



**CALIFORNIA
ENERGY COMMISSION**



**CALIFORNIA
natural
resources
AGENCY**

Energy Research and Development Division

FINAL PROJECT REPORT

Multihazard Investigation of Climate Vulnerability of the Natural Gas Energy System

Gavin Newsom, Governor
October 2020 | CEC-500-2020-071



PREPARED BY:

Primary Authors:

A. AghaKouchak, J. Brouwer, Y-H Lin, A. Hall, K. Reich, N. Berg, I. Mallakpour, O. Mazdiyasn, Z. Heydarzadeh, H-Y Huang, E. Ragno, and C.A. Love

University of California, Irvine
University of California, Los Angeles

Contract Number: 500-15-005

PREPARED FOR:

California Energy Commission

Guido Franco
Project Manager

Jonah Steinbuck, Ph.D.
Office Manager
ENERGY GENERATION RESEARCH OFFICE

Laurie ten Hope
Deputy Director
ENERGY RESEARCH AND DEVELOPMENT DIVISION

Drew Bohan
Executive Director

DISCLAIMER

This report was prepared as the result of work sponsored by the California Energy Commission. It does not necessarily represent the views of the Energy Commission, its employees or the State of California. The Energy Commission, the State of California, its employees, contractors and subcontractors make no warranty, express or implied, and assume no legal liability for the information in this report; nor does any party represent that the uses of this information will not infringe upon privately owned rights. This report has not been approved or disapproved by the California Energy Commission nor has the California Energy Commission passed upon the accuracy or adequacy of the information in this report.

ACKNOWLEDGEMENTS

This study was supported by California Energy Commission Contract Number 500-15-005.

PREFACE

The California Energy Commission's Energy Research and Development Division manages the Natural Gas Research and Development Program, which supports energy-related research, development, and demonstration not adequately provided by competitive and regulated markets. These natural gas research investments spur innovation in energy efficiency, renewable energy and advanced clean generation, energy-related environmental protection, energy transmission and distribution and transportation.

The Energy Research and Development Division conducts this public interest natural gas-related energy research by partnering with RD&D entities, including individuals, businesses, utilities and public and private research institutions. This program promotes greater natural gas reliability, lower costs and increases safety for Californians and focused in these areas:

- Buildings End-Use Energy Efficiency.
- Industrial, Agriculture and Water Efficiency
- Renewable Energy and Advanced Generation
- Natural Gas Infrastructure Safety and Integrity.
- Energy-Related Environmental Research
- Natural Gas-Related Transportation.

Multihazard Investigation of Climate Vulnerability of the Natural Gas Energy System is the final report for the Multi-Hazard Investigation of Climate Vulnerability of the Natural Gas Energy System in Southern California project (Contract Number 500-15-005) conducted by the University of California, Irvine. The information from this project contributes to the Energy Research and Development Division's Natural Gas Research and Development Program.

For more information about the Energy Research and Development Division, please visit the [CEC's research website](http://www.energy.ca.gov/research/) (www.energy.ca.gov/research/) or contact the CEC at 916-327-1551.

ABSTRACT

California needs to address energy security concerns while considering the potential impacts of climate change on the state's energy infrastructure. Infrastructure systems such as natural gas pipelines are experiencing changes in exposure to natural hazards across California. Consequently, infrastructure will likely face more severe climatic conditions in a warming climate with potential societal and economic consequences. Infrastructure design has historically relied on the notion of stationarity, which assumes that statistics of hydroclimatic extremes such as rainfall or streamflow do not change over time. The necessity to adapt infrastructure to climate extremes was recognized by California Legislature in Assembly Bill 2800, which aimed to start the process to ensure the long-term resilience of infrastructure throughout the state. Through California Senate Bill 100, California set goals to eliminate its reliance on fossil fuels and move to zero-carbon energy sources for its electricity needs by 2045. This project explored quantifying climate change impacts on different climatic hazards that can potentially affect natural gas infrastructure systems such as extreme rainfall, coastal and inland flooding, and wildfires. Following scenario guidelines of the California's Fourth Climate Change Assessment, the research team used downscaled climate data with a 1/16 degree spatial resolution from selected Coupled Model Intercomparison Project Phase 5 models. The results show that the exposure of natural gas infrastructure in response to individual and compounding effects of hazards is expected to increase substantially in a warming climate.

Keywords: compound hazards, energy infrastructure, exposure, climate change

Please use the following citation for this report:

AghaKouchak, A., J. Brouwer, Y-H Lin, A. Hall, K. Reich, N. Berg, I. Mallakpour, O. Mazdidasni, Z. Heydarzadeh, H-Y Huang, E. Ragno, and C.A. Love. 2020. *Multi-Hazard Investigation of Climate Vulnerability of the Natural Gas Energy System*. California Energy Commission.
Publication Number: CEC-500-2020-071.

TABLE OF CONTENTS

	Page
ACKNOWLEDGEMENTS.....	i
PREFACE	ii
ABSTRACT	iii
EXECUTIVE SUMMARY	1
Introduction.....	1
Project Purpose.....	1
Project Results.....	1
Knowledge Transfer (Advancing the Research to Market)	3
Benefits to California	3
CHAPTER 1: Introduction	5
CHAPTER 2: Project Approach	9
2.1 Increasing Exposure of Energy Infrastructure to Climate Hazards	9
2.1.1 Data.....	9
2.1.2 Method.....	10
CHAPTER 3: Project Results.....	13
3.1 Increasing Exposure of Energy Infrastructure to Climate Hazards	13
3.1.1 Changes in Precipitation Intensity-Duration-Frequency Curves.....	13
3.1.2 Changes in Inland Flood Hazard.....	21
3.1.3 Changes in Inland Flood Hazard.....	25
3.1.4 Change in Exposure of Gas Pipelines to Climate Hazard.....	28
CHAPTER 4: Knowledge Transfer Activities	37
CHAPTER 5: Conclusions/Recommendations.....	38
CHAPTER 6: Benefits to Ratepayers	40
REFERENCES	42
APPENDIX A-1: Detailed Method	A-1
APPENDIX A-2: Tables of Precipitation Intensity-Duration-Frequency	A-2
APPENDIX B-1: Regarding Twenty-First Century Temperature Changes Over California: 9-km Hybrid Downscaling.....	B-1
APPENDIX B-2: Regarding 1981–2014 90-m Temperature Simulations and End-of-21st-Century 90-m Temperature Simulations	B-14
APPENDIX C: Regional Climate Symposia Summary.....	C-1

LIST OF FIGURES

	Page
Figure 1: Change in 25-Year Intensity-Duration-Frequency Curves Under RCP4.5	14
Figure 2: Change in 50-Year Intensity-Duration-Frequency Curves Under RCP4.5	15
Figure 3: Change in 100-Year Intensity-Duration-Frequency Curves Under RCP4.5.....	16
Figure 4: Change in 25-Year Intensity-Duration-Frequency Curves Under RCP8.5	17
Figure 5: Change in 50-Year Intensity-Duration-Frequency Curves Under RCP8.5	18
Figure 6: Change in 100-Year Intensity-Duration-Frequency Curves Under RCP8.5.....	19
Figure 7: Change in Extreme Precipitation Return Periods for Major Cities in California.....	20
Figure 8: Change in Flood Hazard	21
Figure 9: Change in Flood Hazard Over Leveed Region of California Under RCP4.5	22
Figure 10: Change in Flood Hazard Over Leveed Region of California Under RCP8.5.....	24
Figure 13: Change in Compound Hazard.....	26
Figure 14: Compound Hazards Density Distribution	26
Figure 15: Distribution Natural Gas Pipeline Runoff Exposure	27
Figure 16: Natural Gas Pipeline Wildfire Exposure	27
Figure 17: Length of Natural Gas Pipeline in Leveed Area	29
Figure 18: Number of Power Plants in Leveed Area	30
Figure 19: Natural Gas Pipeline Exposure to Flood Hazard in Leveed Area	31
Figure 20: Natural Gas Pipeline Exposure to Coastal Storm	33
Figure 21: Natural Gas Pipeline Exposure to Tidal Flooding	34
Figure 22: Natural Gas Pipeline Exposure to Coastal Storm and Sea Level Rise Compound Flooding	35
Figure 23: Power Plants Exposure Matrix for Los Angeles County	36
Figure B1-1: Elevation (m) and model setup in this study with two one-way nested WRF domains (labeled D01 and D02) at resolutions of 27 and 9 km.....	B-4
Figure B1-2: Elevation (m) and model setup in this study with two one-way nested WRF domains (labeled D01 and D02) at resolutions of 27 and 9 km.....	B-7

Figure B1-3: (top) WRF March warming patterns (°C). (bottom) StatWRF March warming patterns	B-8
Figure B1-4: Temperature changes between 2081–2100 and 1981–2000 for (top) linearly interpolated GCM ΔT (°C) averaged from 31 RCP8.5 GCMs, and (bottom) as in (top), but for StatWRF ΔT (°C).....	B-9
Figure B1-5: StatWRF ΔT warming estimations in California between 2041-2060 and 1981-2000 periods and between 2081-2100 and 1981-2000 for RCP4.5 and RCP8.5	B-10
Figure B2-1: Study domain’s a) elevation, b) canopy cover fraction, and c) land cover type in 90-m resolution. Abbreviations in c) represent Water body (Wtr), Developed (Dvl), Barren (Brr), Forest (Frs), Shrubland (Shr), Herbaceous land (Hrb), Planted (Pln), and Wetland (Wtl)	B-15
Figure B2-2: Mean changes of surface air temperature (ΔT_a) and daily precipitation (ΔPPT) between future GCM simulations (2081–2100 with scenario RCP 8.5) and historical baseline (1981–2000).....	B-16
Figure B2-3: Comparison of T_a between observations collected in CIMIS sites and model estimates: a) all data from October, 1991 to September 2001, b) monthly mean. Data are averaged across all 137 CIMIS sites	B-18
Figure B2-4: Average air temperature in winter months (December, January, and February): a) historical and b–f) projected temperature change from selected GCMs.	B-19
Figure B2-5: Same as Figure B2-4, but for summer months (June, July, and August).	B-20
Figure B2-6: a) Mean air temperature for winter months (December-February, blue dots) and summer months (June-August, red dots) during the historical time period for major cities in State of California. b) Projected temperature changes from GCMs. The vertical bar represents standard deviation cross GCMs.	B-21
Figure D-1: SoCalGas System Map	D-4
Figure D-2: Schematic of the Hydrogen Energy Storage System.....	D-5
Figure D-3: Annual Hydrogen Energy Storage Capacity Starting at Full Capacity	D-9
Figure D-4: Annual Hydrogen Energy Storage Capacity for Various Scaling Factors Starting at Half Capacity	D-9
Figure D-5: Annual Hydrogen Energy Storage Capacity for Various Scaling Factors Starting at Half Capacity	D-11
Figure D-6: SoCal Transmission Pipelines Used in Modeling	D-12
Figure D-7: Annual Pressure Fluctuation for 100% Hydrogen Delivered Through Pipe 1-2 .	D-13
Figure D-8: Annual Pressure Fluctuation for 100% Hydrogen Delivered Through Pipe 3-4 .	D-13
Figure D- 9: Annual Pressure Fluctuation for 100% Hydrogen Delivered Through Pipe 5-6	D-14
Figure D-10: Annual Pressure Fluctuation for 100% Hydrogen Delivered Through Pipe 7-8	D-14
Figure D-11: Annual Pressure Fluctuation for 40% Hydrogen Delivered Through Pipe 1-2 .	D-15

Figure D-12: Annual Pressure Fluctuation for 40% Hydrogen Delivered Through Pipe 3-4 . D-15

Figure D-13: Annual Pressure Fluctuation for 40% Hydrogen Delivered Through Pipe 5-6 . D-16

Figure D-14: Annual Pressure Fluctuation for 40% Hydrogen Delivered Through Pipe 7-8 . D-16

LIST OF TABLES

	Page
Table 1: Levee Systems That Protect Highest Length of Natural Gas Pipeline.....	32
Table A-1: 25-yr Return Period Intensity-Duration-Frequency curves based on historical records (NOAA) and future climate (RCP 4.5 and RCP 8.5).	A-2
Table A-2: 50-yr Return Period Intensity-Duration-Frequency curves based on historical records (NOAA) and future climate (RCP 4.5 and RCP 8.5).	A-4
Table A-3: 100-yr Return Period Intensity-Duration-Frequency curves based on historical records (NOAA) and future climate (RCP 4.5 and RCP 8.5).	A-6
Table D-1: Southern California Gas Company Natural Gas Underground Storage.....	D-3
Table D-2: Land Use Requirement for Different Solar PV Power Plants in SoCal	D-16

EXECUTIVE SUMMARY

Introduction

Rapid increases in population and fiscal constraints have challenged California's ability to maintain adequate levels of public infrastructure. Combined with increasingly severe and frequent natural hazards, strategic planning for California's infrastructure is essential. The natural gas infrastructure is among the most reliable and resilient to natural disasters. However, California's natural gas lines can be vulnerable to the increased frequency and intensity of wildfires and floods, extreme precipitation events, and sea level rise driven by climate change. For instance, increases in flooding along the coast of California due to sea level rise can result in more pipelines remaining in near water-saturated conditions for longer periods. Therefore, different requirements for pipe materials, strength, and wall thickness are necessary to account for this new condition. If the design of the pipelines did not incorporate the changing climate conditions, then the useful life of gas pipelines may be reduced, and more frequent pipeline replacement and repairs will be necessary. The effects from exposure of natural hazards on the energy infrastructure has the potential to cause significant economic and societal damage (such as power outages). In an effort to plan for and mitigate such damages, studies must be conducted to quantify the impacts of these natural hazards. Studies have been performed on the changes of climate hazards and their associated impacts. However, studies on multiple climate events occurring simultaneously or consecutively are only beginning to be investigated.

Project Purpose

In this study, the research team analyzed climate change impacts on different hazards that can potentially impact natural gas infrastructure systems (for example extreme rainfall, coastal and inland flooding, and wildfires). The study targets the changes and impacts of these natural hazards on natural gas infrastructure. This report addresses technical gaps in the pursuit of achieving California clean energy goals by specifically analyzing the possible exposure of natural gas infrastructure to natural hazards in the future and addressing multiple co-occurring natural hazards. In this report, climate change impacts refer to exposure of natural gas infrastructure to climate extremes, and not necessarily economic or other physical damages. This analysis will guide policy makers to make informed decisions, reducing the economic burden on California ratepayers.

Project Results

The team achieved the project goals and objectives. The changes in natural hazards along key natural gas infrastructure were determined for different future climate scenarios, based on different greenhouse gas concentrations. Climate change is expected to have significant impacts on air temperature in California, but these impacts are not yet quantified at very fine scales (such as hundreds of meters or finer). The possible projected increase in temperatures can increase severity and frequency of climate extreme events such as wildfire activity across California.

Specifically, in this project, floods and wildfires were considered, and it was determined that under a fossil fuel intensive "business as usual" climate scenario, there would be an average of more than double the exposure of natural gas infrastructure to wildfires across most of

California. Furthermore, it was determined that major cities such as Los Angeles, San Francisco, and Sacramento will receive almost twice the precipitation rate over seven days for an extreme precipitation event under 'business as usual' climate scenario by the end of 21st century relative to a 1950-1999 baseline.

Increases in intensity, duration, and frequency of extreme precipitation can adversely impact the integrity of infrastructure and natural and engineered slopes. For example, results demonstrate that levee systems in the northern part of Central Valley and coastal counties of Southern California, which protect hundreds of miles of natural gas pipelines, experience the highest likelihood of changes in flood hazard in the latter half of the 21st century. Therefore, the infrastructure protected by these levee systems may observe higher rates of exposure to flooding in the future.

Additionally, the research shows that regional patterns of exposure of natural gas pipelines to individual/compounding effects of hazards are significantly different. Considering the compounding impacts of concurrent hazards is even more important when dealing with aging infrastructure with declining resilience to natural hazards. The researchers studied the changes of extreme climate events and natural hazards from multiple perspectives, including analyzing the change in how often (on average) an event with a certain magnitude would occur and the change in the magnitude of an event associated with a certain likelihood in a warming climate. This report refers to these occurrences as the return period and return level, respectively, of different natural hazards in a warming climate. The analysis was robust and filled in the knowledge and data gaps necessary to achieve the objectives of the study. It is important to note that the results are based on climate models and statistical methods, making the findings subject to model and parameter uncertainty.

The major lesson learned in this study was the shift in magnitude of extreme events that California's natural gas infrastructure is projected to be exposed to by the latter half of the 21st century. The results show that extreme precipitation-related events — such as those that are expected to occur every 50 or 100 years — will likely become more frequent. (Note: A 50-year event is one that has a 2 percent chance of happening in any year, and a 100-year event is one that has a 1 percent chance of happening in any year.) For example, climate model simulations project that the frequency of what is now referred to as a 50-year event will double in the future in many parts of the state under representative concentration pathways 8.5 (such as in San Diego, Santa Barbara, San Jose, San Francisco and northern California). Additionally, results show that in areas such as Los Angeles County and Orange County the exposure to compounding impacts of SLR and coastal storm increases exponentially (compared to current mean sea level and coastal flooding) when sea levels increase. For example, this may mean that a storm of a certain magnitude that, at present, is considered to be a 100-year coastal storm, would be expected to become frequent tidal flooding when there is a sea level rise of 1.5 m. Thus, any infrastructure that is in the flooding zone will be exposed to extreme flooding more frequently by the end of the century than that it is now. Such information can be used to design new infrastructure and retrofit existing infrastructure.

In considering natural gas infrastructure, the research team modeled integrating hydrogen energy storage with large-scale renewable power using the capabilities of the existing California natural gas infrastructure. The gedanken experiment described in Appendix D gives

insight into the potential contribution that the natural gas system could make toward balancing a highly renewable electric grid in the future.

Knowledge Transfer (Advancing the Research to Market)

In this report, the research team analyzed the impact of rising natural hazards from a warming climate on energy infrastructure. The analysis was informative to policy makers and stakeholders for future climate adaptation plans. The research team met with stakeholders and presented their work in open forums to transfer the knowledge to decision makers and the general public. Furthermore, the researchers will continue to work with the California Energy Commission, Southern California Gas Company and stakeholders to inform them based on the analysis in this report.

In addition to the stakeholder outreach performed by the research team, Local Government Commission (LGC) and Climate Resolve contributed to further public and stakeholder outreach as part of this project. Their work, presented in Appendix C to this report, included the organization of four regional climate symposia in the Inland Desert, Los Angeles, San Joaquin Valley, and Central Coast regions, with speakers from public agencies such as the Strategic Growth Council, the Governor's Office of Planning and Research, and the California Energy Commission; as well as nonprofits, universities, and private sector organizations such as TreePeople, Los Angeles Regional Collaborative for Climate Action and Sustainability, UC Irvine, UCLA, Scripps Institution of Oceanography, and Southern California Gas Company. Participants included representatives from state and local government, academic institutions, and community-based organizations, and each event earned local and regional media coverage.

Benefits to California

This research is important to ratepayers because it provides information to decision makers to plan for and mitigate the costly impacts of rising natural disasters associated with a changing climate. The potential cumulative damage to infrastructure until the end of the century may cost many times more than upgrading existing infrastructure. The results of this study can be used to design improved structures for natural gas pipelines (such as creating levees that guard against more extreme river discharge) considering possible future climate changes.

Parts of this report contributed to California's Fourth Climate Change Assessment. Specifically, this research supported examination of potential changes in extreme precipitation events, developing what is known as intensity-duration-frequency curves. Engineers use these curves in the design of infrastructure including natural gas physical assets. In turn, the authors of the report for AB 2800 (*Paying it Forward: The Path Towards Climate-Safe Infrastructure in California*) used these curves as an example on how to translate information on climate projections in a way that engineers can use. This contributes to a new area of research that brings together climate scientists and engineers. In 2018, the California Public Utilities Commission opened a rulemaking to consider strategies and guidance for climate change adaptation for electric and natural gas utilities (proceeding number R.18-04-019). Studies like this are providing material for consideration in the preparation of plans and guidance documents for the CPUC proceeding and other similar efforts.

CHAPTER 1:

Introduction

In the past decades, anthropogenic emissions have increased triggering more natural hazards that cause damage to infrastructure such as levees, dams, roads and energy infrastructure systems (Das et al., 2011; Jongman et al., 2014). For instance, the observed increase in extreme temperatures can increase the risk of wildfires (Turco et al., 2017). Extensive wildfire during the dry season may enhance the risk of debris flow and sediment transport in the following wet season (Williams et al., 2014), threatening populations and infrastructure. The risk of wildfires is also intensified by those extreme weather conditions leading to power line system failure and consequent fire ignition in highly populated environments (Mitchell, 2013). Higher surface temperatures can also alter the global water cycle by increasing the number of heavy precipitation events. Heavier precipitation events, in turn, exacerbate the risk of fluvial and pluvial flooding (Field et al., 2014). In addition, recent studies have shown that, given the expected increase in future precipitation, there is a high chance of substantial impact on landslide activity in natural slopes (Robinson et al., 2017) and on the performance of man-made earthen structures (Jasim et al., 2017; Vahedifard et al., 2017b), calling into question the current procedure for infrastructure design and risk assessment.

Flood-prone areas can experience additional loss of life because of transport network disruptions and power outage due to flooding, which impede rescue operations and medical assistance. The risk of flooding is also exacerbated by sea level rise, which represents a special threat to the California coast. Critical infrastructure will also be exposed to coastal flooding inundation and the estimated damage is to be nearly \$100 billion (in year 2000 dollars; Heberger et al., 2009).

Moreover, current methods for the design of infrastructure such as levees, dams, roads, and energy infrastructure systems are based on the so-called stationary assumption that assumes the statistics of extremes and distribution of the underlying variables do not change over time (Sadegh et al., 2015). For example, engineers use rainfall Intensity-Duration-Frequency (IDF) curves for estimating the design storm intensity and the corresponding flow. Rainfall IDF curves show the magnitude of an extreme event with a certain duration and expected recurrence interval based on historical observations. The process of estimating IDF curves requires fitting a representative distribution function to the observed rainfall data (Bonnin et al., 2006). Traditionally, the parameters of the distribution function are estimated under the stationary assumption (i.e., time invariant parameters), meaning that no significant changes are expected in the characteristics (e.g., magnitude and frequency) of rainfall extremes over time. However, in a warming climate, the assumption of stationarity may not be necessarily sufficient (Milly et al., 2008).

The projected warming and expected changes in precipitation and snow patterns are anticipated to change river flows (Alfieri et al., 2015; McCabe and Wolock, 2014; Nazemi and Wheeler, 2014). A warmer climate may drive earlier snowmelt, reduce snowpack, change the seasonality of river flows and instigate changes in snow to rain ratio (Cayan et al., 2001; Harpold et al., 2017; Knowles et al., 2006; Mao et al., 2015). These changes are even more

important in regions like California, where streamflow relies on winter snow accumulation (Diffenbaugh et al., 2015; Li et al., 2017). In recent years, California has experienced a series of flooding events (Vahedifard et al., 2017a) on the heels of a 5-year drought (AghaKouchak et al., 2014; Hardin et al., 2017). In 2017, a major flood in Northern California led to structural failure of Oroville Dam's spillway that triggered the evacuation of about 200,000 people. Several studies have documented that warm and wet storms brought by atmospheric rivers (AR) during winter may cause severe flooding in California (Barth et al., 2016; Dettinger, 2011; Leung and Qian, 2009; Ralph et al., 2013). Jeon et al. (2015) used 10 CMIP5 climate models to show that AR events in warming climate would bring more frequent and severe storms to California in the future. Similarly, Payne and Magnúsdóttir (2015) used 28 CMIP5 models in a study where they projected up to 35 percent increase in AR landfall days. Dettinger (2011) have shown that potential increases in the magnitude and frequency of AR events in the future can cause more severe and frequent flooding events in California.

It is essential to recognize that climate change impacts do not occur in isolation but are strongly coupled. For instance, floods and debris flow pose a significant threat to energy infrastructure, especially when extreme rain falls over burned areas. A recent example was the devastating debris flow in Montecito, California that killed at least 20 people and injured many more. The event occurred about a month after a major wildfire that scorched over 440 square miles in Southern California. This is an example of compound events in which two concurrent or consecutive events lead to extreme impacts.

Though there is significant variability in the ways to define/discuss extreme events across disciplines (McPhillips et al., 2018), in general, compound events (or compound hazards) correspond to combinations of two or more dependent drivers that yield extreme impacts and pose significant societal or environmental risk (Leonard et al., 2014; Zscheischler and Seneviratne, 2017). The compounding impacts can be grouped into the following categories:

1. Two or more extreme events occurring simultaneously or successively.
2. Combinations of extreme events with underlying conditions that amplify the impact of the events.
3. Combinations of events that are not themselves extremes but lead to an extreme event or impact when combined (IPCC, 2012).

In these situations, the resulting impacts due to compounding effects are expected to be significantly more severe than those due to individual hazard drivers in isolation, and thus ignoring these compounding effects may yield inappropriate characterization of posed risk (Sadegh et al., 2018).

Wildfires followed by severe flooding in the western United States are examples of compound hazards, under which the impacts are intensified by the succession of two natural hazards (NFIP, 2012). Both the frequency and intensity of wildfires in the western US have significantly increased over the last few decades (Dennison et al., 2014). This rise is associated with many factors including human-caused climate change, and more specifically climate warming and drought severity (Abatzoglou and Williams, 2016; Westerling, 2016). This extensive wildfire during the dry season may enhance the risk of flooding by increased hydrologic vulnerability stemming from elevating soil exposure to runoff and erosion processes (Williams et al., 2014). Wildfires disturb hydrologic characteristics of the watershed such as evapotranspiration (Poon

and Kinoshita, 2018), baseflow (Kinoshita and Hogue, 2011) and surface water yield, which not only affect the quantity of the delivered runoff, but also the quality and concentration of suspended materials (Burke et al., 2013; Florsheim et al., 2017). That makes debris-flow activity among the most destructive consequences of post-wildfire effects. Fire-related debris flows can be intensified by erosion and entrainment of material by surface runoff and infiltration-triggered failure and mobilization of a discrete, shallow landslide mass (Parise and Cannon, 2017).

On the other hand, there is robust evidence of increased coastal flooding due to sea level rise (SLR) (Kriebel et al., 2015; Moftakhari et al., 2017, 2015; Vitousek et al., 2017; Woodruff et al., 2013). The rate of exposure to flooding may, however, depart from sea level rates due to local patterns of topography and development (Kulp and Strauss, 2017). The projected increase in the risk of coastal flooding is partially explained by raised exposure due to population and economic growth (Curtis and Schneider, 2011; Garschagen and Romero-Lankao, 2015; Hallegatte et al., 2013). While the research team expected this more frequent flooding would adversely affect the coastal infrastructures, there are limited assessments on projected impacts of long-term changes in the literature (Forzieri et al., 2018; Hill, 2015; Wang et al., 2017).

Energy infrastructure is vulnerable to climate conditions in numerous ways (Cruz and Krausmann, 2013; Mukherjee et al., 2018; Schaeffer et al., 2012). By the 2080s, for example, an overall climate risk of € 8.2 million/year to the energy sector is expected in Europe (Forzieri et al., 2018). In California, substantial new investment is required for an additional 38.5 percent peak generation capacity to compensate the decreased efficiency of generators and substations, and the increased demand by the end of the 21st century (Sathaye et al., 2012). Also, about two thirds of mega-cities with populations above 5 million are located in the low-elevation coastal zone (Abadie et al., 2016). Coastal population densities are nearly three times that of inland areas, and they are increasing exponentially (Field et al., 2014; Neumann et al., 2015). This growth in urbanization/population is usually accompanied by costly infrastructural development in coastal regions (Mansur et al., 2016; Tessler et al., 2015). Energy infrastructure is among the most basic and vulnerable coastal infrastructures, where interruption in their serviceability may yield disastrous conditions (Brown et al., 2014). Natural gas pipelines are especially sensitive to change in flooding and wildfires (Forzieri et al., 2018; Schaeffer et al., 2012). Therefore, the exposure of natural gas pipelines to possible changes in climatic hazards must be further explored to accurately estimate the failure probability (Moftakhari et al., 2017).

The overarching goal of this report is to determine the changes and exposure of natural hazards (precipitation events, floods, sea level rise, and wildfires) on natural gas infrastructure due to a warming climate. To do this, historical and future projections are used to assess the exposure of energy infrastructure under single or multiple climatic drivers. This study focuses on assessing the exposure of energy infrastructure due to extreme precipitation, flooding, and wildfires. Hydroclimatic extremes are interdependent, so the research team further investigate the impact on infrastructure system resulting from the interaction between multiple drivers. Climate change is predicted to have notable impacts on air temperature however impacts are not yet quantified at very fine scales. Therefore, UCLA researcher used a hybrid dynamical–statistical approach to develop high resolution (i.e., 9 km and 90 m) temperature projections

over California (Appendix B1 and B2). In a warmer climate, intense rainfall hazard is also expected to be higher due to increased water vapor holding capacity of the atmosphere and change in precipitation pattern (Hirabayashi et al., 2013). Thus, the expected climate change-induced alteration in heavy-precipitation and high-temperature extremes (Fischer and Knutti, 2015) may yield growing susceptibility to compound hazards. The more intense/frequent extreme compound hazards significantly threaten infrastructures, depending on their vulnerability to each specific hazard (Forzieri et al., 2018).

In this study, the research team first quantify the climate-induced stressors on California natural gas pipelines, resulting from a single climatic extreme or from concurrent/consecutive climatic extremes. Then the research team quantify the change in the exposure of natural gas pipelines as a consequence of single or multiple natural hazards and determine the regions with elevated projected hazard. They also seek to address the possible changes in flood hazard over the leveed area of California and quantify the change in the exposure of natural gas pipelines to flooding over the levee protected regions. Finally, the researchers quantify the change in the exposure of natural gas pipelines to coastal flooding for Los Angeles and Orange counties in Southern California due to sea level rise. The results of this report are based on model outputs and statistical tools, making them subject to uncertainty. However, they are a means to provide valuable information about possible exposure of energy infrastructure to natural disasters.

CHAPTER 2:

Project Approach

2.1 Increasing Exposure of Energy Infrastructure to Climate Hazards

2.1.1 Data

The climatic data used in this study are all based on the downscaled climate simulations and projections from Localized Constructed Analogs (LOCA) by Scripps Institution of Oceanography (Pierce et al., 2014). There are two major uncertainties in climate models when projecting future climate changes. First, there is uncertainty in the physics contained in the global climate models (GCMs) simulations of future environments, such as hydrological processes, cloud formation, and wind circulations. Second, there is uncertainty due to the spatial scale of GCMs, which cannot accurately resolve the complex topography of California, including its coasts, valleys, and high mountains. Therefore, the use of downscaling techniques to convert the coarse spatial resolution in GCMs to high resolution hydrological variables is an inevitable step for the climate change impacts assessment studies (Mehrotra and Sharma, 2016).

The Variable Infiltration Capacity (VIC; Lohmann et al., 1998) model is driven by the high-resolution Localized Constructed Analogs (LOCA) downscaled and bias-corrected minimum and maximum temperature, and precipitation. The LOCA downscaling method has shown, for California, a superior performance to its predecessors including Multivariate Adapted Constructed Analogs (MOCA). California's Fourth California Climate Change Assessment used LOCA projections as a basis for climate resilience research. The LOCA method "produces downscaled estimates suitable for hydrological simulations using a multiscale spatial matching scheme to pick appropriate analog days from observations" (Pierce et al., 2014). LOCA reduces the averaging of analog days that other existing methods typically use and constructs a downscaled area (field) that best matches (historically observed) weather in a local region around the point being considered.

Cal-Adapt (<http://cal-adapt.org>) provides access to LOCA climate data including precipitation and generated total runoff at spatial resolution of $1/16^\circ$ (approximately 6 km) and daily temporal resolution all over the State of California for the period of 1950 to 2099. LOCA data have also been used as input to models for wildfire intensity projections. The projections from four General Circulation Models (GCMs) prioritized by the Fourth Assessment, namely HadGEM2-ES, CNRM-CM5, CanESM2 and MIROC5 under Representative Concentration Pathways (RCP) 4.5 and 8.5 are obtained to represent warm/dry, cool/wet, average and complement climate conditions in California. While the daily values for precipitation and runoff are provided in $\text{kg}/\text{m}^2/\text{s}$ and m^3/s , the monthly wildfire intensity is estimated in hectares.

For infrastructure exposure assessment the researchers obtain data about the distribution of natural gas pipelines of California from U.S. Energy Information Administration (<https://www.eia.gov>). This dataset includes information about the interstate and intrastate natural gas pipelines for states with State Natural Gas Pipeline Programs in the USA (Stafford, 2017), including California. Worth noted that the data set does not include information

regarding the elevation of pipelines, so exposure here could either refer to complete/partial inundation of pipeline or exposure of supporting structures (e.g. piers). Information related to the leveed area of California are obtained from the National Levee Database (NLD) maintained by the U.S. Army Corps of Engineers (USACE; <https://levees.sec.usace.army.mil/>). Flooding hazards maps for the counties of Los Angeles and Orange are obtained from the Coastal Storm Modeling System (CoSMoS) by United States Geological Survey (USGS; Barnard et al., 2015, 2014). CoSMoS provides information about the severity (i.e. extent, depth, etc.) of flooding along the coasts of Southern California. Here the researchers emphasize that climate model simulations are subject to biases and uncertainties (e.g., Liu et al., 2014; Mehrotra and Sharma, 2016). While climate models exhibit a wide range of uncertainty that can influence the estimation of flood hazard, they are a means to provide valuable information about possible future hydrological conditions.

2.1.2 Method

2.1.2.1 Precipitation Intensity-Duration-Frequency Curves

Precipitation Intensity-Duration-Frequency (IDF) curves provided by National Oceanic and Atmospheric Administration (NOAA) involve fitting a representative distribution function to observed (historical) extreme precipitation. Two main underlying assumptions have been considered (see Appendix A.1): (i) annual precipitation maxima follow a Generalized Extreme Value (GEV) distribution; (ii) the statistics of the distribution are time-invariant (stationarity assumption). The assumption (ii) refers to the expectation of a climate in which precipitation characteristics do not change over time. However, for a more realistic representation of the time series behavior the research team needed to account for changes in the statistics of the extremes if they are significant (Cheng and AghaKouchak, 2014).

Based on the above considerations, the researchers employ time series of annual maxima precipitation intensity to retrieve historical and projected IDF curves based on Ragno et al. (2018). For each location, they independently analyze daily precipitation products of each GCM to retrieve time series of annual maxima intensity in a water year (October through September, as defined by the United States Geological Survey) for events of 1-day to 7-day duration. It is worth noting that any storm duration can be investigated. Here, the researchers focused on daily duration because the downscaled GCM simulations provided for the Fourth Assessment are daily. The simulations include Representative Concentration Pathways (RCP) 4.5 and 8.5. The researchers consider daily precipitation estimates for 1950-1999 and 2050-2099 to be representative of the historical and future climate, respectively. Given that the focus of this report is on frequency analysis, the researchers have chosen a 50-year baseline to be consistent with the typical length of record used in the current historical IDF curves. Also, the researchers have chosen a 50-year projection period to ensure consistency of sample sizes in the baseline and projection periods. A time series of annual maxima is obtained as follows. Consider that the time series of daily precipitation of the j th water year, $P^j = \{p_1^j, \dots, p_{n_j}^j\}$, where n_j is the number of days in the j th water year. The annual precipitation intensity of a d -day event for the j th water year is:

$$P_{d,max}^j = \max\left\{\frac{\sum_{t=1}^d p_t^j}{d}, \dots, \frac{\sum_{t=i}^{i+d-1} p_t^j}{d}, \dots, \frac{\sum_{t=n_j-d+1}^{n_j} p_t^j}{d}\right\} \quad (2.1)$$

The time series of annual maxima is then $P_{d,max} = \{P_{d,max}^1, \dots, P_{d,max}^{ny}\}$, where ny is the total number of water years (49 years in this study). For each model, the researchers process the historical simulations and the future projections independently.

The project team retrieved historical IDF curves using historical simulations and a stationary GEV distribution to reproduce NOAA IDF curves. On the other hand, the researchers retrieved future IDF curves using future projections and a GEV distribution with parameters that change over time (hereafter, non-stationary GEV), to incorporate trends in the data when observed. Indeed, the non-stationary GEV is used when the Mann-Kendall trend test result detects a statistically significant trend in precipitation (i.e. null-hypothesis of no trend is rejected at a 0.05 level of significance).

2.1.2.2 Change in Flood Hazard

Researchers use GEV distribution to estimate the flood frequency distribution for gridded runoff over California. In this study, the research team used annual maximum daily simulated runoff as a proxy to examine the direction of change in flood hazard. For this, the research team firstly utilize annual block maximum sampling technique to extract the maximum daily value of runoff for each year and for each of the four climate models and scenarios. Then, they fit the GEV distribution to estimate the flood frequency distribution for each pixel using extreme 2.0 package in R (Gilleland and Katz, 2016). To estimate the parameters of the GEV distribution the researchers used the maximum likelihood method (Coles, 2001). This statistical model has been used in many hydrological studies to characterize the behavior of extreme events (AghaKouchak, 2013; Cheng et al., 2014; Katz et al., 2002). With the means of extreme value theory, the researchers then compute the percentage change between the magnitudes of a 100-year flow ($T=1/p$ where exceedance probability $p=0.01$) in the future (2020–2099) relative to the historical (1950–2005) periods as an indicator of change in the flood hazard for each pixel and for each model and scenario using normalized percent change:

$$\frac{Future - Historical}{Historical} \times 100 \quad (2.2)$$

To compute the change in the flood hazard for each levee system the researchers spatially average the percentage change in the magnitude of the 100-year flow over each levee system. They used the 100-year flow concept since the majority of levee systems in California have been designed to withstand the peak flow with a 1 percent annual chance of occurrence (i.e. 100-year flood; Burton and Cutter, 2008; Ludy and Kondolf, 2012). Note that a comprehensive flood risk assessment in leveed area is a function of three components, hazard (likelihood of the flood event), exposure (assets and population exposed to the flood events), and vulnerability (capacity of system to damp the impact of a flood event; e.g., Collenteur et al., 2015; USACE, 2018). Here, the researchers are only focusing on the flood hazard changes and energy infrastructure exposure to these changes.

2.1.2.3 Change in Hazard Exposure

In this study for wildfire and precipitation compound hazard assessment the research team take the product of largest monthly wildfire in a given dry season and the 95th percentile of daily precipitation in the following wet season as a representative of compound wildfire-flooding hazard. They assume that a watershed hit by wildfire can recover after a year and so

the history of fire experience (i.e. lag times greater than one year) is not transferred to calculate the compound hazard. Using this data the research team quantify the length of pipelines located in each pixel with wildfire intensity and runoff projection. Then the exposure of pipelines to natural hazards is calculated by multiplying the length of pipeline to the estimated intensity of the given natural hazard.

The research team used the SLR projections for Los Angeles, provided in the State of California Sea Level Rise Guidance (State of California, 2018), to analyze the timeline associated with studied scenarios. Here the research team used 40 scenarios combining ten SLR scenarios (0, 0.25 m, 0.5 m, 0.75 m, 1.0 m, 1.25 m, 1.5 m, 1.75 m, 2.0 m, and 5 m) with four possible coastal storm conditions (daily/background conditions, 1-year storm, 20-year storm, and 100-year storm). These coastal storm conditions include sea level anomalies, waves, storm surge and river discharge. The document uses SLR projections from Kopp et al. (2014) and tabulate the 19-year average values centered on the specified year with respect to a 1991-2009 baseline, under high and low emission scenarios (e.g. Representative Concentration Pathways (RCPs) 8.5 and 2.6, respectively). Finally, the research team calculate the lengths of natural gas pipelines located in the flood prone zones from CoSMoS. In this manner the research team analyze the extent to which natural gas pipeline are located in flood prone zones and determine the likelihood of each scenario given the regional sea level projections in Southern California. They emphasize that exposure of natural gas pipelines in this study could either refer to complete or partial inundation of pipeline or exposure of supporting structures (e.g. piers). Therefore, the analysis in this report does not indicate that natural gas pipelines are in danger, but the research team argues that under a changing climate the possible exposure of this infrastructure to climate extremes will change.

CHAPTER 3:

Project Results

3.1 Increasing Exposure of Energy Infrastructure to Climate Hazards

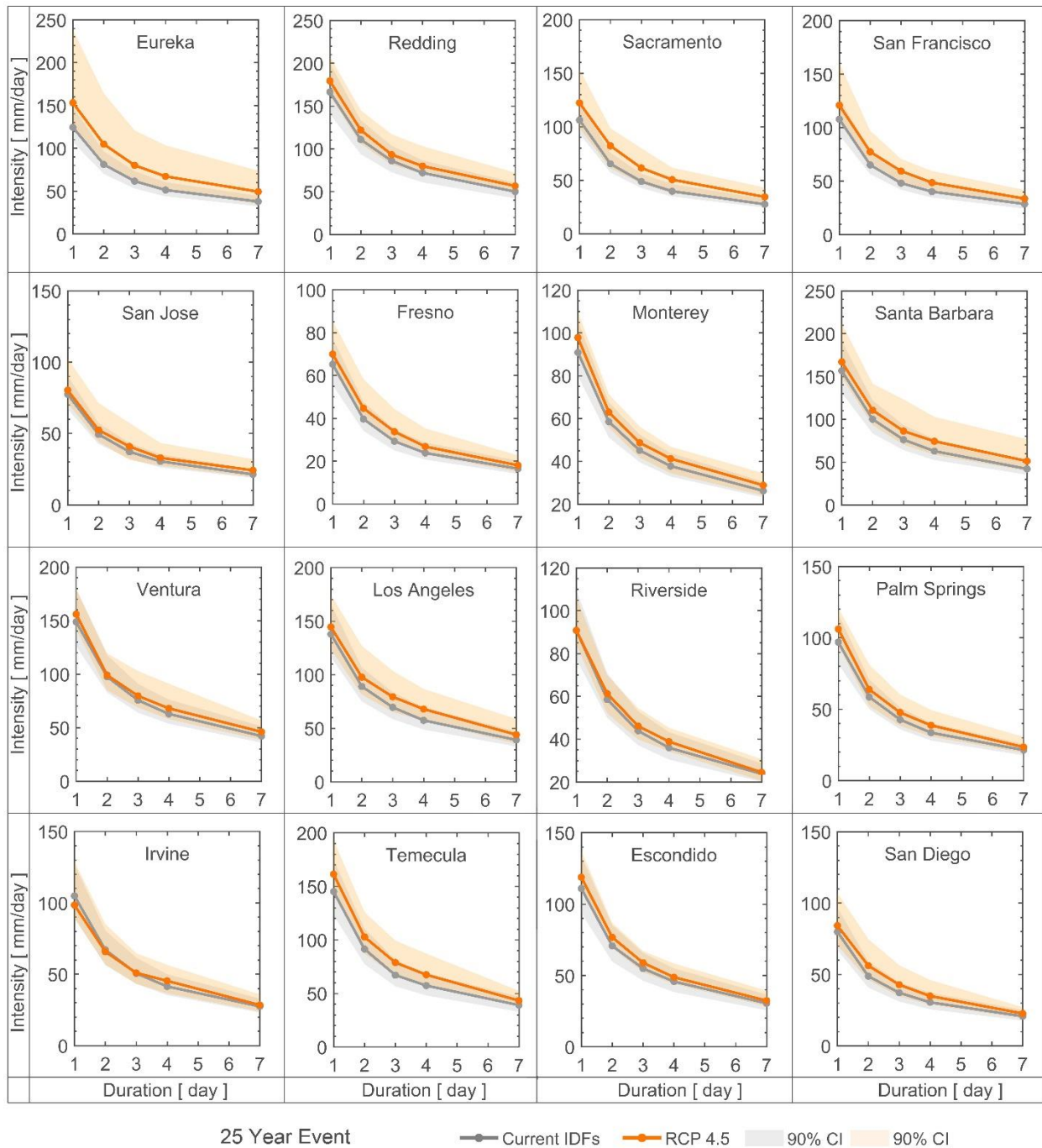
3.1.1 Changes in Precipitation Intensity-Duration-Frequency Curves

Under the chosen future scenarios, their results show an overall upward shift of the Intensity-Duration-Frequency (IDF) curves, indicating that more severe events are expected to occur. Figures 1-3 and Figures 4-6 show IDF curves based on RCP4.5 and RCP8.5 scenarios, respectively. The interested readers can find the numerical values of the expected IDF curves in Appendix A-2.

An overall pattern towards more intense precipitation is observable under both RCPs for events with 25-, 50-, and 100-year return period. In southern California (i.e., Irvine, Riverside, and Escondido) the research team can observe that, for the RCP 4.5 scenario, changes in extreme precipitation intensity are minimal across different storm durations (Figures 1–3). The same pattern can be detected in northern California. Whereas, the RCP 8.5 scenario shows an overall increase in the intensity of extreme events across the state of California.

It is worth noting that precipitation is highly dependent on local climate, so high spatial variability is not surprising. Moreover, high uncertainty bounds are mainly associated with the climate models that are subject to biases and uncertainties.

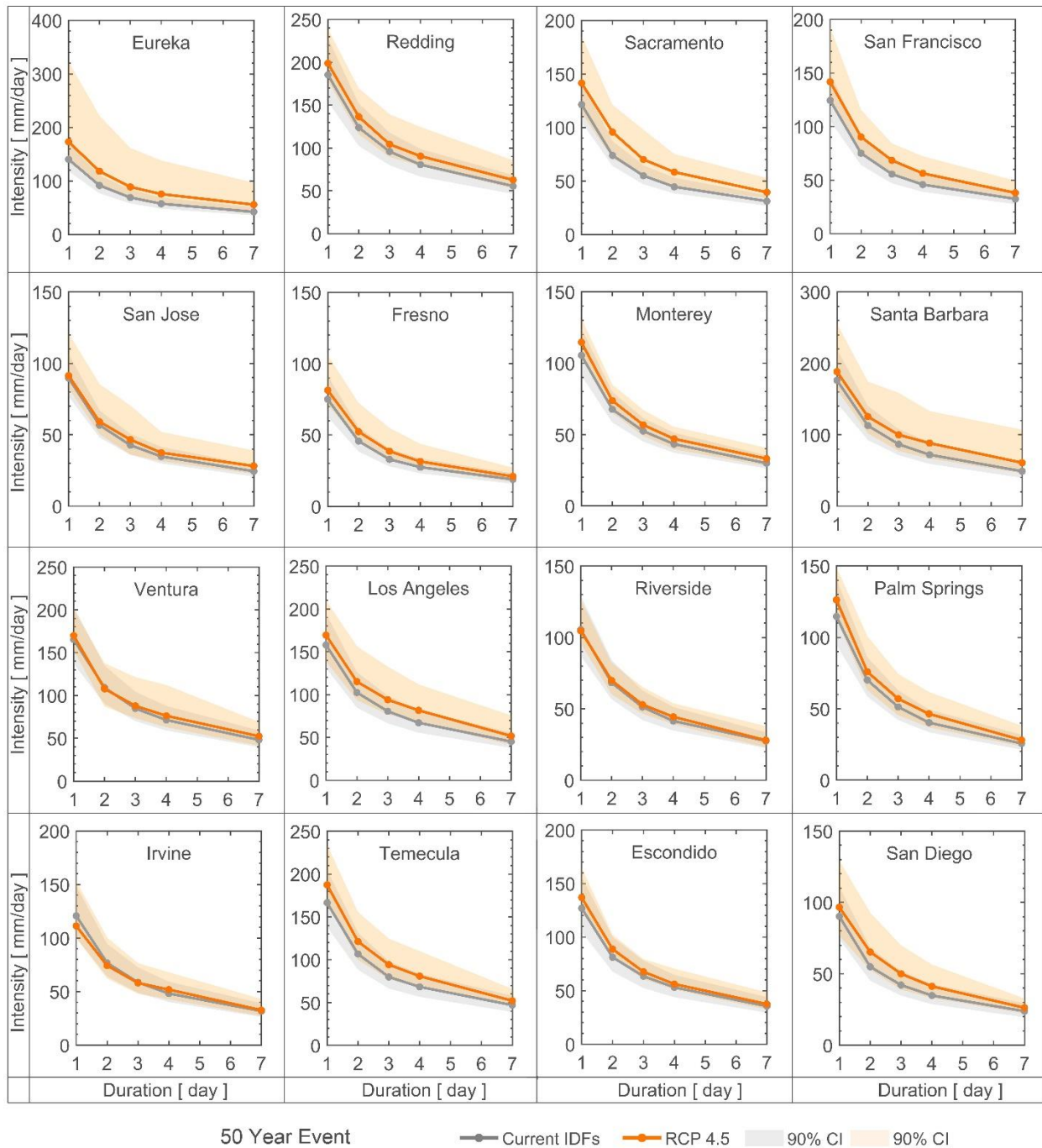
Figure 1: Change in 25-Year Intensity-Duration-Frequency Curves Under RCP4.5



Comparison between the current (grey lines) and future climate (orange lines) 25-yr Intensity-Duration-Frequency (IDF) curves (RCP4.5), along with 90 percent confidence intervals (after Ragno et al., 2018).

Source: University of California, Irvine and University of California, Los Angeles.

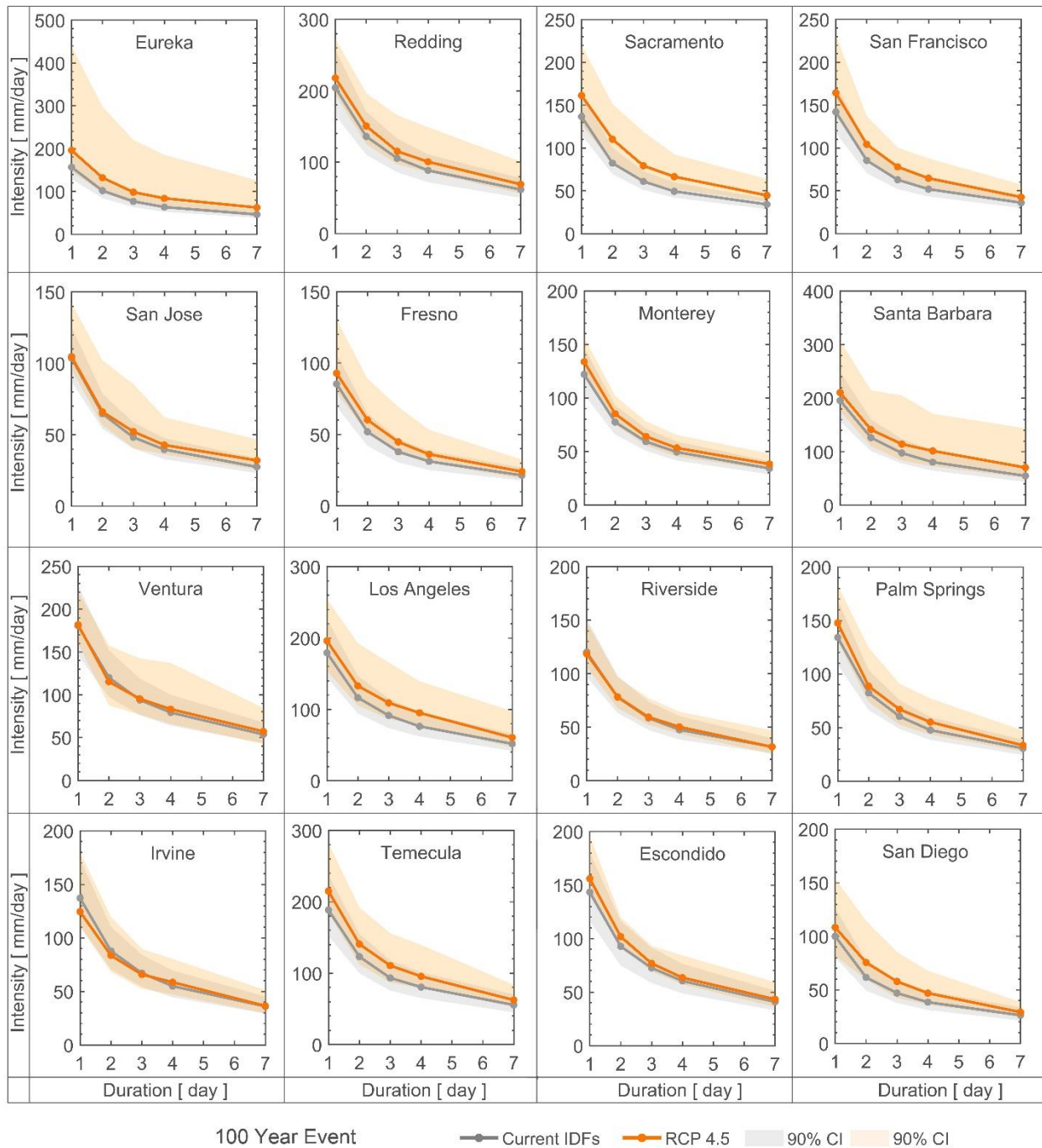
Figure 2: Change in 50-Year Intensity-Duration-Frequency Curves Under RCP4.5



Comparison between the current (grey lines) and future climate (orange lines) 50-yr Intensity-Duration-Frequency (IDF) curves (RCP4.5), along with 90 percent confidence intervals (after Ragno et al., 2018).

Source: University of California, Irvine and University of California, Los Angeles.

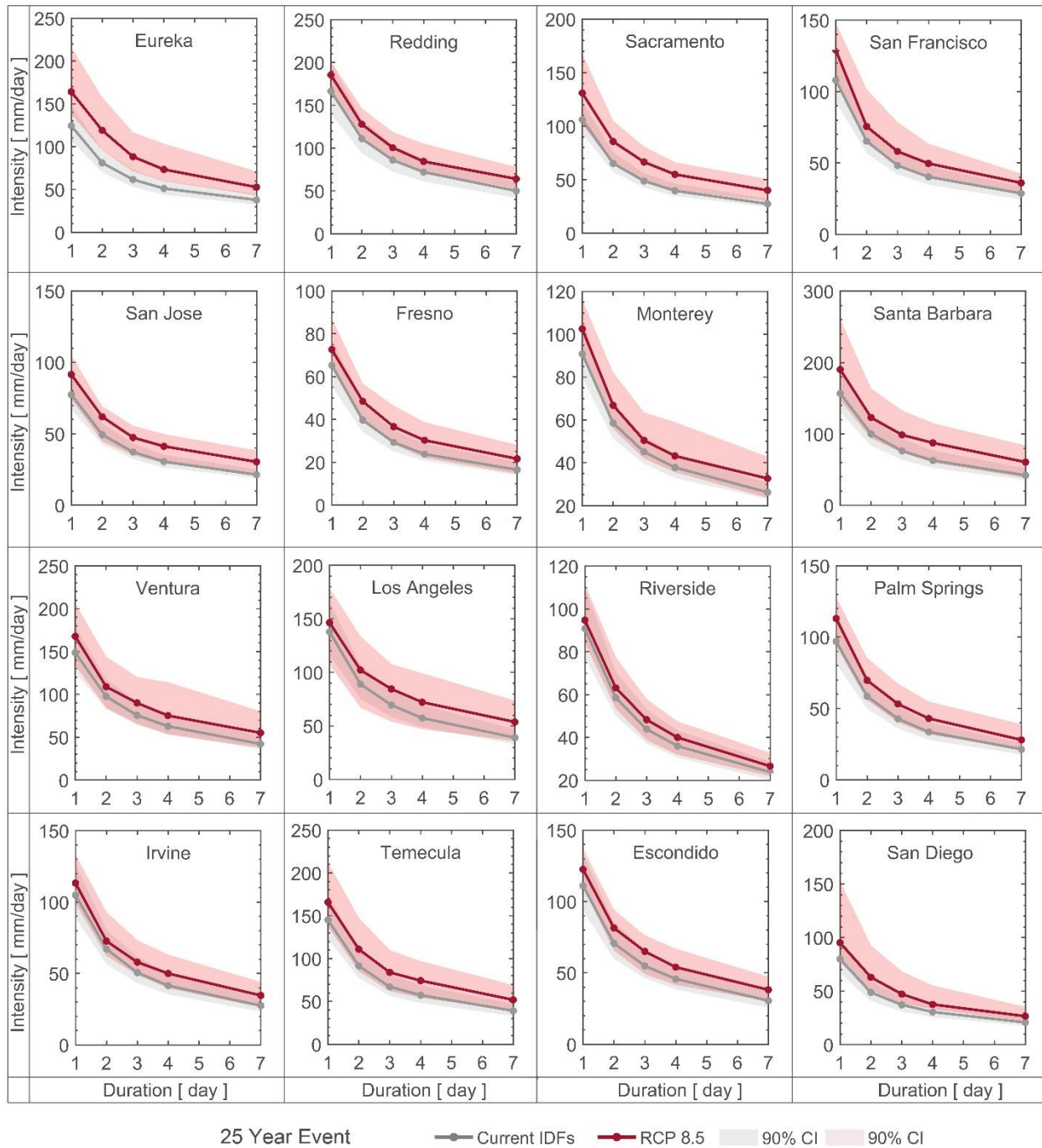
Figure 3: Change in 100-Year Intensity-Duration-Frequency Curves Under RCP4.5



Comparison between the current (grey lines) and future climate (orange lines) 100-yr Intensity-Duration-Frequency (IDF) curves (RCP4.5), along with 90 percent confidence intervals (after Ragno et al., 2018).

Source: University of California, Irvine and University of California, Los Angeles.

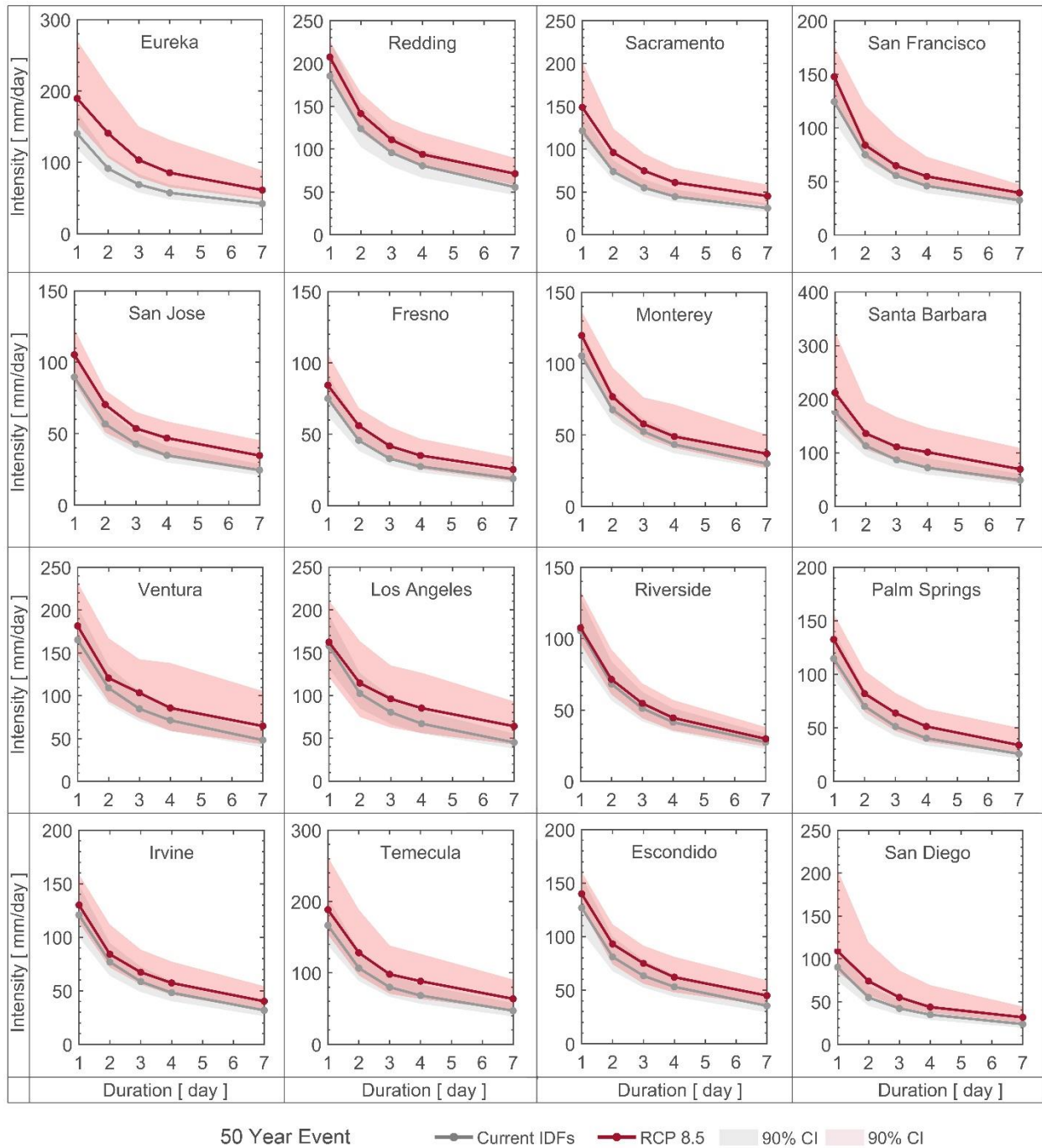
Figure 4: Change in 25-Year Intensity-Duration-Frequency Curves Under RCP8.5



Comparison between the current (grey lines) and future climate (orange lines) 25-yr Intensity-Duration-Frequency (IDF) curves (RCP8.5), along with 90 percent confidence intervals (after Ragno et al., 2018).

Source: University of California, Irvine and University of California, Los Angeles.

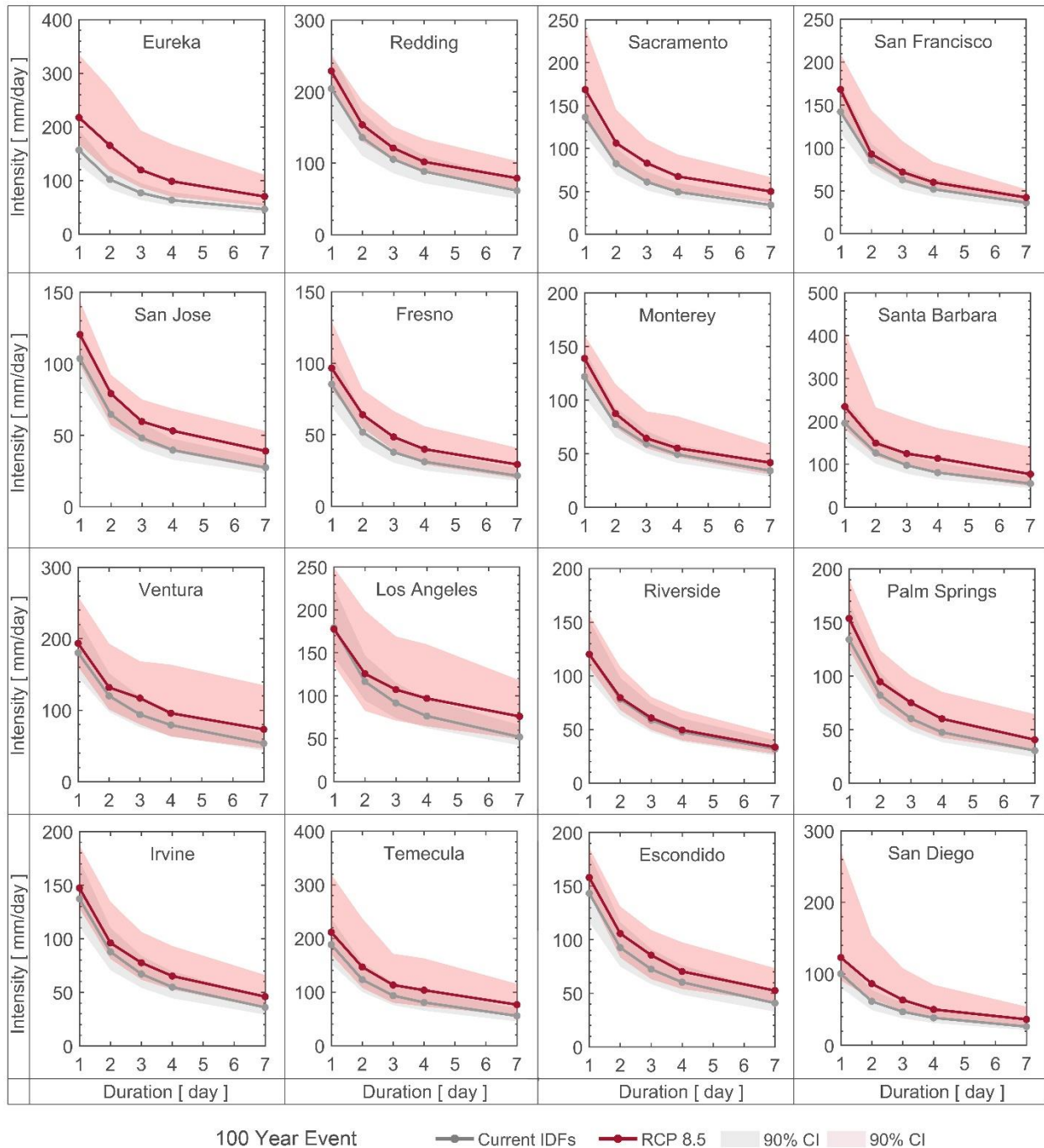
Figure 5: Change in 50-Year Intensity-Duration-Frequency Curves Under RCP8.5



Comparison between the current (grey lines) and future climate (orange lines) 50-yr Intensity-Duration-Frequency (IDF) curves (RCP8.5), along with 90 percent confidence intervals (after Ragno et al., 2018).

Source: University of California, Irvine and University of California, Los Angeles.

Figure 6: Change in 100-Year Intensity-Duration-Frequency Curves Under RCP8.5



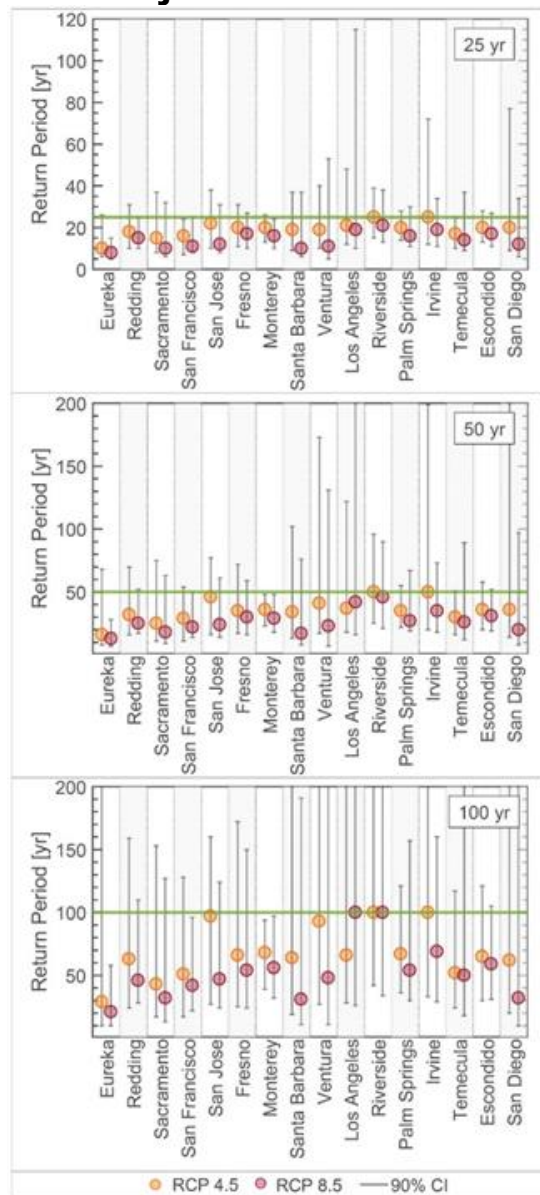
Comparison between the current (grey lines) and future climate (orange lines) 100-yr Intensity-Duration-Frequency (IDF) curves (RCP8.5), along with 90 percent confidence intervals (after Ragno et al., 2018).

Source: University of California, Irvine and University of California, Los Angeles.

After investigating the change in extreme event intensity for a fixed return period, the research team now explore the changes in frequency of extreme events with 1-day duration for a given event magnitude. Specifically, the research team choose the intensity of three baseline events corresponding to 25-, 50- and 100-year events (retrieved from current NOAA IDF curves) to estimate their expected recurrence intervals in the future, along with their confidence intervals. Figure 7 illustrates the return periods expected in the future of the

baseline events (dots), along with their 90 percent confidence intervals (gray lines). The results show that the extreme events - such as those that are presently expected to occur every 50, or 100 years - will likely become more frequent. For example, climate model simulations project that the frequency of a 50-year event in the future will double in San Diego, and Santa Barbara under RCP8.5. The same behavior can be observed in northern California, in San Jose and San Francisco (Figure 7). The high uncertainties in the estimated values reflect the intermodal variability in climate model projections (here, four different climate models) and parameter fitting uncertainties.

Figure 7: Change in Extreme Precipitation Return Periods for Major Cities in California



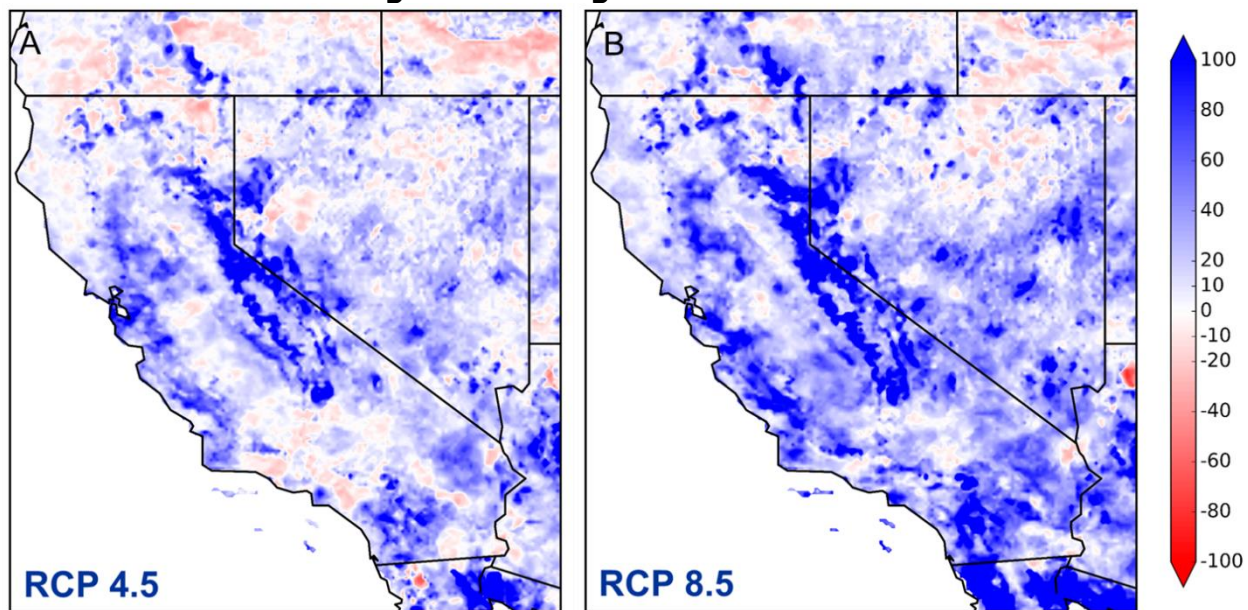
Return periods of future events (orange and red dots), historically associated with return periods of 25-, 50-, and 100-year in California (green lines). Panels a, b, and c show the projected return periods considering two future scenarios: RCP 4.5 (orange dots) and RCP 8.5 (red dots) along with their 90 percent confidence interval (gray lines; after Ragno et al., 2018).

Source: University of California, Irvine and University of California, Los Angeles.

3.1.2 Changes in Inland Flood Hazard

Projected changes in the intensity and frequency of extreme precipitation that have been shown in the previews section (3.1.1) are anticipated to result in possible future changes in the risk posed by flooding hazards to infrastructure. Therefore, the researchers analyze the percent change in the magnitude of 100-year flow in the projected period relative to the historical period spatially distributed over California using gridded simulated runoff (Figure 8). The research team use this metric as a proxy to investigate the direction of changes in the flood hazard in the future. Overall, there is a significantly higher number of pixels showing at least a slight increase in the multi-model median of the 100-year flow in the projection period. Note that relative change is computed for each model separately, and then median of all models for each grid is calculated. This reveals that the direction of change in the frequency of high flow events, given the uncertainty, are likely to increase over the study area. This increasing pattern is expectedly more pronounced under the RCP8.5 (Figure 8B). The most noticeable change is the increasing pattern in peak runoff over the eastern side of their study domain extended over the Sierra Nevada mountain range. This finding is in agreement with Das et al. (2011), which projected an increasing trend in the magnitude and frequency of 3-day flood over the Sierra Nevada region.

Figure 8: Change in Flood Hazard

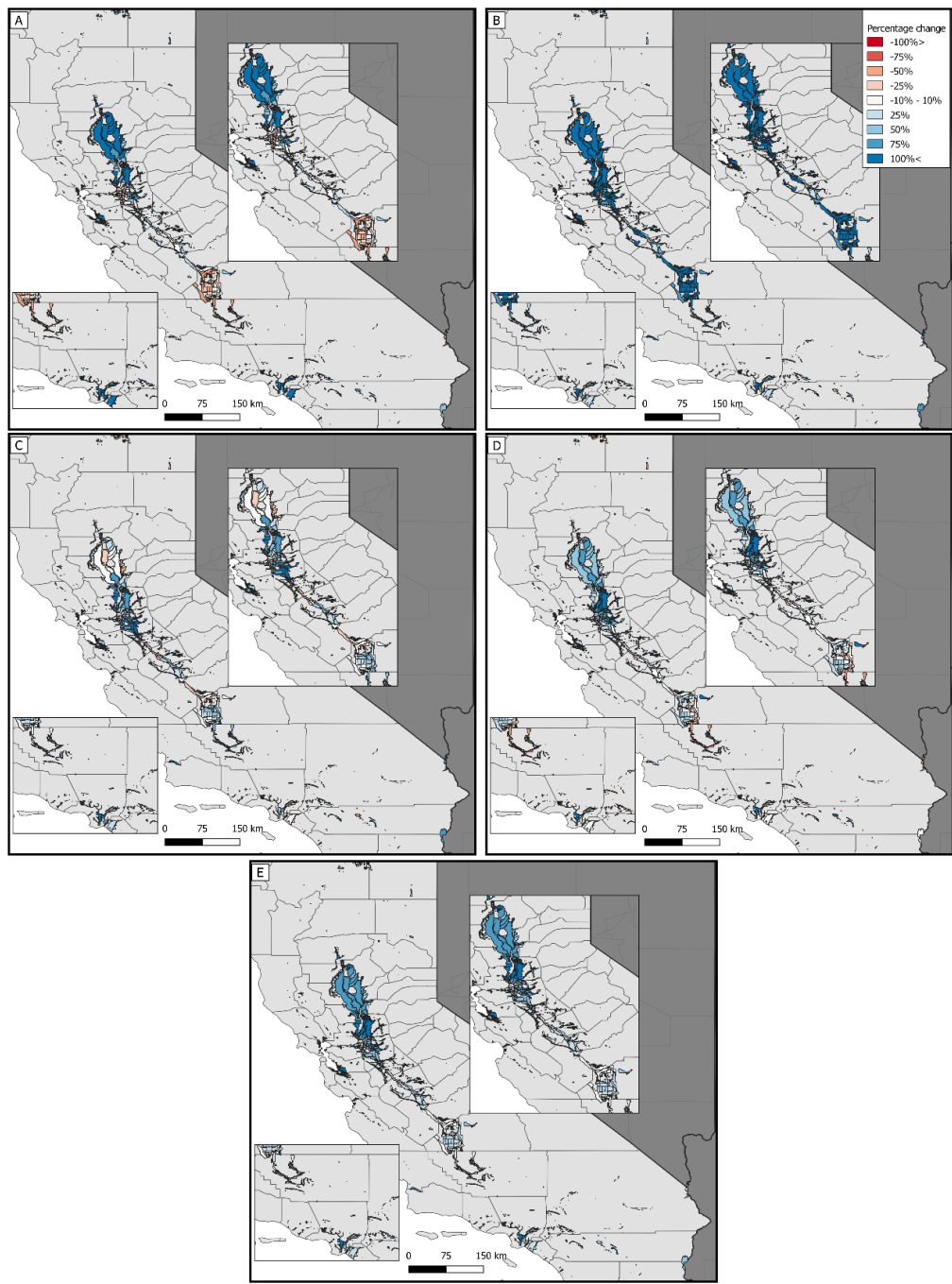


Percentage changes between multi-model median of gridded simulated runoff associated with projected 100-year flood level under RCP4.5 (A) and RCP8.5 (B) relative to historical period (1950-2005) over northern and central California. The blue (red) color reveals locations that magnitude of 100-year flood projected to increase (decrease) in the future. The color bar shows the percentage difference [%] in the 100-year flood level in the projection period relative to the historical period (after Mallakpour et al. (2019)).

Source: University of California, Irvine and University of California, Los Angeles.

Next, the researchers investigate how flood hazard will possibly change for the leveed regions under a warming climate. Figures 9 and 10 show the percent change in the magnitude of a 100-year flow in the future relative to the baseline period as a proxy to examine the direction of changes in the flood hazard under RCP 4.5 and 8.5, respectively.

Figure 9: Change in Flood Hazard Over Leveed Region of California Under RCP4.5



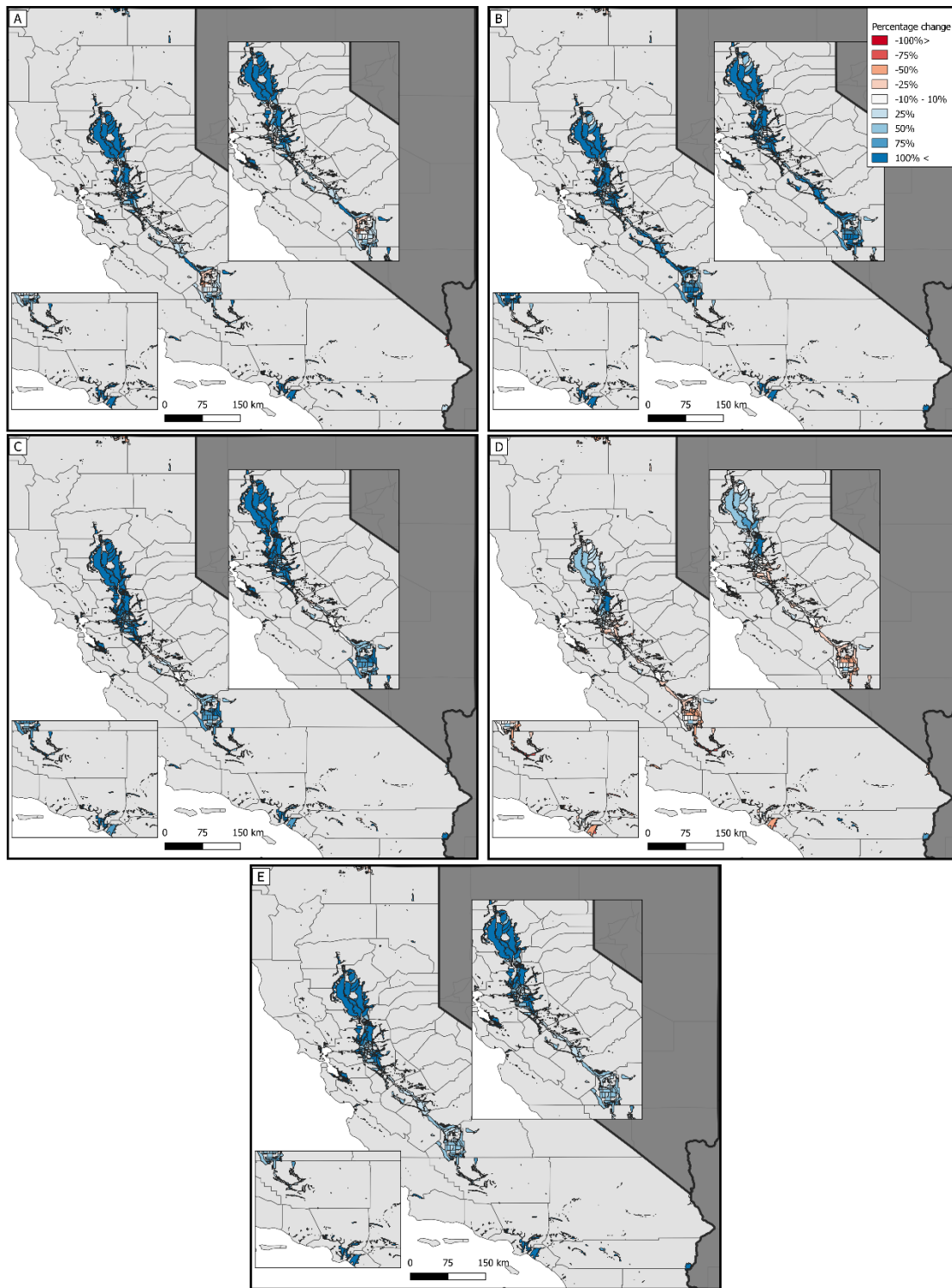
Percentage changes in the magnitude of 100-year flow in the projected period (2020-2099) relative to the baseline period (1950-2005) for (A) CanESM2, (B) CNRM-CM5, (C) HadGEM2-ES, (D) MIROC5, and (E) ensemble median of aforementioned climate models under RCP4.5 over the leveed region of California. The color bar displays the percentage change [%] in the magnitude of 100-year flow where the blue (red) color shows levee systems that magnitude of the 100-year flow expected to increase (decrease) under a warming climate in the future. Inset maps in each panel show the zoomed in map of levee systems of California's Central Valley (right inset map) and levees over Southern California (left inset map).

Source: University of California, Irvine and University of California, Los Angeles.

The spatially distributed results show that there is a significantly higher number of levee systems that exhibit an increase in the magnitude of 100-year flow in the projection period relative to the historical period. The CanESM2 climate model, which is known to be associated with an average climate condition for the state of California in the future, shows that other than several levee systems in the central and southern parts of Central Valley, all the levee systems will likely experience a higher flooding hazard (Figure 9A). The CNRM-CM5 climate model that represents a cool and wet condition over California in the future shows the highest increase in the magnitude of 100-year flow relative to the results from other models (Figure 9B). Under this climate model, almost all of the levee systems display an increasing pattern in the flood hazard in the future. Figure 9C shows the result for HadGEM2-ES, a model that represents a warmer and dryer future over California, where relative to other climate models higher number of levee systems display a decreasing pattern in the magnitude of 100-year flow in the future. However, even with this climate model, a significant number of levee systems are projected to have at least a slight increase in the magnitude of 100-year flow. The results for projected change in the magnitude of 100-year flow for MIROC5 climate model (representing a complement climate condition) reveal that the levee systems over northern and central parts of Central Valley show an increasing pattern in flood hazard in the future while southern regions show a slightly decreasing pattern in the magnitude of 100-year flow (Figure 9D). Figure 9E is summarizing the projected change in the flood hazard over the leveed area of California based on the median of the four climate models in this study. The results depict that the direction of change in the frequency of high runoff events is likely toward increasing over the leveed area of California. Note that the increasing pattern is more marked under the RCP8.5 (Figure 10) for all the cases. In general, the most evident change is the increasing pattern in the magnitude of 100-year runoff over the northern region of Central Valley including Butte, Glenn, Yuba, Sutter, Sacramento, and San Joaquin Counties. These counties can experience up to threefold increase in the flood hazard relative to the historical period. In general, total precipitation amounts in northern California are higher than in southern California (Jones, 2000).

There are several possible explanations for this projected change in the magnitude of the 100-year flow. Studies that investigate possible flood generating mechanisms have indicated that most of the flooding events in California, historically, occurred during the winter season due to atmospheric river systems and in spring due to snowmelt (e.g., Berghuijs et al., 2014; Das et al., 2011; Mallakpour et al., 2018; Villarini, 2016). However, climate warming is changing the hydrology of California, so that temperature in winter and spring is likely to increase, resulting in earlier snowmelt, decline in snowpack, and more precipitation falling as rain and less falling as snow (Das et al., 2011; Dettinger and Cayan, 1995; Hidalgo et al., 2009). Therefore, while the annual average daily discharge is projected to remain almost similar to the historical period, magnitude of the annual maximum discharge is projected to increase (Mallakpour et al., 2018).

Figure 10: Change in Flood Hazard Over Leveed Region of California Under RCP8.5



Percentage changes in the magnitude of 100-year flow in the projected period (2020-2099) relative to the baseline period (1950-2005) for (A) CanESM2, (B) CNRM-CM5, (C) HadGEM2-ES, (D) MIROC5, and (E) ensemble median of aforementioned climate models under RCP8.5 over the leveed region of California. The color bar displays the percentage change [%] in the magnitude of 100-year flow where the blue (red) color shows levee systems that magnitude of the 100-year flow expected to increase (decrease) under a warming climate in the future. Inset maps in each panel show the zoomed in map of levee systems of California's Central Valley (right inset map) and levees over Southern California (left inset map).

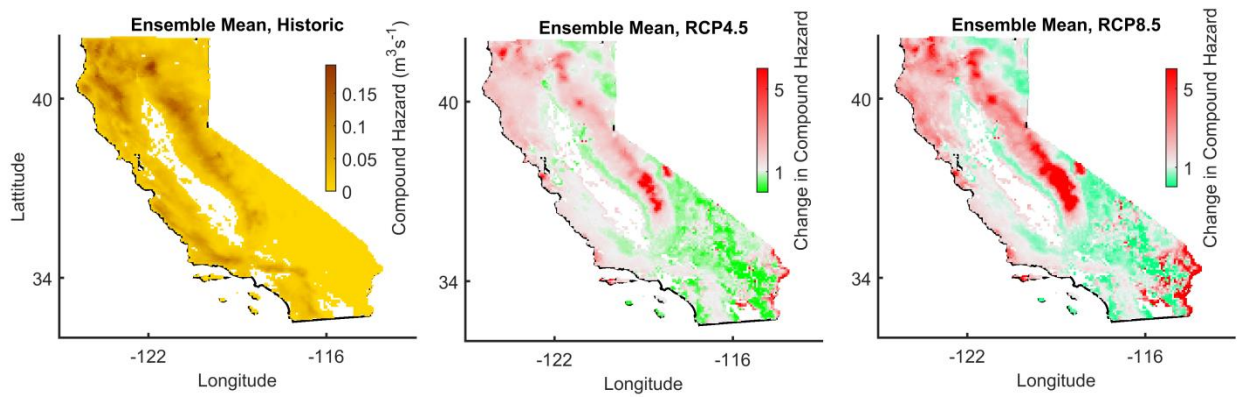
Source: University of California, Irvine and University of California, Los Angeles.

Recently, Li et al. (2017) also have shown that the future contribution of snow to runoff is likely to decline in California. Thus, most of the changes the researchers projected in flood peaks may be attributed to earlier snowmelt, rain-on-snow events and more precipitation falling as rain, resulting in possible higher peak flow events during winter and early spring. This becomes even more important given the majority of levee breaks over California historically happened during November to June period that emphasizes the important role of winter storms (Florsheim and Dettinger, 2015, 2007). For instance, Florsheim and Dettinger (2015) identified wintertime AR precipitation events as the main reason for levee failures in California's Central Valley. Impacts of the projected changes in the magnitude of 100-year flow over the Sierra Nevada bears important implications for water management in California as this region is the main source of water for California.

3.1.3 Changes in Inland Flood Hazard

Floods and debris flows can result in a significant threat to energy infrastructure, especially when extreme rain falls over burned areas. In section 3.1.1 the researchers have projected that many major cities in California will suffer by more frequent extreme precipitation events. It should also recognize that that climate extremes can result in compounding effects when occurring simultaneously or in a cascading fashion, which may lead to more frequent and more severe hazards than otherwise expected (AghaKouchak et al., 2018). Figure 13 shows the change in expected compound wildfire and intense precipitation events in the future (2047 – 2099) relative to the past (1953 – 2005). The shading on the left panel (Historic) shows the intensity of estimated compound hazard over the historic period. The intensity of compound hazards is generally larger in the North compared to the Southern California. The north part of California is the region of this state where the researchers have shown that they anticipate the highest change in both flooding and heavy precipitation (sections 3.1.1 and 3.1.2). Therefore, this difference can be attributed to the significant spatial variability of precipitation across the State. The total rainfall amounts received during a typical winter season in northern California could be 2 to 4 times higher than the southern California (Jones, 2000). This yields large differences in vegetation pattern and so the wildfire dynamics that combined with precipitation variability explains the aforementioned spatial pattern in compound hazard intensity. Another detectable pattern is the difference between coastal watersheds and mountain ranges with low lying inland watersheds. Indeed, out of various known bioregions in California (Lenihan et al., 2003), forests (Northwest, Cascade Ranges, and Sierra Nevada) and coastal shrublands/woodlands (Central Western and Southwestern) are experiencing more intense compound hazards. In the future, forests are expected to experience even more severe compound hazards (up to 6X), with south part of Sierra Nevada experiencing the highest rise under both RCPs 4.5 and 8.5. Coastal shrublands/woodlands though expect to experience either low-to-moderate rise (i.e. Central Western) or no-significant rise (i.e. Southwestern). Interestingly, East of Sierra Nevada, South of Mojave Desert and Sonoran Desert that in the current situation show relatively low potential for compound hazards are projected to experience significantly more intense compound events in the future. This may stem from the potential for land cover change due to change in climatic patterns.

Figure 13: Change in Compound Hazard

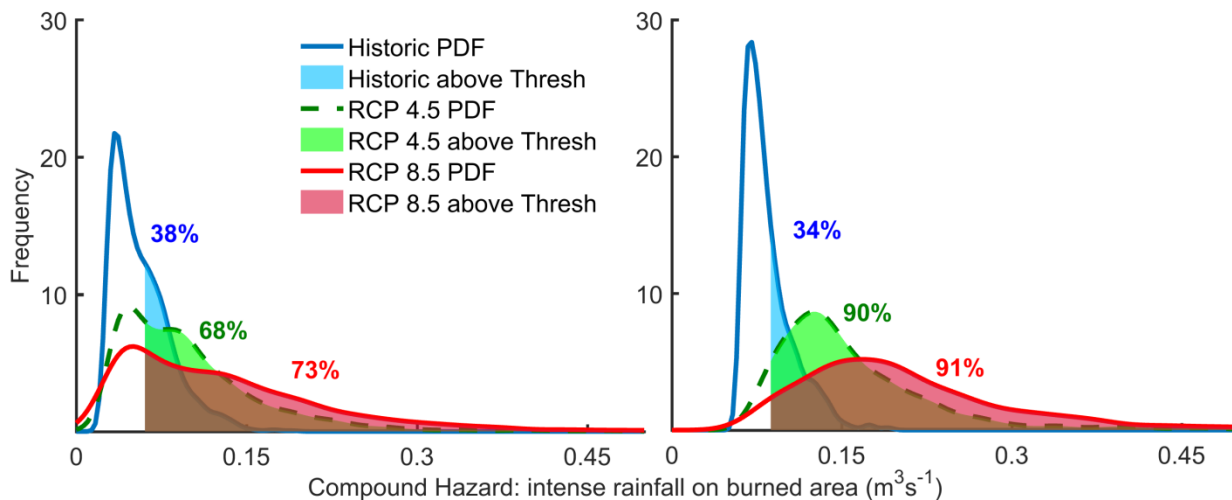


Relative change in compound hazard (burned area x precipitation intensity) in the future (2047 – 2099) compared with the past (1953 – 2005) based on ensemble mean of climate models. Red (green) means increased (decreased) likelihood of compound hazards.

Source: University of California, Irvine and University of California, Los Angeles.

Figure 14 shows the temporal evolution in the distribution of compound hazard intensities. The left panel shows the empirical probability distribution function (PDF) of median values.

Figure 14: Compound Hazards Density Distribution



Distribution of median and 90th quantile of the ensemble average estimates of compound hazards. The shaded areas represent the exceedance likelihood with respect to the mean of the historic distribution.

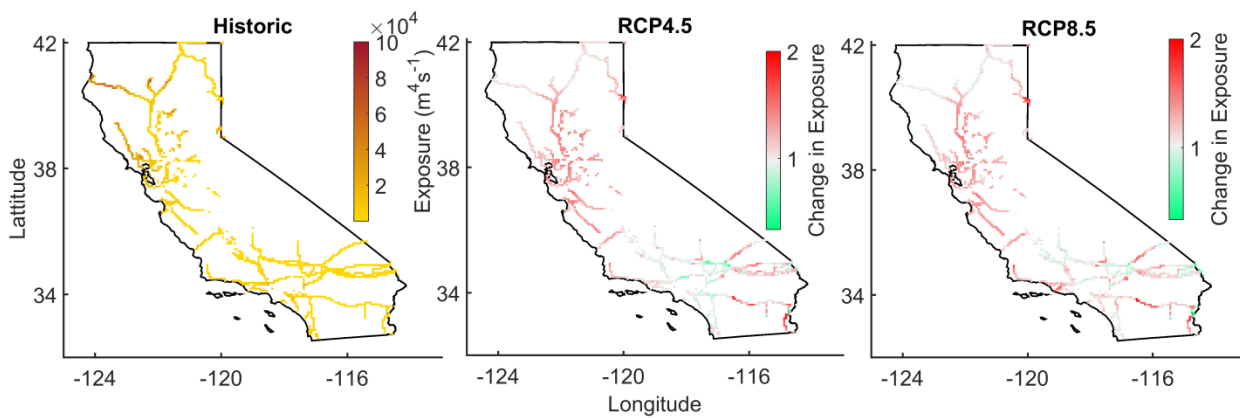
Source: University of California, Irvine and University of California, Los Angeles.

To obtain this PDF, first the ensemble mean of estimated compound hazards from the four studied GCMs are calculated, and then the distribution of median of estimated hazards for the pixels all around the California is calculated. Then, the mean of historic values is considered as a threshold to calculate the exceedance likelihood above the given threshold. Indeed, the shaded area (and the percentage associated with that) represent the likelihood that historic mean to be surpassed by above-average events. The right panel shows the empirical PDFs of 90th quantiles. The distributions of compound hazards are expected to be significantly different in the future relative to past. While, in the past there has been 38 percent chance that the historic mean of median values to be exceeded, this likelihood is projected to double in the future under both RCPs 4.5 (68%) and 8.5 (73%). The difference between distributions

becomes even more significant on the extreme events. The likelihood that mean of 90th quantiles to be exceeded in the future is almost three times higher than the past (34%), under both RCPs 4.5 (90%) and 8.5 (91%). The statistics of compound hazards are ought to be totally different, and if this non-stationarity would not be taken into account, hazards may not be appropriately characterized in the future (Cheng et al., 2014; Ragno et al., 2018).

Analysis of exposure of energy infrastructure to the projected hazards highlighted in the previews sections may provide a better understanding of the expected change in risk towards these infrastructure systems in the future relative to past. For this purpose, the researchers calculate the length of pipelines within each pixel with runoff and wildfire estimates. Then the product of hazard intensity and pipeline length in each pixel provides an estimate of the exposure of the natural gas pipelines to these hazard drivers. Figures 15 and 16 show the results for the ensemble mean estimates.

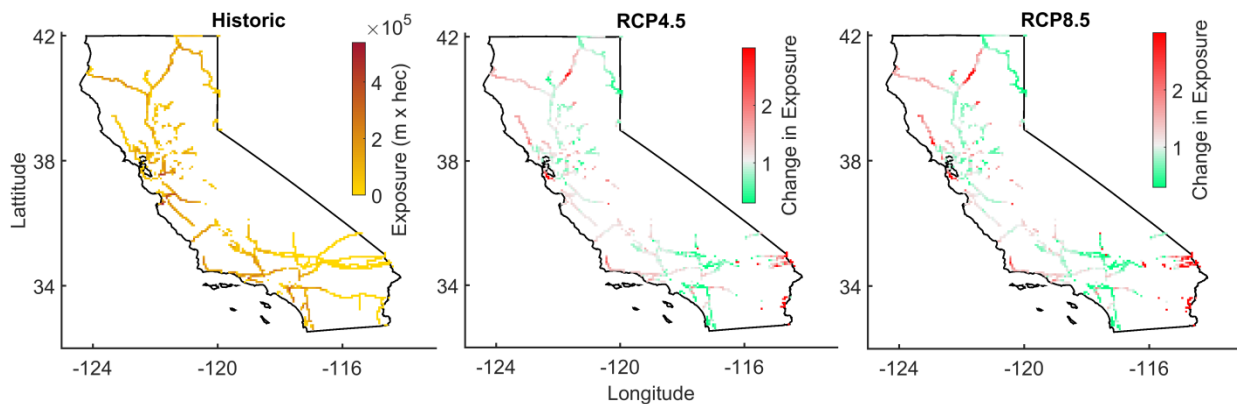
Figure 15: Distribution Natural Gas Pipeline Runoff Exposure



Natural gas pipeline exposure to runoff in the past (left; 1953 – 2005), and its expected change in the future (2047-2099) under RCPs 4.5 (middle) and 8.5 (right). Red (green) means increased (decreased) exposure to runoff.

Source: University of California, Irvine and University of California, Los Angeles.

Figure 16: Natural Gas Pipeline Wildfire Exposure



Natural gas pipeline exposure to wildfire in the past (left; 1953 – 2005), and its expected change in the future (2047-2099) under RCPs 4.5 (middle) and 8.5 (right). Red (green) means increased (decreased) exposure to wildfire.

Source: University of California, Irvine and University of California, Los Angeles.

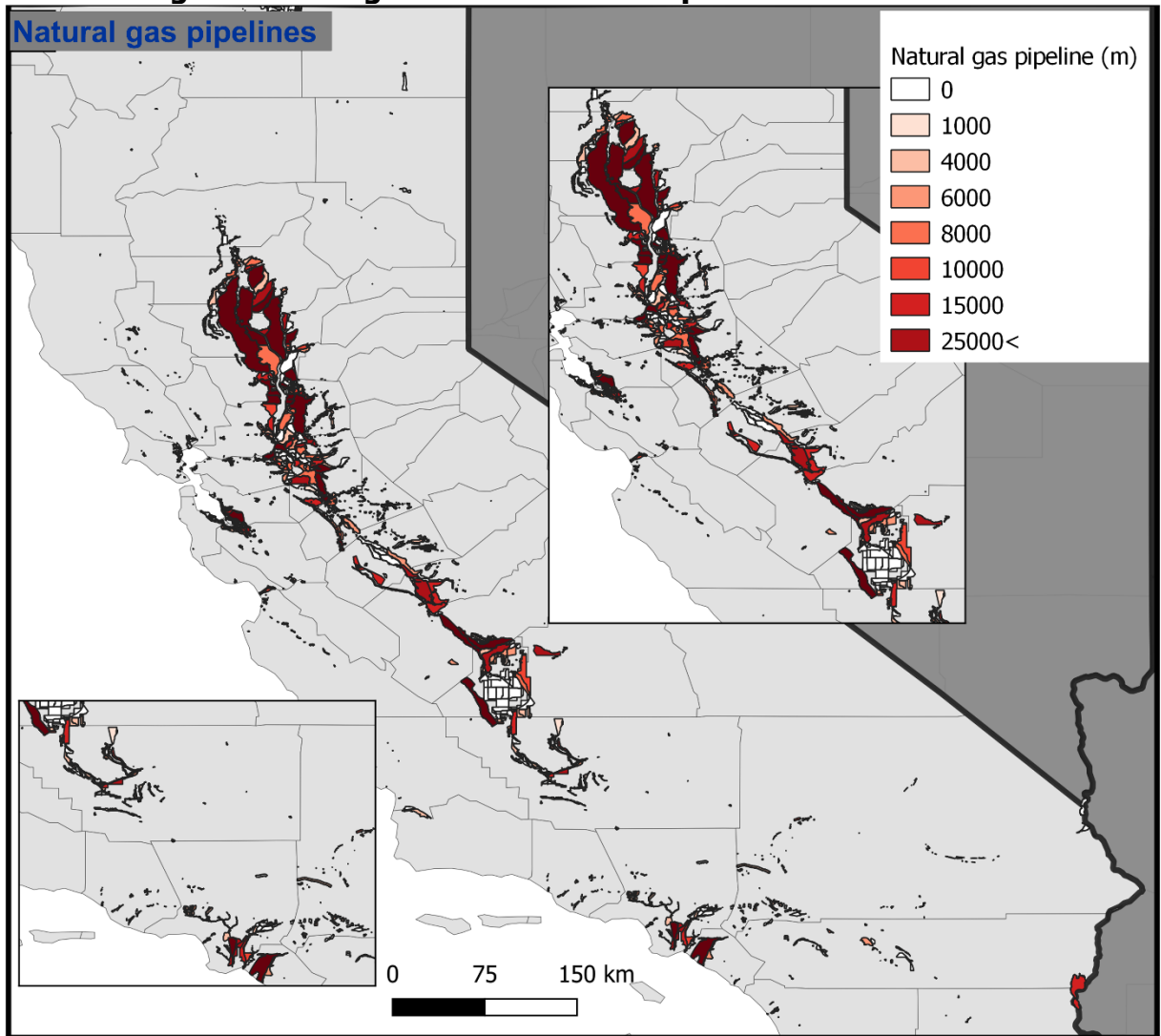
3.1.4 Change in Exposure of Gas Pipelines to Climate Hazard

The estimated exposure of pipelines to runoff is significantly higher over the northern parts of California. Since their analysis shows no notable difference between average lengths of pipelines in each pixel between south and north, the researchers conclude that the exposure difference between northern and southern California to be attributed to variation in received precipitation across California (Jones, 2000). The exposures have been highest in the Northwest and lowest in the deserts of the south (e.g. Mojave, and Sonoran) as expected from their flooding and precipitation analyses. In the future, however, the infrastructure in the north of Central Valley, Modoc Plateau, and the San Francisco Bay area along with parts of the South (e.g. Southwestern, Mojave Desert and Sonoran Desert) will experience a raised (2+ times) exposure to runoff. Should be noted that this raise is estimated based on the assumption that no flood mitigation measures will be implemented and thus (if available) the effects of runoff control projects (i.e. storm water drainage systems implementation) must be taken into account for more accurate projections.

The exposure to wildfire is somehow different and is expected to vary differently over time (Figure 16). The exposure is relatively higher (up to three times) in coastal regions (e.g. Northwest, Central Western and Southwestern) and cascade ranges and relatively low in the deserts of the South. While expected to rise in Northwest, Cascade ranges, and the east of Mojave and Sonoran deserts, it shows no significant change or tends to decrease in the future in the rest of State. A considerable decreasing trend (down to one-third) is expected in Modoc Plateau, the north of Central Valley and the Bay area, wets of Mojave and Sonoran deserts and the Southwestern regions.

In order to identify which levee system is more susceptible to projected changes in the flood hazard in term of energy infrastructure systems, the researchers first quantify the length of natural gas pipelines (Figure 17) and number of power plants (Figure 18) that are located behind each of California's levee systems using the National Levee Database. Note that the energy infrastructure dataset used in this study does not contain information about the elevation of pipelines and location of the power plants. Therefore, their exposure analysis could either refer to complete or partial exposure of pipeline and power plant facilities and their supporting structures. Figure 17 displays the length of natural gas pipelines located behind each of the levee systems across California, where the Sacramento River West Bank levee system (~ 183 km) has the highest length of pipelines. For Southern California, exposure of pipelines is higher in the levee systems that are closer to the coast. The highest length of natural gas pipelines in this region is located in the Santa Ana River 1 levee system (~ 54 km) in Orange County. For Los Angeles County, the Los Angeles River/Compton Creek 2 levee system (~40 km) has the highest length of natural gas pipelines. Figure 18 displays the number of power plant protected by each of the levee systems. Here, MA-09 of City of Sacramento and Santa Ana River 1 levee systems (with 10 power plants) followed by Feather River west bank - Sutter Bypass east bank (with 9 power plants) have the highest number of power plants.

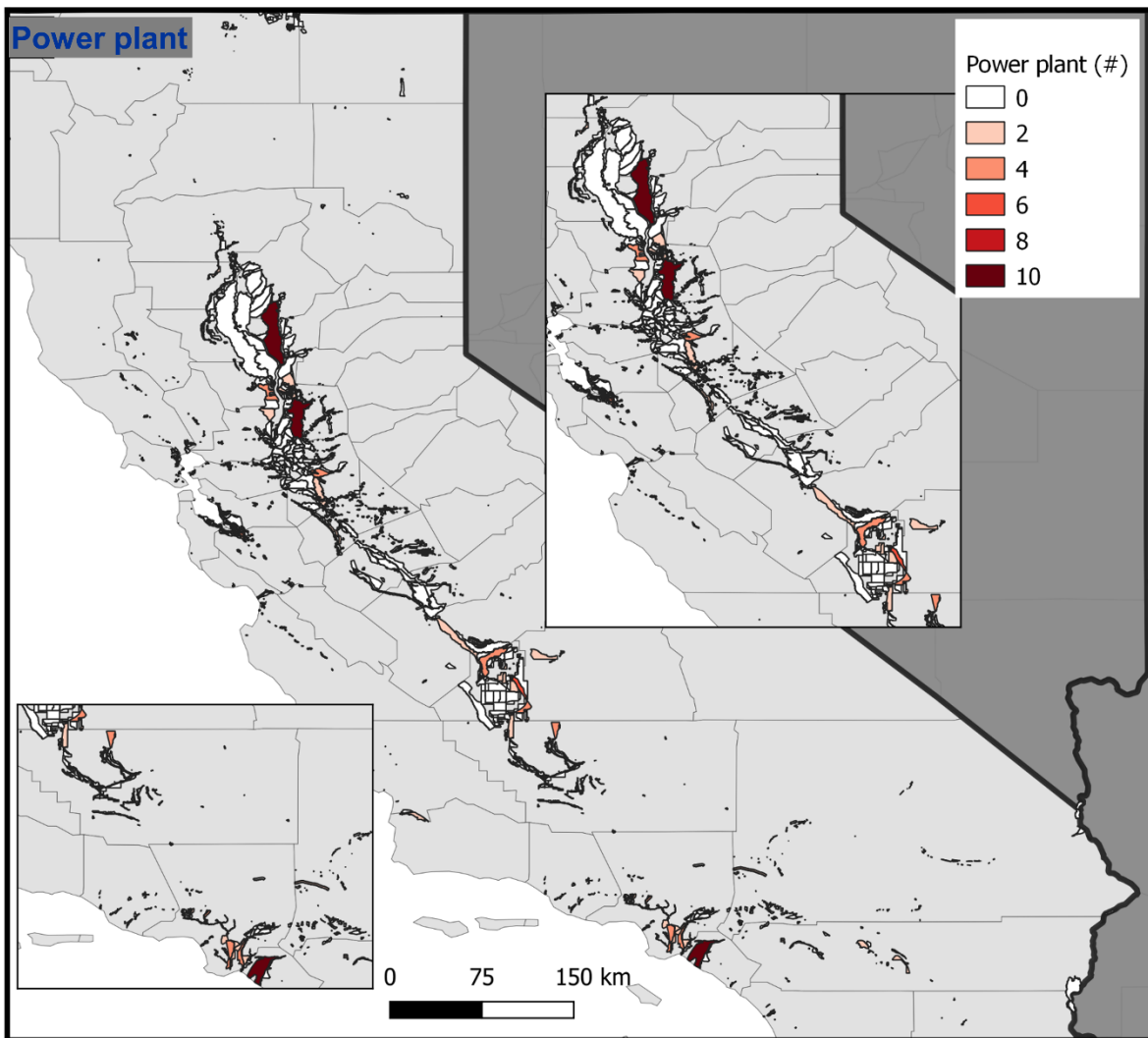
Figure 17: Length of Natural Gas Pipeline in Leveed Area



Map showing the length of natural gas pipelines that are protected by the levee systems over California. Inset maps in each panel show the zoomed in map of levee systems of California's Central Valley (right inset map) and levees over Southern California (left inset map). Darker red color shows a higher length of the infrastructure is protected by a levee system.

Source: University of California, Irvine and University of California, Los Angeles.

Figure 18: Number of Power Plants in Leveed Area



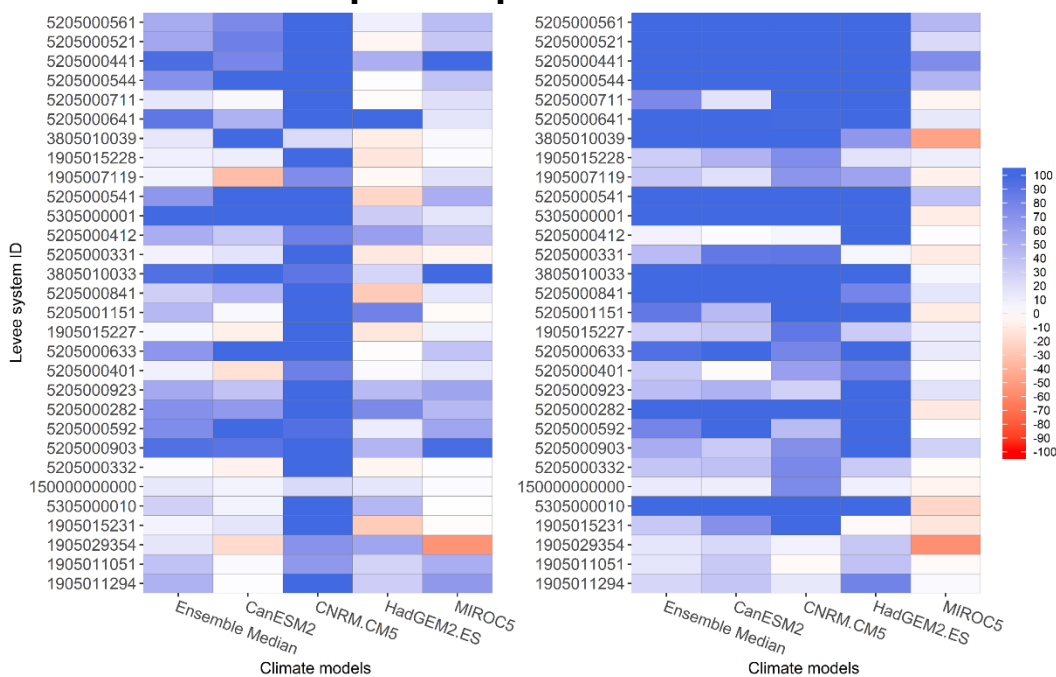
Map showing the number of power plants that are protected by the levee systems over California. Inset maps in each panel show the zoomed in map of levee systems of California's Central Valley (right inset map) and levees over Southern California (left inset map). Darker red color shows a higher length of the infrastructure is protected by a levee system.

Source: University of California, Irvine and University of California, Los Angeles.

Next, the researchers provide a detailed analysis of which of the levee systems, given the associated uncertainties, are more susceptible to exposure of gas pipelines to the projected changes in the flood hazards in the future (Figure 19 and Table 1). For the sake of brevity, here the research team present results for the thirty levee systems that encompass the highest length of natural gas pipelines. In figure 19, each cell represents the percentage change in the magnitude of 100 year runoff as a proxy to evaluate future changes in the flood hazard for each levee system based on the aforementioned four climate models and an ensemble median of the climate models. Here, the multi-model median values summarize the possible values of the magnitude and direction of changes in the flood hazard for the future. Also, the magnitudes and direction for the four climate models represent the possible range of uncertainties associated with the use of different climate models. By using the information provided in Figure 19 and Table 1 the research team can identify that 5 of the thirty levees that protect the highest length of the natural gas pipeline show at least 80 percent increase in

ensemble median of the flood hazard under RCP 4.8. These numbers increase to 15 levee systems under RCP 8.5. As expected, under the RCP 8.5 scenario increase in the flood hazard are more marked and larger on average. As expected from their precipitation and flood analyses the majority of these levee systems are located in northern California. The information provided here can be used by water managers to prioritize resources allocated for rebuilding and maintaining the assets behind the levee systems based on possible changes in the flooding hazard and exposure of the critical infrastructure to the projected change in flood hazard in a changing climate. For example, the highest length of the natural gas pipeline is located within Sacramento River West Bank (System ID=5205000561) followed by Feather River west bank - Sutter Bypass east bank (System ID=5205000521) system that both of these systems show a relatively small increase in the flood hazard under RCP 4.5. However, the next levee system with the highest length of the natural gas pipeline is MA 09 - City of Sacramento (System ID=5205000441), which is relatively more susceptible to change in flood hazard under RCP 4.5. Flood-prone areas can experience additional loss of lives because of disruptions in power outages, which impedes rescue operations and medical assistance. Based on these results, energy and water managers can invest on emergency preparedness plans to increase resiliency and improve evacuation effectiveness that can lead to a reduction in potential life loss during a possible levee incident (Ludy and Kondolf, 2012), by starting from the levee systems that show a higher relative change in the flood hazard for the future.

Figure 19: Natural Gas Pipeline Exposure to Flood Hazard in Leveed Area



Heatmaps showing possible changes in the flood hazard in the future relative to the baseline period for each of the levee systems based on different climate models used in this study. In each of the panels, the levee system are sorted descending based on the length of natural gas pipelines, where the topmost levee system on the Y-axis represents the levee system that has the highest length of natural gas pipelines it. Left panels depict the result for RCP 4.5 whereas the right panels represent future projections under RCP 8.5 scenario. The color bar shows the percentage change [%] in the magnitude of 100-year flow. The blue (red) color displays levee systems that the magnitude of the 100-year flow expected to increase (decrease) in the future. Refer to Table 1 for the name of the levee systems.

Source: University of California, Irvine and University of California, Los Angeles.

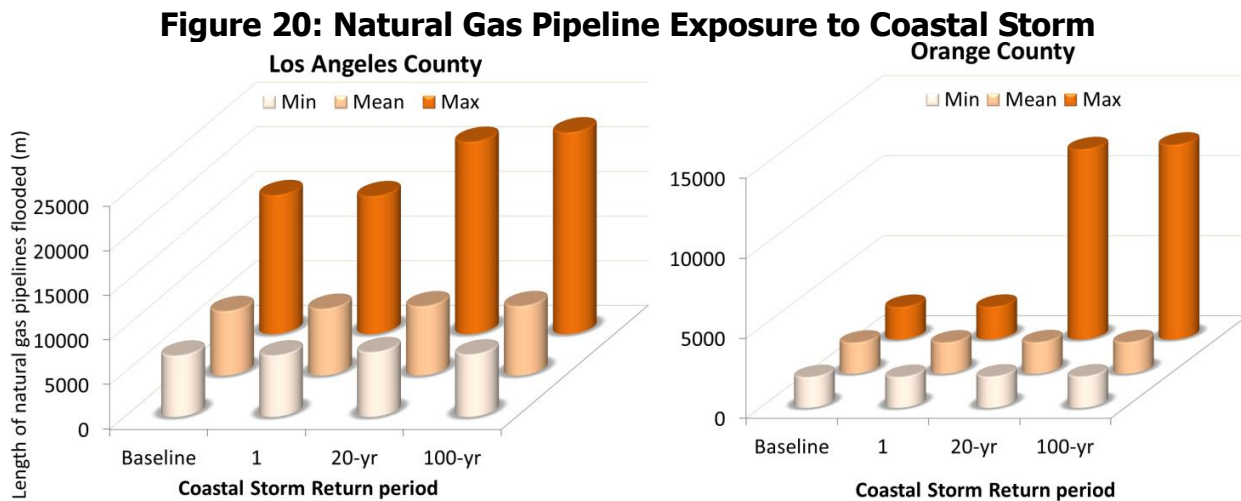
Table 1: Levee Systems That Protect Highest Length of Natural Gas Pipeline

System-Id	System Name	Length of Natural Gas Pipelines (km)
5205000561	Sacramento River west bank	183.22
5205000521	Feather River right bank - Sutter Bypass east bank	174.43
5205000441	MA 09 - City of Sacramento - American R left bank	145.78
5205000544	RD 0070 and RD 1660 - Sutter Basin North	79.92
5205000711	RD 0341 - Sherman Island	59.83
5205000641	Putah Cr Unit 1 - Yolo Bypass - Willow Slgh Unit 2	54.57
3805010039	Santa Ana River 1	53.33
1905015228	San Joaquin County Levee 30	51.34
1905007119	Kings County Levee 171	47.40
5205000541	Sacramento River East Levee - LD 3 Glenn County	46.93
5305000001	Alameda Creek - LB	42.68
5205000412	Cache Creek - RD 2035 - Willow Bypass	41.99
5205000331	Kings River - Units 6, 9, and 11 north and James Bypass	41.83
3805010033	Los Angeles River/Compton Creek 2	39.91
5205000841	RD 0784 - Plumas Lakes Basin	34.70
5205001151	RD 0017, 2094, 2096, 2075, 2064 - SJ River East	32.35
1905015227	San Joaquin County Levee 7	31.28
5205000633	MA 13 Unit 2 south - Cherokee Canal left bank	29.98
5205000401	Brannan-Andrus LMD - RD 0556	28.70
5205000923	RD 1000 - Natomas	28.66
5205000282	Mormon Slough-Calaveras left bank - RD 0404 - Duck Creek	27.94
5205000592	MA 05 Unit 2 - Butte Creek right bank	27.72
5205000903	West Sacramento	26.24
5205000332	Kings River - Units 1, 3, 5, 13, and 14	25.94
1.50005E+11	LSJLD-Units 3, 6, 18 - Eastside-Chowchilla Bypass	24.46
5305000010	Coyote Creek, Santa Clara - RB	23.22
1905015231	Merced County Levee 1	22.97
1905029354	Kern County Levee 53	21.79
1905011051	San Joaquin County Levee 56	20.84
1905011294	Sacramento County Levee 32	20.42

Source: University of California, Irvine and University of California, Los Angeles.

There is robust evidence of increased coastal flooding due to SLR and energy infrastructure are among the vulnerable coastal infrastructures (Moftakhari et al., 2017, 2015). Figure 20 shows the exposure of natural gas pipelines to coastal flooding under design storm events in the current system (e.g. with no SLR). Figure 20 includes a range of possible exposures from minimum to mean and maximum estimates, reflecting the underlying uncertainties. The sources of uncertainties include numerical model errors, digital elevation model uncertainty,

and vertical land motion. While in Los Angeles County the uncertainties could cover a relatively wide range of possibilities (i.e. from 7 kilometers (km) to 15.5 km) for frequent events (e.g. background and 1-yr storms), Orange County estimates are insensitive to the underlying uncertainties and ~2 km of pipeline is expected to be exposed to frequent coastal flooding. This is, however, different for infrequent storm events (e.g. 20-yr and 100-yr) and in these cases the exposure could be significantly higher in both counties. In Los Angeles County the exposure is estimated to be ~3X higher under maximum inundation scenario (21.5 – 22.5 km) compared to minimum and mean scenarios (7 – 7.7 km). In Orange County too, while the lower range of possibilities remains around 2 km of exposure, the upper range is estimated to be ~6 times higher (~12 km). Compatible with the findings of (Moftakhari et al., 2017), their results suggest coastal infrastructure in Orange County have some level of protection against high-to-mid frequency events, but the exposure exponentially increases after a threshold. This significant higher exposure rate suggests careful consideration of rare oceanic events in future design/development purposes and their associated risk factors (e.g. vulnerability) in Orange County.

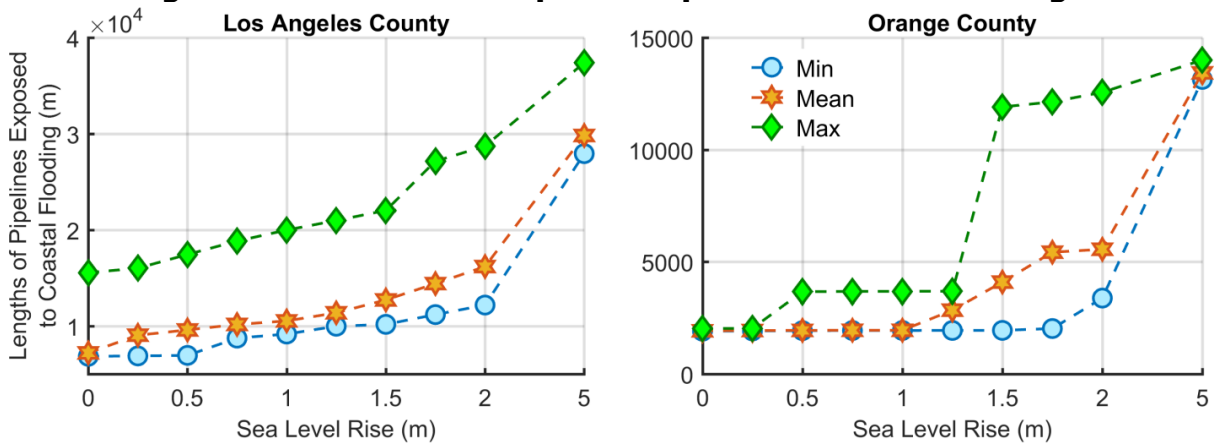


Exposure of natural gas pipelines in Los Angeles County (left) and Orange County (right) to coastal storms with design return periods in the current mean sea level.

Source: University of California, Irvine and University of California, Los Angeles.

At higher mean sea levels, energy infrastructure would be exposed to coastal flooding, even without significant coastal storm activities. Figure 21 shows how rates of exposure increase with sea level rise at the studied counties. While exposure in Los Angeles County gradually increases with SLR, Orange County exposure rates again show step changes at maximum probable flooding in 0.5 and 1.5 m of SLR scenarios. Without storm activity, 1 m of SLR increases both the minimum and maximum estimated exposure by ~30%. This means at some SLR levels tidal flooding becomes so severe in impacts, somehow comparable to current infrequent storm flooding. The maximum estimated exposure due to a 100-yr coastal storm, for example, with current mean sea level in both counties, could be achieved by astronomic tides on top of 1.5 m of SLR. This much of SLR, however less likely by the end of this century (0.7 – 2 percent probable under RCPs 2.6 and 8.5, respectively (State of California, 2018)), is 23 percent probable to be met or exceeded by 2050, and also projected to be reached by 2070 under H++ scenario (State of California, 2018).

Figure 21: Natural Gas Pipeline Exposure to Tidal Flooding



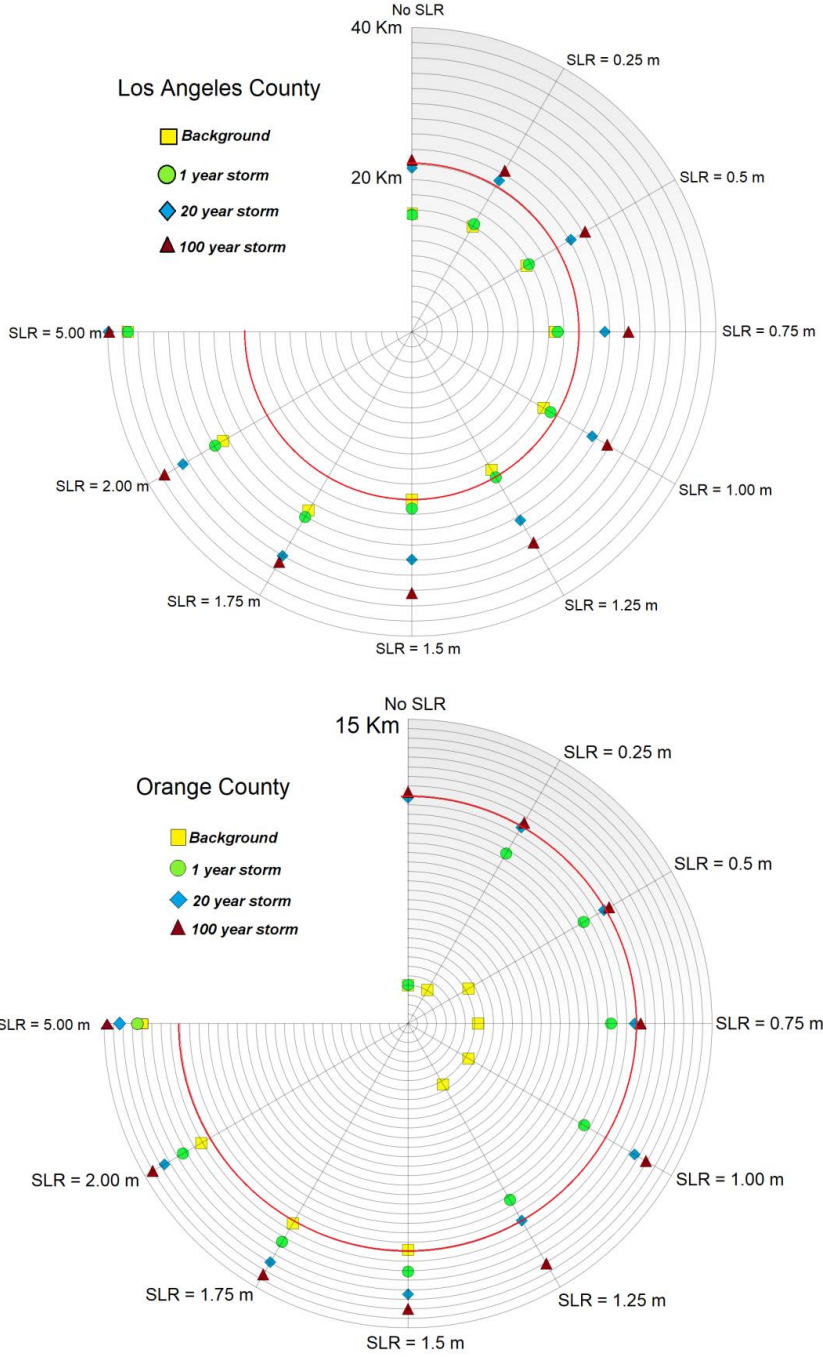
Exposure of natural gas pipelines to tidal flooding (no storm activity) in Los Angeles County (left) and Orange County (right) under different sea level rise scenarios.

Source: University of California, Irvine and University of California, Los Angeles.

In Los Angeles County, with the current mean sea level, up to 22 km of pipelines are exposed to coastal flooding, about 7 km of which exposed to regular tidal flooding (Figure 22). These rates, however, exponentially rise under the compounding impacts of SLR and coastal storm up to ~38 km when a 100-year coastal storm hits the coast on top of 2 m of SLR. The SLR both intensifies the extreme events and minor-moderate flood events. One and half meters of SLR make the estimated mean and maximum exposure to a 100-year coastal storm to rise by 92 percent and 52 percent, respectively. This rise, however, is not limited to extreme flooding. The same 1.5 m of SLR make the estimated mean and maximum exposure to tidal flooding (no coastal storm activity) to rise by 76 percent and 42 percent, respectively. This means the exposure rate to a 100-year coastal storm in the current system would be expected to become frequent tidal flooding with 1.5 of SLR.

In Orange County also, the compounding effects may exacerbate the risk of flooding (Figure 22). The maximum expected exposure to a 1-year coastal storm (with 99 percent chance of occurrence in a given year) with one foot of SLR jumps to five times higher. This suggests that County of Orange is near a tipping point that, if SLR would not be taken seriously into account, unprecedented relatively frequent flooding may threaten its energy infrastructure. In this county too, with a rise of 1.5 m in mean sea level, the maximum expected rate of exposure to tidal flooding would be equal to the one due to a 100-year coastal storm under current mean sea level.

Figure 22: Natural Gas Pipeline Exposure to Coastal Storm and Sea Level Rise Compound Flooding



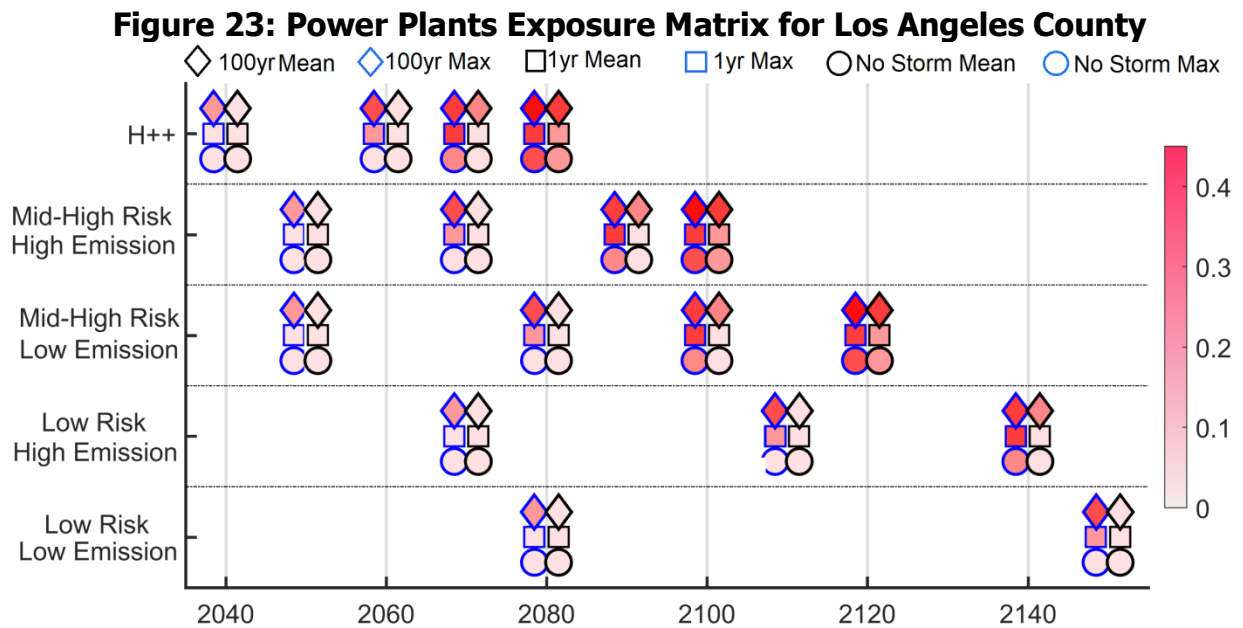
Estimated maximum natural gas pipeline exposure to coastal storm and sea level rise compound flooding.

Source: University of California, Irvine and University of California, Los Angeles.

Coastal flooding threatens both energy transmission and production infrastructure. Up to 45 percent of energy production infrastructure in Los Angeles County is expected to be exposed to flooding due to sea level rise and coastal storms combined. Figure 23 shows the matrix of expected exposure for different time horizons. The researchers follow the recommendations by the State of California Sea Level Rise Guide to provide useful information for evaluating a

range of projections based on low, medium-high and extreme levels of risk aversion (www.opc.ca.gov/updating-californias-sea-level-rise-guidance/). To depict the matrix in Figure 23 the research team have considered the SLR projections under different scenarios including Low and Mid-High Risk Aversion (under both high and low emission scenarios) plus Extreme Risk Aversion (a.k.a. H++ scenario) discussed in the Ocean Protection Council’s State of California Sea Level Rise Guidance 2018 Update (Ocean Protection Council, 2018).

In Figure 23, the color bar represents the estimated mean and maximum exposure of power plant capacity of Los Angeles County to coastal flooding relative to the total power plant capacity of the County, which is ~14,000 MW. In this figure, the circle, square and diamond symbols represent the estimated exposure due to the no storm activity, 1-year and 100-year coastal storm scenarios, respectively; These results show by the year 2100, for example, with mid-high risk aversion under low emission scenario, the mean (black edge) and maximum (blues edge) estimates for power plants capacity exposed to tidal flooding (circle) would be 3 percent and 21 percent of the total capacity of County, respectively. This rate would be 21 percent and 36 percent in the same year due to a 100-year coastal storm (diamond). Under H++ scenario (extreme risk aversion), by the year 2080, at least 18 percent (mean estimates of tidal flooding) and at most 45 percent (maximum estimates due to a 100-year coastal storm) of Los Angeles County power plant capacity is expected to be exposed to coastal flooding.



Color bar shows the ratio of power generation capacity exposed to coastal flooding. Under each sea level rise projection (on y-axis) circle, square and diamond, represent the estimated exposure due to background scenario (i.e. no storm activity), 1-year and 100-year coastal storm, respectively; while marker edge colors black and blue are associated with mean estimated exposure and the maximum estimates. These estimates cover SLR projections between 0.5 m and 2 m.

Source: University of California, Irvine and University of California, Los Angeles.

CHAPTER 4:

Knowledge Transfer Activities

In this report, the research team analyzed the impact rising natural hazards due to a warming climate on energy infrastructure. The analysis was informative to policy makers and stakeholders for future climate adaptation plans. They have set meetings with stakeholders and presented their work in open forums to transfer the knowledge to decision makers and the public. The details about the regional climate symposia held by Local Government Commission (LGC) as part of this project is presented in the Appendix C. The researchers will continue to work with the CEC, SoCal Gas, and other stakeholders to inform them based on the analysis in this report.

CHAPTER 5:

Conclusions/Recommendations

In this report, the research team showed the potential impacts of a warming climate on natural gas system infrastructure. This was done through quantification of climate induced stressors on California natural gas pipelines, and quantification of the change in exposure of natural gas pipelines as a consequence of single or multiple natural hazards.

The conclusions of the report are:

1. There is a rise in the impacts of extreme precipitation intensity and recurrence interval due to a warming climate. The results show that in most cities, extreme precipitation events are projected to intensify. Urban areas in California may struggle against increases in severity and frequency of rare events. Increases in intensity, duration, and frequency of extreme precipitation can adversely impact the integrity of infrastructure and natural and engineered slopes. Severe rainfall causes flooding, landslides, soil erosion and jeopardizes functionality or integrity of infrastructure systems. Infrastructure built with soil (for example, earthen dams, levees, embankments), or the ones that interface with soil (for example, roads, bridge, pipelines, foundations) are often more vulnerable. The IDF curves presented in this report can be used to evaluate the risk of existing infrastructure systems in a changing climate.
2. Projected changes in the characteristic of extreme precipitation are anticipated to result in possible future changes in the flood characteristics, and consequently, the risk posed by flooding hazards to infrastructure. The results using simulated runoff as a proxy to investigate the direction of change in the flood hazard point to amplification of flood hazard in the future. This can be attributed to increases in the frequency of extreme flows in a warming climate. While climate model simulations contain biases and uncertainties the results reveal that a historical 100-year flood event is 5 times more likely in the future under a fossil fuel intensive "business as usual" scenario (RCP8.5). The results also demonstrate that levee systems in the northern part of Central Valley and coastal counties of Southern California, which protect hundreds of miles of natural gas pipelines, experience the highest likelihood of changes in flood hazard. Therefore, the infrastructure protected by these levee systems may observe higher rates of exposure to flooding in the future. These possible changes in flood hazard are neither considered in the current levee assessments nor in the future water resource planning and management for the levee operation and maintenance.
3. Sea level rise not only raises the mean water level but also affects the free surface wave (for example, tide and storm surge) propagation (Devlin et al., 2017; Schindelegger et al., 2018; Wahl, 2017). The interactions between SLR and coastal storm activities are non-linear and their compounding effects are complicated to estimate. Future projection of risk of coastal flooding is therefore a complicated process that needs to both deal with compounding effects of interdependent flooding drivers and also systematically take the uncertainties associated with the hazard prediction estimates into account for reliable estimates of the threat to coastal communities. In

this study the research team quantify the exposure of natural gas pipelines in Los Angeles County and Orange County of California, USA to compound coastal flooding. Combined impacts of sea level rise scenarios with design coastal storms are considered for exposure assessment. Results suggest that, if no adaptation measure is implemented, 1-1.5 m of sea level rise may trigger tidal flooding (without significant storm activity) equal in exposure to a 100-year coastal storm today.

4. The research shows that regional patterns of exposure of natural gas pipelines to individual/compounding effects of hazards are significantly different. The results show Northwest and Cascade ranges are the regions with highest exposure and they are expected to experience significantly higher rates of exposure to compound hazards in the future. These compound hazards can be detrimental to critical energy infrastructure, because their combined effects have impacts that are more significant. Considering the compounding impacts of concurrent hazards is even more important when dealing with aging infrastructure with declining resilience to natural hazards. The research team emphasized that natural gas pipelines infrastructure are typically underground and therefore, the chance of being directly affected by climate hazards are relatively small. The hazards discussed in this study can cause significant impact both directly and indirectly. For instance, a flooding event may disrupt the transportation network making it difficult to resolve natural gas pipeline incidents. This may result in possible power outages which in turn impede rescue operations and medical assistance and thus potentially leading to additional loss of lives. Also, in these analyses, interactions between hazard drivers and anthropogenic effects (that is, risk prevention/mitigation measures) are not included. A more thorough understanding of risk in the future needs holistic approaches that take the post-disaster dynamic interactions between natural and human processes into account.
5. In this project, a hybrid dynamical–statistical approach was used to downscale the CMIP5 GCMs to 9 km resolution for fine-scale temperature projections over California during the 21st century. The downscaled ensemble of temperature over California reveals that statewide temperatures under RCP4.5 (RCP8.5) are projected to increase by about 2.0 (2.5) °C in the middle of the 21st century and 2.6 (5.0) °C at the end of 21st century compared to the historical (1981-2000) climate. Overall, the findings in this report indicate that a hybrid-downscaling approach that combines the benefits of physical realism associated with dynamical downscaling and the computational efficiency of statistical downscaling can provide a credible way to downscale a large ensemble of GCM temperature projections. Using Weather Research and Forecasting (WRF) model found that in winter months, temperatures in southern California cities are generally higher than those in northern California cities, as expected. However, in summer months, Sacramento and Fresno are hotter than other cities in northern California. The reason could be the lack of sea breeze cooling down the air temperature in these cities located in the Central Valley. It is important to note that all exposure estimates in this study are based on the current installations, and future developments and adaptation measures are not considered here. While successful adaptation (Adger et al., 2018, 2013), depending on a number of socioeconomic and geophysical factors (Arkema et al., 2013; Barbier, 2014; Cheong et al., 2013), is expected to mitigate the risk, and should be considered for integrated risk assessment (Nicholls and Cazenave, 2010).

CHAPTER 6:

Benefits to Ratepayers

Climate change impacts are projected to worsen in the future altering vulnerability of the existing infrastructure systems. The changes in the climate extremes and the importance of incorporating climate change impacts on infrastructure have been recognized by California State Legislature as an emerging problem through AB-2800. The goal of California's AB-2800 is to achieve a set of climate adaptive strategies and guidelines to ensure safety and durability of infrastructure in the future. California also is also decarbonizing its electricity system. In September 2018, California senate passed SB100, which requires the Golden State to obtain 100 percent of its power from clean sources by 2045. Considering the State consumes more than 206 billion kilowatt hours (bn kWh) of electricity per year, achieving this goal requires significant investment in the infrastructure needed for the production, transportation, and storage of alternative green sources of energy. Anticipating the threats to California's energy infrastructure and developing new techniques to move toward utilizing green energies can help Californians achieve climate adaptive strategies to ensure the safety and durability of energy infrastructure in the future.

Here the research team shows that extreme precipitation is expected to increase across most cities in California based on the current multi-model climate simulations. The research team argues that the increase in intensity, duration, and frequency of extreme precipitation can adversely impact the integrity of infrastructure. Indeed, severe rainfall causes flooding, landslides, soil erosion and jeopardizes functionality or integrity of infrastructure systems. The future developments over the leveed regions in particular need to incorporate the possible changes in the flood hazard in a changing climate. To ensure the adaptation and mitigation strategies can lead to reducing flood impacts in the leveed area, also there is a need to include hydrological risks into guidelines and actions that address water challenges in the leveed area. These strategies, if informed by climate change analyses, can lead to increased public safety and security of infrastructure systems protected by the levees.

Also, the research team has shown that projected increased of coastal flooding in southern California threatens both energy transmission and production infrastructure. For instance, up to 45 percent of energy production infrastructure in Los Angeles County is expected to be exposed to flooding due to sea level rise and coastal storms combined. In general, the results show that the exposure of natural gas infrastructure in response to individual and compounding effects of hazards is expected to increase substantially in a warming climate. Understanding possible future climate risks and developing context-sensitive adaptive strategies and options for infrastructure provision and management will give the state a solid scientific foundation from which to prioritize policies, guidelines, activities and economic investments to protect infrastructure systems. Effective adaptation and mitigation strategies for reducing the impact of extreme events on infrastructure systems require community engagement, public risk and safety education, economic and regulatory analysis, and close, iterative collaboration with stakeholders. Therefore, this research benefits ratepayers in the future, because the results of this work show the projected changes in damaging and costly compound (cascading) hazards.

Sections of this report contributed to California’s Fourth Climate Change Assessment examining potential changes of extreme precipitation. The research team developed what is known as intensity-duration-frequency curves using non-stationary techniques. Engineers use these curves in the design of infrastructure including natural gas physical assets. In turn, the authors of the report for AB 2800 (*Paying it Forward: The Path Towards Climate-Safe Infrastructure in California*) used these curves as an example on how to translate information on climate projections in a way that engineers can use. This contributes to a new area of research that brings together climate scientists and engineers.

In 2018, the California Public Utilities Commission opened a rulemaking (ongoing at the time of this publication) to consider strategies and guidance for climate change adaptation for electric and natural gas utilities (proceeding number R.18-04-019). Studies like this are providing material for consideration in the preparation of plans and guidance documents for the CPUC proceeding and other similar efforts.

REFERENCES

- Abadie, L.M., Sainz de Murieta, E., Galarraga, I., 2016. Climate Risk Assessment under Uncertainty: An Application to Main European Coastal Cities. *Front. Mar. Sci.* 3. <https://doi.org/10.3389/fmars.2016.00265>
- Abatzoglou, J.T., Williams, A.P., 2016. Impact of anthropogenic climate change on wildfire across western US forests. *Proceedings of the National Academy of Sciences* 113, 11770–11775. <https://doi.org/10.1073/pnas.1607171113>
- Adger, W.N., Barnett, J., Brown, K., Marshall, N., O'Brien, K., 2013. Cultural dimensions of climate change impacts and adaptation. *Nature Clim Change* 3, 112–117. <https://doi.org/10.1038/nclimate1666>
- Adger, W.N., Brown, I., Surminski, S., 2018. Advances in risk assessment for climate change adaptation policy. *Philosophical Transactions of the Royal Society A: Mathematical, Physical and Engineering Sciences* 376, 20180106. <https://doi.org/10.1098/rsta.2018.0106>
- AghaKouchak, A. (Ed.), 2013. *Extremes in a changing climate: detection, analysis and uncertainty*, Water science and technology library. Springer, Dordrecht; New York.
- AghaKouchak, A., Cheng, L., Mazdidasni, O., Farahmand, A., 2014. Global warming and changes in risk of concurrent climate extremes: Insights from the 2014 California drought. *Geophys. Res. Lett.* 41, 2014GL062308. <https://doi.org/10.1002/2014GL062308>
- AghaKouchak, A., Huning, L.S., Chiang, F., Sadegh, M., Vahedifard, F., Mazdidasni, O., Moftakhari, H., Mallakpour, I., 2018. How do natural hazards cascade to cause disasters? *Nature* 561, 458–460. <https://doi.org/10.1038/d41586-018-06783-6>
- Alfieri, L., Burek, P., Feyen, L., Forzieri, G., 2015. Global warming increases the frequency of river floods in Europe. *Hydrol. Earth Syst. Sci.* 19, 2247–2260. <https://doi.org/10.5194/hess-19-2247-2015>
- Arkema, K.K., Guannel, G., Verutes, G., Wood, S.A., Guerry, A., Ruckelshaus, M., Kareiva, P., Lacayo, M., Silver, J.M., 2013. Coastal habitats shield people and property from sea-level rise and storms. *Nature Clim Change* 3, 913–918. <https://doi.org/10.1038/nclimate1944>
- Barbier, E.B., 2014. A global strategy for protecting vulnerable coastal populations. *Science* 345, 1250–1251. <https://doi.org/10.1126/science.1254629>
- Barnard, P.L., Erikson, L.H., Foxgrover, A.C., Limber, P.W., O'Neill, A.C., Vitousek, S., 2015. Coastal Storm Modeling System (CoSMoS) for Southern California, v3.0, Phase 2. <https://doi.org/10.5066/f7t151q4>
- Barnard, P.L., van Ormondt, M., Erikson, L.H., Eshleman, J., Hapke, C., Ruggiero, P., Adams, P.N., Foxgrover, A.C., 2014. Development of the Coastal Storm Modeling System

- (CoSMoS) for predicting the impact of storms on high-energy, active-margin coasts. *Nat Hazards* 74, 1095–1125. <https://doi.org/10.1007/s11069-014-1236-y>
- Barth, N.A., Villarini, G., NAYak, M., White, K., 2016. Mixed populations and annual flood frequency estimates in the western United States: The role of atmospheric rivers. *Water Resour. Res.* n/a-n/a. <https://doi.org/10.1002/2016WR019064>
- Berghuijs, W.R., Woods, R.A., Hrachowitz, M., 2014. A precipitation shift from snow towards rain leads to a decrease in streamflow. *Nature Climate Change* 4, 583–586. <https://doi.org/10.1038/nclimate2246>
- Bonnin, G.M., Martin, D., Lin, B., Parzybok, T., Yekta, M., Riley, D., 2006. Precipitation-frequency atlas of the United States. NOAA atlas 14, 1–65.
- Brown, S., Hanson, S., Nicholls, R.J., 2014. Implications of sea-level rise and extreme events around Europe: a review of coastal energy infrastructure. *Climatic Change* 122, 81–95. <https://doi.org/10.1007/s10584-013-0996-9>
- Burke, M.P., Hogue, T.S., Kinoshita, A.M., Barco, J., Wessel, C., Stein, E.D., 2013. Pre- and post-fire pollutant loads in an urban fringe watershed in Southern California. *Environmental Monitoring and Assessment* 185, 10131–10145. <https://doi.org/10.1007/s10661-013-3318-9>
- Burton, C., Cutter, S.L., 2008. Levee Failures and Social Vulnerability in the Sacramento-San Joaquin Delta Area, California. *Nat. Hazards Rev.* 9, 136–149. [https://doi.org/10.1061/\(ASCE\)1527-6988\(2008\)9:3\(136\)](https://doi.org/10.1061/(ASCE)1527-6988(2008)9:3(136))
- Cayan, D.R., Dettinger, M.D., Kammerdiener, S.A., Caprio, J.M., Peterson, D.H., 2001. Changes in the Onset of Spring in the Western United States. *Bull. Amer. Meteor. Soc.* 82, 399–415. [https://doi.org/10.1175/1520-0477\(2001\)082<0399:CITOOS>2.3.CO;2](https://doi.org/10.1175/1520-0477(2001)082<0399:CITOOS>2.3.CO;2)
- Cheng, L., AghaKouchak, A., 2014. Nonstationary Precipitation Intensity-Duration-Frequency Curves for Infrastructure Design in a Changing Climate. *Scientific Reports* 4. <https://doi.org/10.1038/srep07093>
- Cheng, L., AghaKouchak, A., Gilleland, E., Katz, R.W., 2014. Non-stationary extreme value analysis in a changing climate. *Climatic Change* 127, 353–369. <https://doi.org/10.1007/s10584-014-1254-5>
- Cheong, S.-M., Silliman, B., Wong, P.P., van Wesenbeeck, B., Kim, C.-K., Guannel, G., 2013. Coastal adaptation with ecological engineering. *Nature Clim Change* 3, 787–791. <https://doi.org/10.1038/nclimate1854>
- Coles, S., 2001. *An Introduction to Statistical Modeling of Extreme Values*, Springer Series in Statistics. Springer-Verlag, London.
- Collenteur, R.A., de Moel, H., Jongman, B., Di Baldassarre, G., 2015. The failed-levee effect: Do societies learn from flood disasters? *Nat Hazards* 76, 373–388. <https://doi.org/10.1007/s11069-014-1496-6>

- Cruz, A.M., Krausmann, E., 2013. Vulnerability of the oil and gas sector to climate change and extreme weather events. *Climatic Change* 121, 41–53. <https://doi.org/10.1007/s10584-013-0891-4>
- Curtis, K.J., Schneider, A., 2011. Understanding the demographic implications of climate change: estimates of localized population predictions under future scenarios of sea-level rise. *Popul Environ* 33, 28–54. <https://doi.org/10.1007/s11111-011-0136-2>
- Das, T., Dettinger, M.D., Cayan, D.R., Hidalgo, H.G., 2011. Potential increase in floods in California's Sierra Nevada under future climate projections. *Climatic Change* 109, 71–94. <https://doi.org/10.1007/s10584-011-0298-z>
- Dennison, P.E., Brewer, S.C., Arnold, J.D., Moritz, M.A., 2014. Large wildfire trends in the western United States, 1984-2011: DENNISON ET. AL.; LARGE WILDFIRE TRENDS IN THE WESTERN US. *Geophysical Research Letters* 41, 2928–2933. <https://doi.org/10.1002/2014GL059576>
- Dettinger, M., 2011. Climate Change, Atmospheric Rivers, and Floods in California - A Multimodel Analysis of Storm Frequency and Magnitude Changes1: Climate Change, Atmospheric Rivers, and Floods in California - A Multimodel Analysis of Storm Frequency and Magnitude Changes. *JAWRA Journal of the American Water Resources Association* 47, 514–523. <https://doi.org/10.1111/j.1752-1688.2011.00546.x>
- Dettinger, M.D., Cayan, D.R., 1995. Large-Scale Atmospheric Forcing of Recent Trends toward Early Snowmelt Runoff in California. *J. Climate* 8, 606–623. [https://doi.org/10.1175/1520-0442\(1995\)008<0606:LSAFOR>2.0.CO;2](https://doi.org/10.1175/1520-0442(1995)008<0606:LSAFOR>2.0.CO;2)
- Devlin, A.T., Jay, D.A., Zaron, E.D., Talke, S.A., Pan, J., Lin, H., 2017. Tidal Variability Related to Sea Level Variability in the Pacific Ocean: TIDAL VARIABILITY IN THE PACIFIC OCEAN. *J. Geophys. Res. Oceans* 122, 8445–8463. <https://doi.org/10.1002/2017JC013165>
- Diffenbaugh, N.S., Swain, D.L., Touma, D., 2015. Anthropogenic warming has increased drought risk in California. *PNAS* 112, 3931–3936. <https://doi.org/10.1073/pnas.1422385112>
- Field, C.B., Barros, V.R., Intergovernmental Panel on Climate Change (Eds.), 2014. Climate change 2014: impacts, adaptation, and vulnerability: Working Group II contribution to the fifth assessment report of the Intergovernmental Panel on Climate Change. Cambridge University Press, New York, NY.
- Fischer, E.M., Knutti, R., 2015. Anthropogenic contribution to global occurrence of heavy-precipitation and high-temperature extremes. *Nature Climate Change* 5, 560–564. <https://doi.org/10.1038/nclimate2617>
- Florsheim, J.L., Chin, A., Kinoshita, A.M., Nourbakhshbeidokhti, S., 2017. Effect of storms during drought on post-wildfire recovery of channel sediment dynamics and habitat in the southern California chaparral, USA: Effect of storms on post-wildfire sediment

dynamics and habitat. *Earth Surface Processes and Landforms* 42, 1482–1492.
<https://doi.org/10.1002/esp.4117>

- Florsheim, J.L., Dettinger, M.D., 2015. Promoting Atmospheric-River and Snowmelt-Fueled Biogeomorphic Processes by Restoring River-Floodplain Connectivity in California's Central Valley, in: Hudson, P.F., Middelkoop, H. (Eds.), *Geomorphic Approaches to Integrated Floodplain Management of Lowland Fluvial Systems in North America and Europe*. Springer New York, New York, NY, pp. 119–141. https://doi.org/10.1007/978-1-4939-2380-9_6
- Florsheim, J.L., Dettinger, M.D., 2007. Climate and floods still govern California levee breaks. *Geophysical Research Letters* 34. <https://doi.org/10.1029/2007GL031702>
- Forzieri, G., Bianchi, A., Silva, F.B. e, Marin Herrera, M.A., Leblois, A., Lavallo, C., Aerts, J.C.J.H., Feyen, L., 2018. Escalating impacts of climate extremes on critical infrastructures in Europe. *Global Environmental Change* 48, 97–107.
<https://doi.org/10.1016/j.gloenvcha.2017.11.007>
- Garschagen, M., Romero-Lankao, P., 2015. Exploring the relationships between urbanization trends and climate change vulnerability. *Climatic Change* 133, 37–52.
<https://doi.org/10.1007/s10584-013-0812-6>
- Gilleland, E., Katz, R.W., 2016. extRemes 2.0: An Extreme Value Analysis Package in R. *Journal of Statistical Software* 72. <https://doi.org/10.18637/jss.v072.i08>
- Hallegatte, S., Green, C., Nicholls, R.J., Corfee-Morlot, J., 2013. Future flood losses in major coastal cities. *Nature Climate Change* 3, 802–806. <https://doi.org/10.1038/nclimate1979>
- Hardin, E., AghaKouchak, A., Qomi, M.J.A., Madani, K., Tarroja, B., Zhou, Y., Yang, T., Samuelsen, S., 2017. California drought increases CO2 footprint of energy. *Sustainable Cities and Society* 28, 450–452. <https://doi.org/10.1016/j.scs.2016.09.004>
- Harpold, A.A., Rajagopal S., Crews J. B., Winchell T., Schumer R., 2017. Relative Humidity Has Uneven Effects on Shifts From Snow to Rain Over the Western U.S. *Geophysical Research Letters* 44, 9742–9750. <https://doi.org/10.1002/2017GL075046>
- Hidalgo, H.G., Das, T., Dettinger, M.D., Cayan, D.R., Pierce, D.W., Barnett, T.P., Bala, G., Mirin, A., Wood, A.W., Bonfils, C., Santer, B.D., Nozawa, T., 2009. Detection and Attribution of Streamflow Timing Changes to Climate Change in the Western United States. *J. Climate* 22, 3838–3855. <https://doi.org/10.1175/2009JCLI2470.1>
- Hill, K., 2015. Coastal infrastructure: a typology for the next century of adaptation to sea-level rise. *Frontiers in Ecology and the Environment* 13, 468–476.
<https://doi.org/10.1890/150088>
- Hirabayashi, Y., Mahendran, R., Koirala, S., Konoshima, L., Yamazaki, D., Watanabe, S., Kim, H., Kanae, S., 2013. Global flood risk under climate change. *Nature Climate Change* 3, 816–821. <https://doi.org/10.1038/nclimate1911>

- IPCC (Ed.), 2012. Managing the risks of extreme events and disasters to advance climate change adaptation: special report of the Intergovernmental Panel on Climate Change. Cambridge University Press, New York, NY.
- Jasim, F.H., Vahedifard, F., Ragno, E., AghaKouchak, A., Ellithy, G., 2017. Effects of Climate Change on Fragility Curves of Earthen Levees Subjected to Extreme Precipitations, in: Geo-Risk 2017. Presented at the Geo-Risk 2017, American Society of Civil Engineers, Denver, Colorado, pp. 498–507. <https://doi.org/10.1061/9780784480724.045>
- Jeon, S., Prabhat, Byna, S., Gu, J., Collins, W.D., Wehner, M.F., 2015. Characterization of extreme precipitation within atmospheric river events over California. *Advances in Statistical Climatology, Meteorology and Oceanography* 1, 45–57. <https://doi.org/10.5194/asmo-1-45-2015>
- Jones, C., 2000. Occurrence of Extreme Precipitation Events in California and Relationships with the Madden–Julian Oscillation. *Journal of Climate* 13, 3576–3587. [https://doi.org/10.1175/1520-0442\(2000\)013<3576:OOEPEI>2.0.CO;2](https://doi.org/10.1175/1520-0442(2000)013<3576:OOEPEI>2.0.CO;2)
- Jongman, B., Hochrainer-Stigler, S., Feyen, L., Aerts, J.C.J.H., Mechler, R., Botzen, W.J.W., Bouwer, L.M., Pflug, G., Rojas, R., Ward, P.J., 2014. Increasing stress on disaster-risk finance due to large floods. *Nature Climate Change* 4, 264–268. <https://doi.org/10.1038/nclimate2124>
- Katz, R.W., Parlange, M.B., Naveau, P., 2002. Statistics of extremes in hydrology. *Advances in Water Resources* 25, 1287–1304. [https://doi.org/10.1016/S0309-1708\(02\)00056-8](https://doi.org/10.1016/S0309-1708(02)00056-8)
- Kinoshita, A.M., Hogue, T.S., 2011. Spatial and temporal controls on post-fire hydrologic recovery in Southern California watersheds. *CATENA* 87, 240–252. <https://doi.org/10.1016/j.catena.2011.06.005>
- Knowles, N., Dettinger, M.D., Cayan, D.R., 2006. Trends in Snowfall versus Rainfall in the Western United States. *J. Climate* 19, 4545–4559. <https://doi.org/10.1175/JCLI3850.1>
- Kriebel, D.L., Geiman, J.D., Henderson, G.R., 2015. Future Flood Frequency under Sea-Level Rise Scenarios. *Journal of Coastal Research* 315, 1078–1083. <https://doi.org/10.2112/JCOASTRES-D-13-00190.1>
- Kulp, S., Strauss, B.H., 2017. Rapid escalation of coastal flood exposure in US municipalities from sea level rise. *Climatic Change* 142, 477–489. <https://doi.org/10.1007/s10584-017-1963-7>
- Lenihan, J.M., Drapek, R., Bachelet, D., Neilson, R.P., 2003. CLIMATE CHANGE EFFECTS ON VEGETATION DISTRIBUTION, CARBON, AND FIRE IN CALIFORNIA. *Ecological Applications* 13, 1667–1681. <https://doi.org/10.1890/025295>
- Leonard, M., Westra, S., Phatak, A., Lambert, M., van den Hurk, B., McInnes, K., Risbey, J., Schuster, S., Jakob, D., Stafford-Smith, M., 2014. A compound event framework for understanding extreme impacts. *Wiley Interdisciplinary Reviews: Climate Change* 5, 113–128. <https://doi.org/10.1002/wcc.252>

- Leung, L.R., Qian, Y., 2009. Atmospheric rivers induced heavy precipitation and flooding in the western U.S. simulated by the WRF regional climate model: ATMOSPHERIC RIVER, PRECIPITATION, FLOOD. *Geophysical Research Letters* 36, n/a-n/a. <https://doi.org/10.1029/2008GL036445>
- Li, D., Wrzesien, M.L., Durand, M., Adam, J., Lettenmaier, D.P., 2017. How much runoff originates as snow in the western United States, and how will that change in the future? *Geophys. Res. Lett.* 44, 2017GL073551. <https://doi.org/10.1002/2017GL073551>
- Liu, Z., Mehran, A., Phillips, T., AghaKouchak, A., 2014. Seasonal and regional biases in CMIP5 precipitation simulations. *Climate Research* 60, 35–50. <https://doi.org/10.3354/cr01221>
- Lohmann, D., Raschke, E., Nijssen, B., Lettenmaier, D.P., 1998. Regional scale hydrology: I. Formulation of the VIC-2L model coupled to a routing model. *Hydrological Sciences Journal* 43, 131–141. <https://doi.org/10.1080/02626669809492107>
- Ludy, J., Kondolf, G.M., 2012. Flood risk perception in lands “protected” by 100-year levees. *Natural Hazards* 61, 829–842. <https://doi.org/10.1007/s11069-011-0072-6>
- Mallakpour, I., AghaKouchak, A., Sadegh, M., 2019. Climate - Induced Changes in the Risk of Hydrological Failure of Major Dams in California. *Geophys. Res. Lett.* 46, 2130 – 2139. <https://doi.org/10.1029/2018GL081888>
- Mallakpour, I., Sadegh, M., AghaKouchak, A., 2018. A new normal for streamflow in California in a warming climate: Wetter wet seasons and drier dry seasons. *Journal of Hydrology* 567, 203–211. <https://doi.org/10.1016/j.jhydrol.2018.10.023>
- Mansur, A.V., Brondízio, E.S., Roy, S., Hetrick, S., Vogt, N.D., Newton, A., 2016. An assessment of urban vulnerability in the Amazon Delta and Estuary: a multi-criterion index of flood exposure, socio-economic conditions and infrastructure. *Sustainability Science* 11, 625–643. <https://doi.org/10.1007/s11625-016-0355-7>
- Mao, Y., Nijssen, B., Lettenmaier, D.P., 2015. Is climate change implicated in the 2013–2014 California drought? A hydrologic perspective. *Geophys. Res. Lett.* 42, 2015GL063456. <https://doi.org/10.1002/2015GL063456>
- McCabe, G.J., Wolock, D.M., 2014. Spatial and temporal patterns in conterminous United States streamflow characteristics. *Geophys. Res. Lett.* 41, 2014GL061980. <https://doi.org/10.1002/2014GL061980>
- McPhillips, L.E., Chang, H., Chester, M.V., Depietri, Y., Friedman, E., Grimm, N.B., Kominoski, J.S., McPhearson, T., Méndez-Lázaro, P., Rosi, E.J., Shiva, J.S., 2018. Defining Extreme Events: A Cross-Disciplinary Review. *Earth’s Future*. <https://doi.org/10.1002/2017EF000686>
- Mehrotra, R., Sharma, A., 2016. A Multivariate Quantile-Matching Bias Correction Approach with Auto- and Cross-Dependence across Multiple Time Scales: Implications for

- Downscaling. *Journal of Climate* 29, 3519–3539. <https://doi.org/10.1175/JCLI-D-15-0356.1>
- Milly, P.C.D., Betancourt, J., Falkenmark, M., Hirsch, R.M., Kundzewicz, Z.W., Lettenmaier, D.P., Stouffer, R.J., 2008. Stationarity Is Dead: Whither Water Management? *Science* 319, 573–574. <https://doi.org/10.1126/science.1151915>
- Mitchell, J.W., 2013. Power line failures and catastrophic wildfires under extreme weather conditions. *Engineering Failure Analysis* 35, 726–735. <https://doi.org/10.1016/j.engfailanal.2013.07.006>
- Moftakhari, H., Salvadori, G., AghaKouchak, A., Sanders, B.F., Matthew, R.A., 2017. Compounding effects of sea level rise and fluvial flooding. *Proceedings of the National Academy of Sciences* 114, 9785–9790. <https://doi.org/10.1073/pnas.1620325114>
- Moftakhari, H.R., AghaKouchak, A., Sanders, B.F., Feldman, D.L., Sweet, W., Matthew, R.A., Luke, A., 2015. Increased nuisance flooding along the coasts of the United States due to sea level rise: Past and future: INCREASED NUISANCE FLOODING DUE TO SLR. *Geophysical Research Letters* 42, 9846–9852. <https://doi.org/10.1002/2015GL066072>
- Mukherjee, S., Nateghi, R., Hastak, M., 2018. A Multi-Hazard Approach to Assess Severe Weather-Induced Major Power Outage Risks in the U.S. *Reliability Engineering & System Safety*. <https://doi.org/10.1016/j.ress.2018.03.015>
- Nazemi, A. (Ali), Wheeler, H.S., 2014. Assessing the Vulnerability of Water Supply to Changing Streamflow Conditions. *Eos Trans. AGU* 95, 288–288. <https://doi.org/10.1002/2014EO320007>
- Neumann, B., Vafeidis, A.T., Zimmermann, J., Nicholls, R.J., 2015. Future Coastal Population Growth and Exposure to Sea-Level Rise and Coastal Flooding - A Global Assessment. *PLoS ONE* 10, e0118571. <https://doi.org/10.1371/journal.pone.0118571>
- NFIP, 2012. Flood After Fire Fact Sheet, Risks and Protection. FEMA.
- Nicholls, R.J., Cazenave, A., 2010. Sea-Level Rise and Its Impact on Coastal Zones. *Science* 328, 1517–1520. <https://doi.org/10.1126/science.1185782>
- Ocean Protection Council, 2018, State of California Sea Level Rise Guidance, 2018 Update. Ocean Protection Council: Sacramento, CA, USA, p.84., Link: http://www.opc.ca.gov/webmaster/ftp/pdf/agenda_items/20180314/Item3_Exhibit-A OPC_SLR_Guidance-rd3.pdf
- Parise, M., Cannon, S.H., 2017. Debris Flow Generation in Burned Catchments, in: Mikoš, M., Casagli, N., Yin, Y., Sassa, K. (Eds.), *Advancing Culture of Living with Landslides*. Springer International Publishing, Cham, pp. 643–650. https://doi.org/10.1007/978-3-319-53485-5_74
- Payne, A.E., Magnusdottir, G., 2015. An evaluation of atmospheric rivers over the North Pacific in CMIP5 and their response to warming under RCP 8.5: NORTH PACIFIC

- ATMOSPHERIC RIVERS IN CMIP5. *Journal of Geophysical Research: Atmospheres* 120, 11,173–11,190. <https://doi.org/10.1002/2015JD023586>
- Pierce, D.W., Cayan, D.R., Thrasher, B.L., 2014. Statistical Downscaling Using Localized Constructed Analogs (LOCA)*. *Journal of Hydrometeorology* 15, 2558–2585. <https://doi.org/10.1175/JHM-D-14-0082.1>
- Poon, P.K., Kinoshita, A.M., 2018. Spatial and temporal evapotranspiration trends after wildfire in semi-arid landscapes. *Journal of Hydrology* 559, 71–83. <https://doi.org/10.1016/j.jhydrol.2018.02.023>
- Ragno, E., AghaKouchak, A., Love, C.A., Cheng, L., Vahedifard, F., Lima, C.H.R., 2018. Quantifying Changes in Future Intensity-Duration-Frequency Curves Using Multimodel Ensemble Simulations. *Water Resources Research*. <https://doi.org/10.1002/2017WR021975>
- Ralph, F.M., Coleman, T., Neiman, P.J., Zamora, R.J., Dettinger, M.D., 2013. Observed Impacts of Duration and Seasonality of Atmospheric-River Landfalls on Soil Moisture and Runoff in Coastal Northern California. *Journal of Hydrometeorology* 14, 443–459. <https://doi.org/10.1175/JHM-D-12-076.1>
- Robinson, J.D., Vahedifard, F., AghaKouchak, A., 2017. Rainfall-triggered slope instabilities under a changing climate: comparative study using historical and projected precipitation extremes. *Can. Geotech. J.* 54, 117–127. <https://doi.org/10.1139/cgj-2015-0602>
- Sadegh, M., Moftakhari, H., Gupta, H.V., Ragno, E., Mazdidasni, O., Sanders, B., Matthew, R., AghaKouchak, A., 2018. Multi-hazard scenarios for analysis of compound extreme events. *Geophysical Research Letters*. <https://doi.org/10.1029/2018GL077317>
- Sadegh, M., Vrugt, J.A., Xu, C., Volpi, E., 2015. The stationarity paradigm revisited: Hypothesis testing using diagnostics, summary metrics, and DREAM: REVISITING STATIONARITY PARADIGM. *Water Resources Research* 51, 9207–9231. <https://doi.org/10.1002/2014WR016805>
- Sathaye, J., Dale, L., Larsen, P., Fitts, G., Ko, K., Lewis, S., Lucena, A., 2012. Estimating Risk to California Energy Infrastructure From Projected Climate Change (No. CEC-500-2012-057). California Energy Commission, Berkeley, CA.
- Schaeffer, R., Szklo, A.S., Pereira de Lucena, A.F., Moreira Cesar Borba, B.S., Pupo Nogueira, L.P., Fleming, F.P., Troccoli, A., Harrison, M., Boulahya, M.S., 2012. Energy sector vulnerability to climate change: A review. *Energy* 38, 1–12. <https://doi.org/10.1016/j.energy.2011.11.056>
- Schindelegger, M., Green, J.A.M., Wilmes, S.-B., Haigh, I.D., 2018. Can We Model the Effect of Observed Sea Level Rise on Tides? *J. Geophys. Res. Oceans* 123, 4593–4609. <https://doi.org/10.1029/2018JC013959>

- Stafford, S.L., 2017. Pipeline Performance and Safety in a Federal System: A Study of Natural Gas Pipeline Enforcement by States in the USA. *Journal of Transport Economics and Policy (JTEP)* 51, 193–207.
- Tessler, Z.D., Vorosmarty, C.J., Grossberg, M., Gladkova, I., Aizenman, H., Syvitski, J.P.M., Foufoula-Georgiou, E., 2015. Profiling risk and sustainability in coastal deltas of the world. *Science* 349, 638–643. <https://doi.org/10.1126/science.aab3574>
- Turco, M., Hardenberg, J. von, AghaKouchak, A., Llasat, M.C., Provenzale, A., Trigo, R.M., 2017. On the key role of droughts in the dynamics of summer fires in Mediterranean Europe. *Scientific Reports* 7, 81. <https://doi.org/10.1038/s41598-017-00116-9>
- USACE, 2018. A Summary of Risks and Benefits Associated with the USACE Levee Portfolio. The United States Army Corps of Engineers.
- Vahedifard, F., AghaKouchak, A., Ragno, E., Shahrokhadi, S., Mallakpour, I., 2017a. Lessons from the Oroville dam. *Science* 355, 1139. <https://doi.org/10.1126/science.aan0171>
- Vahedifard, F., Tehrani, F.S., Galavi, V., Ragno, E., AghaKouchak, A., 2017b. Resilience of MSE Walls with Marginal Backfill under a Changing Climate: Quantitative Assessment for Extreme Precipitation Events. *Journal of Geotechnical and Geoenvironmental Engineering* 143, 04017056. [https://doi.org/10.1061/\(ASCE\)GT.1943-5606.0001743](https://doi.org/10.1061/(ASCE)GT.1943-5606.0001743)
- Villarini, G., 2016. On the seasonality of flooding across the continental United States. *Advances in Water Resources* 87, 80–91. <https://doi.org/10.1016/j.adwatres.2015.11.009>
- Vitousek, S., Barnard, P.L., Fletcher, C.H., Frazer, N., Erikson, L., Storlazzi, C.D., 2017. Doubling of coastal flooding frequency within decades due to sea-level rise. *Sci Rep* 7, 1399. <https://doi.org/10.1038/s41598-017-01362-7>
- Wahl, T., 2017. Sea-level rise and storm surges, relationship status: complicated! *Environ. Res. Lett.* 12, 111001. <https://doi.org/10.1088/1748-9326/aa8eba>
- Wang, R.-Q., Herdman, L.M., Erikson, L., Barnard, P., Hummel, M., Stacey, M.T., 2017. Interactions of Estuarine Shoreline Infrastructure With Multiscale Sea Level Variability: INFRASTRUCTURE AND SEA LEVEL VARIABILITY. *Journal of Geophysical Research: Oceans* 122, 9962–9979. <https://doi.org/10.1002/2017JC012730>
- Westerling, A.L., 2016. Increasing western US forest wildfire activity: sensitivity to changes in the timing of spring. *Philosophical Transactions of the Royal Society B: Biological Sciences* 371, 20150178. <https://doi.org/10.1098/rstb.2015.0178>
- Williams, C.J., Pierson, F.B., Robichaud, P.R., Boll, J., 2014. Hydrologic and erosion responses to wildfire along the rangeland–xeric forest continuum in the western US: a review and model of hydrologic vulnerability. *International Journal of Wildland Fire* 23, 155. <https://doi.org/10.1071/WF12161>

Woodruff, J.D., Irish, J.L., Camargo, S.J., 2013. Coastal flooding by tropical cyclones and sea-level rise. *Nature* 504, 44–52. <https://doi.org/10.1038/nature12855>

Zscheischler, J., Seneviratne, S.I., 2017. Dependence of drivers affects risks associated with compound events. *Science Advances* 3, e1700263. <https://doi.org/10.1126/sciadv.1700263>

APPENDIX A-1:

Detailed Method

The cumulative distribution function of the GEV distribution is (Cheng et al., 2014):

$$\Psi(x) = \exp\left\{-\left(1 + \xi \cdot \left(\frac{x - \mu}{\sigma}\right)\right)^{-\frac{1}{\xi}}\right\}$$

where, μ , σ , and ξ are the location parameter representing the center of the distribution, the scale parameter describing the distribution of the data around the center, and the shape parameter that defines the tail behavior of the distribution, respectively.

The researchers employed the Non-Stationary Extreme Value Analysis (NEVA; Cheng et al., 2014) toolbox to estimate the parameters of the GEV distribution in the case of both stationary and non-stationary analysis. NEVA framework has two main advantages: (i) it is versatile enough to deal with temporal stationary and non-stationary extremes (including annual maxima and extremes over a particular threshold); (ii) it estimates Return Level curves along with their uncertainty bounds through Bayesian inference and the Differential Evolution Markov Chain (DE-MC) approach (Cheng et al., 2014). Indeed, a Bayesian approach allows for uncertainty quantification, which is crucial especially when dealing with small sample size and rare events.

In this study, non-stationarity is characterized by a time-dependent location parameter $\mu(t)$, $\mu(t) = \mu_1 \cdot t + \mu_0$, where the regression parameters μ_1 and μ_0 are calibrated. A longer data set is required to reliably model the σ and ξ variability over time (Coles, 2001; Papalexiou and Koutsoyiannis, 2013), so it is assumed the scale and shape parameters to be time-invariant, as suggested by (Cheng et al., 2014).

We use NEVA to process the historical and future time series of annual maxima and obtain IDF curves of 25-, 50-, and 100-year return period along with their associated uncertainties. The return period is defined as $1/(1-p)$ where p is the non-exceedance probability of a given event. The intensity of the p -year event is given by:

$$q_p = \left(\left(-\frac{1}{\ln(p)}\right)^\xi - 1\right) \cdot \frac{\sigma}{\xi} + \hat{\mu}$$

where the location parameter $\hat{\mu} = \text{median}(\mu(t))$ if the Null-Hypothesis of no monotonic trend is rejected, and $\hat{\mu} = \mu$ elsewhere.

Generally, for the i th-set of GEV parameters, the expected return period T_i is given by $\frac{1}{1-\psi(I_T)}$ where $\psi(I_T)$ is estimated as:

$$\Psi(I_T) = \exp\left\{-\left(1 + \xi_i \cdot \left(\frac{I_T - \mu_i}{\sigma_i}\right)\right)^{-\frac{1}{\xi_i}}\right\}$$

APPENDIX A-2:

Tables of Precipitation Intensity-Duration-Frequency

Table A-1: 25-yr Return Period Intensity-Duration-Frequency curves based on historical records (NOAA) and future climate (RCP 4.5 and RCP 8.5).

Location	Based on	1-day mm/day	2-day mm/day	3-day mm/day	4-day mm/day	7-day mm/day
Eureka	NOAA	124.36	81.08	61.57	51.21	37.80
	RCP 4.5	153.14	104.77	80.04	67.14	49.31
	RCP 8.5	164.06	119.08	88.22	73.33	52.70
Redding	NOAA	166.42	110.95	85.95	71.93	49.99
	RCP 4.5	179.33	121.94	93.28	79.84	56.63
	RCP 8.5	185.35	127.83	100.41	84.32	64.01
Sacramento	NOAA	106.07	65.23	48.77	39.62	27.43
	RCP 4.5	122.13	82.08	61.39	50.45	34.31
	RCP 8.5	130.90	85.62	66.48	54.92	39.98
San Francisco	NOAA	107.90	65.23	48.16	40.23	28.65
	RCP 4.5	120.97	77.45	59.38	48.69	33.71
	RCP 8.5	129.05	75.45	58.05	49.61	35.99
San Jose	NOAA	77.42	49.38	37.19	30.48	21.34
	RCP 4.5	80.33	52.45	40.84	32.91	24.18
	RCP 8.5	91.47	61.91	47.35	41.19	30.30
Fresno	NOAA	65.23	39.62	29.26	23.77	16.46
	RCP 4.5	69.97	44.66	33.75	26.78	18.02
	RCP 8.5	72.60	48.42	36.58	30.24	21.59
Monterey	NOAA	90.83	58.52	45.11	37.80	26.21
	RCP 4.5	97.80	63.01	48.69	41.27	28.83
	RCP 8.5	102.52	66.83	50.44	43.19	32.65
Santa Barbara	NOAA	156.67	99.97	76.20	62.79	42.06
	RCP 4.5	166.95	110.57	86.21	74.32	51.17

Location	Based on	1-day mm/day	2-day mm/day	3-day mm/day	4-day mm/day	7-day mm/day
	RCP 8.5	190.19	122.94	98.64	87.44	60.51
Ventura	NOAA	148.74	97.54	75.59	62.79	42.06
	RCP 4.5	155.93	99.02	79.64	67.98	46.02
	RCP 8.5	167.73	108.96	89.99	75.19	55.06
Los Angeles	NOAA	137.77	89.00	69.49	57.30	39.01
	RCP 4.5	144.52	97.65	79.31	67.84	43.93
	RCP 8.5	146.43	102.12	84.48	72.10	53.67
Riverside	NOAA	90.83	58.52	43.89	35.97	23.77
	RCP 4.5	90.78	61.28	46.13	38.82	24.49
	RCP 8.5	94.75	63.12	48.28	39.97	26.57
Palm Springs	NOAA	96.93	58.52	42.67	33.53	21.34
	RCP 4.5	106.08	63.82	47.65	38.67	23.43
	RCP 8.5	113.01	69.70	53.12	42.93	27.96
Irvine	NOAA	104.85	67.06	50.60	41.45	27.43
	RCP 4.5	98.43	65.77	50.91	45.33	28.40
	RCP 8.5	113.29	72.69	57.90	49.96	34.58
Temecula	NOAA	145.08	91.44	67.06	57.30	39.01
	RCP 4.5	161.32	102.76	78.84	67.44	43.31
	RCP 8.5	165.76	110.86	83.87	74.25	51.82
Escondido	NOAA	110.95	70.71	54.86	45.72	30.48
	RCP 4.5	118.78	76.77	58.87	48.72	32.33
	RCP 8.5	122.49	81.44	65.01	53.99	38.13
San Diego	NOAA	79.86	48.77	37.19	30.48	20.73
	RCP 4.5	84.20	56.16	42.81	34.88	22.61
	RCP 8.5	95.25	62.92	47.19	37.55	26.53

Source: University of California, Irvine and University of California, Los Angeles.

Table A-2: 50-yr Return Period Intensity-Duration-Frequency curves based on historical records (NOAA) and future climate (RCP 4.5 and RCP 8.5).

Location	Based on	1-day mm/day	2-day mm/day	3-day mm/day	4-day mm/day	7-day mm/day
Eureka	NOAA	140.21	91.44	68.88	57.30	42.06
	RCP 4.5	172.97	118.04	88.67	75.36	55.58
	RCP 8.5	189.50	140.80	103.22	85.40	61.09
Redding	NOAA	185.32	123.75	95.71	80.47	55.47
	RCP 4.5	198.84	136.41	104.23	90.39	62.60
	RCP 8.5	207.40	141.53	110.81	93.78	71.22
Sacramento	NOAA	121.31	73.76	54.86	44.50	31.09
	RCP 4.5	141.37	95.58	70.00	58.27	39.41
	RCP 8.5	148.79	95.99	74.68	61.00	45.10
San Francisco	NOAA	124.36	74.98	55.47	45.72	32.31
	RCP 4.5	141.70	90.23	68.35	56.21	37.98
	RCP 8.5	147.84	83.90	64.70	54.67	39.35
San Jose	NOAA	89.61	56.69	42.67	34.75	24.38
	RCP 4.5	91.41	59.10	46.52	37.42	28.04
	RCP 8.5	105.26	70.34	53.57	46.85	34.60
Fresno	NOAA	74.98	45.72	32.92	27.43	18.90
	RCP 4.5	81.34	52.31	38.61	31.41	20.94
	RCP 8.5	84.31	56.04	41.80	35.09	25.31
Monterey	NOAA	105.46	67.67	52.43	43.28	29.87
	RCP 4.5	114.63	73.74	56.77	46.95	33.06
	RCP 8.5	119.70	76.76	57.75	48.93	36.83
Santa Barbara	NOAA	176.17	112.78	86.56	71.93	48.77
	RCP 4.5	188.34	125.40	99.82	88.17	60.70
	RCP 8.5	211.95	135.88	110.89	100.93	69.14
Ventura	NOAA	165.20	109.12	84.73	71.32	48.16
	RCP 4.5	169.79	107.70	87.75	76.19	52.34
	RCP 8.5	181.50	120.64	103.41	85.71	64.56

Location	Based on	1-day mm/day	2-day mm/day	3-day mm/day	4-day mm/day	7-day mm/day
Los Angeles	NOAA	157.89	102.41	80.47	67.06	45.11
	RCP 4.5	169.39	115.15	93.96	81.55	51.64
	RCP 8.5	162.22	114.43	96.06	85.21	64.06
Riverside	NOAA	105.46	68.28	51.21	41.45	27.43
	RCP 4.5	104.61	69.87	52.93	44.35	27.92
	RCP 8.5	107.55	71.51	54.69	44.48	29.79
Palm Springs	NOAA	114.60	70.10	51.21	40.23	25.60
	RCP 4.5	126.22	75.86	56.97	46.38	28.02
	RCP 8.5	132.55	81.91	63.77	51.26	33.82
Irvine	NOAA	120.70	76.81	58.52	48.16	31.70
	RCP 4.5	111.23	74.22	58.01	51.75	32.56
	RCP 8.5	130.08	84.07	67.26	57.25	40.17
Temecula	NOAA	166.42	106.68	79.86	68.28	46.94
	RCP 4.5	187.46	121.21	94.22	80.75	52.06
	RCP 8.5	188.48	128.21	98.03	88.31	63.62
Escondido	NOAA	126.80	81.08	63.40	53.04	35.36
	RCP 4.5	136.92	88.71	67.56	56.05	37.35
	RCP 8.5	139.90	93.05	74.96	62.04	44.88
San Diego	NOAA	90.22	54.86	42.06	34.75	23.77
	RCP 4.5	96.59	65.26	49.95	41.17	26.14
	RCP 8.5	109.12	74.00	54.92	43.63	31.66

Source: University of California, Irvine and University of California, Los Angeles.

Table A-3: 100-yr Return Period Intensity-Duration-Frequency curves based on historical records (NOAA) and future climate (RCP 4.5 and RCP 8.5).

Location	Based on	1-day mm/day	2-day mm/day	3-day mm/day	4-day mm/day	7-day mm/day
Eureka	NOAA	156.67	101.80	76.81	63.40	46.33
	RCP 4.5	195.87	132.00	98.25	83.83	62.30
	RCP 8.5	217.38	165.12	119.57	98.39	70.06
Redding	NOAA	204.22	135.94	105.46	88.39	61.57
	RCP 4.5	218.00	150.56	115.23	100.52	68.92
	RCP 8.5	228.86	153.77	121.17	101.84	79.06
Sacramento	NOAA	136.55	82.30	60.96	49.38	34.14
	RCP 4.5	161.28	110.22	79.24	66.52	44.64
	RCP 8.5	168.65	106.32	82.85	67.39	49.95
San Francisco	NOAA	142.04	85.34	62.79	51.82	35.97
	RCP 4.5	164.26	104.17	77.84	64.53	42.50
	RCP 8.5	168.08	92.77	71.76	59.88	42.19
San Jose	NOAA	103.63	64.62	48.16	39.62	27.43
	RCP 4.5	104.61	66.00	52.14	42.78	31.96
	RCP 8.5	120.43	79.20	59.61	53.12	38.98
Fresno	NOAA	85.34	51.82	37.80	31.09	21.34
	RCP 4.5	92.87	60.19	44.72	36.07	23.96
	RCP 8.5	96.62	64.03	48.47	39.88	29.20
Monterey	NOAA	121.92	77.42	59.13	49.38	34.14
	RCP 4.5	133.72	85.13	63.90	53.17	38.11
	RCP 8.5	138.92	87.48	64.43	55.24	41.75
Santa Barbara	NOAA	195.68	126.19	97.54	80.47	54.86
	RCP 4.5	210.45	141.20	114.21	101.52	70.38
	RCP 8.5	234.34	149.30	124.80	113.57	76.86
Ventura	NOAA	180.44	120.09	93.88	79.25	53.64
	RCP 4.5	181.77	115.17	95.28	83.15	57.15
	RCP 8.5	193.64	131.89	116.90	95.80	73.26

Location	Based on	1-day mm/day	2-day mm/day	3-day mm/day	4-day mm/day	7-day mm/day
Los Angeles	NOAA	179.22	116.43	91.44	76.20	51.82
	RCP 4.5	196.07	132.96	109.11	95.11	60.47
	RCP 8.5	177.50	125.57	107.05	96.81	75.81
Riverside	NOAA	120.09	78.03	58.52	47.55	31.70
	RCP 4.5	118.41	78.24	59.46	50.28	31.55
	RCP 8.5	120.00	79.58	60.63	49.37	33.46
Palm Springs	NOAA	134.11	82.30	60.35	47.55	30.48
	RCP 4.5	147.65	88.61	66.96	55.06	33.27
	RCP 8.5	153.82	94.73	75.18	60.17	40.63
Irvine	NOAA	137.16	87.78	67.06	54.86	35.97
	RCP 4.5	124.44	83.58	65.75	58.50	36.42
	RCP 8.5	147.25	96.12	77.55	65.17	45.98
Temecula	NOAA	188.37	123.14	93.27	80.47	55.47
	RCP 4.5	214.92	140.70	110.63	95.45	62.35
	RCP 8.5	211.41	146.70	113.00	103.39	76.40
Escondido	NOAA	143.26	92.66	72.54	60.35	40.84
	RCP 4.5	155.95	101.78	76.82	63.40	43.26
	RCP 8.5	158.02	105.79	85.60	70.38	52.55
San Diego	NOAA	99.97	61.57	46.94	38.40	26.21
	RCP 4.5	108.27	75.48	57.76	46.85	29.08
	RCP 8.5	122.84	86.23	63.41	50.17	36.24

Source: University of California, Irvine and University of California, Los Angeles.

APPENDIX B-1: Regarding Twenty-First Century Temperature Changes Over California: 9-km Hybrid Downscaling

By Yen-heng Lin (yenhenglin@g.ucla.edu), Alex Hall, and Neil Berg
University of California, Los Angeles
Department of Atmospheric and Oceanic Sciences
Institute of the Environment and Sustainability

Acronyms

Term	Description
CMIP5	Coupled Model Intercomparison Project, Phase 5
CMIP6	Coupled Model Intercomparison Project, Phase 6
CNRM-CM5	GCM from Centre National de Recherches Météorologiques (France)
GCM	Global climate model
GFDL-CM3	GCM from National Atmospheric and Oceanic Administration/Geophysical Fluid Dynamics Laboratory (USA)
INMCM4	GCM from Institute of Numerical Mathematics (Russia)
IPCC	Intergovernmental Panel on Climate Change
IPSL-CM5A-LR	GCM from L'Institut Pierre-Simone Laplace (France)
MPI-ESM-LR	GCM from Max Planck Institute for Meteorology (Germany)
RCM	Regional climate model
SAF	Snow albedo feedback
SCF	Snow cover fraction
StatWRF	Statistical emulator of the high-resolution temperature changes produced by the Weather Research and Forecasting Model simulations
WRF	Weather Research and Forecasting Model

Abstract

This study projects future temperature changes over the state of California using a hybrid dynamical–statistical framework to achieve high-resolution patterns. Projections from 31 global climate models (GCMs) in phase 5 of the Coupled Model Intercomparison Project (CMIP5) are downscaled to a 9-km resolution over California. The study focuses on temperature changes during the middle (2041–2060) and the end (2081–2100) of the 21st century compared to the historical climate (1981–2000) under two Representative Concentration Pathway (RCP) scenarios: RCP8.5 (business as usual) and RCP4.5 (stabilization scenario). The hybrid downscaling ensemble projections indicate that during the middle of the 21st century under RCP4.5 (RCP8.5), average temperature across California is expected to be about 2.0 °C (2.5 °C) warmer than the historical value. During the end of the 21st century, temperature is

expected to increase by 2.6 °C annually under the RCP4.5, and by 4.2 °C in the winter and spring and 5.6 °C in the summer and fall under RCP8.5. Moreover, due to the rapid loss of snow in mountain regions under future warming scenarios, the snow albedo feedback leads to localized zones of concentrated warming in regions of strong snow reductions compared to non-mountainous regions.

1. Introduction

There are two major uncertainties in climate models when projecting future climate changes over California. First, there is large uncertainty in the physics contained in global climate model (GCM) simulations of future environments, such as hydrological processes, cloud formation, and wind circulations. To capture a range of how these processes may unfold in the future, large ensembles of climate models are simulated and analyzed to form a range of possible future scenarios. Specifically, the World Meteorology Organization Intergovernmental Panel on Climate Change (IPCC) organizes the Coupled Model Intercomparison Project (CMIP) [Taylor et al., 2012] to conduct multiple climate model simulations forced by different scenarios of greenhouse gas emissions. The ensemble results provide a range of future projections, which presents more reliable results than only analyzing a single model [Knutti and Sedláček, 2013]. Over 30 GCMs participated in phase 5 of CMIP (CMIP5), which informed the IPCC's Fifth Assessment Report (AR5).

Second, there is uncertainty due to the spatial scale of GCMs (on the order of 100 km), which cannot accurately resolve the complex topography of California, including its coasts, valleys, and high mountains. For example, the Sierra Nevada is only represented by a few grid cells that have poorly interpolated elevations in most GCMs. As such, these global-scale projections are heavily biased and inaccurate in their projections over much of California and need to be translated to finer scales for more credible assessments of future climates.

Two primary techniques are used to “downscale” coarse-scale GCM projections down to finer scales: dynamical downscaling and statistical downscaling. The dynamical downscaling approach utilizes GCM simulation data as boundary conditions to drive a high-resolution regional climate model (RCM) over the region of focus. The RCM provides the most physically consistent projection as it solves the equations of motion over limited regions – and more accurately resolves physics for regions with a complex environment [e.g., Mass et al. 2002; Plummer et al. 2006] - however, it requires a high demand of computing capacity. This often leads to a tradeoff of not being able to downscale many GCMs (or different greenhouse gas scenarios for a given GCM) to finer scales, which limits the range of possible future scenarios that can be analyzed.

Statistical downscaling is another approach to generate high-resolution regional climate change projections. This approach develops various statistics-based empirical relationships between coarse-scale and fine-scale historical data and applies those relationships to downscale future GCM data to estimate regional changes from GCM output. This method has a much lower computational demand than dynamical downscaling, which allows for an efficient downscaling of many GCMs and emissions scenarios, helping reduce the uncertainty across models/scenarios [Benestad et al., 2018]. However, the empirical relationships are derived from historical data and they may not hold in a non-stationary future climate. This limitation is particularly relevant for regions like the Sierra Nevada, where changing snow conditions and

the presence of the snow albedo feedback can significantly alter coarse-to-fine-scale relationships in the future [Walton et al., 2017].

Berg et al. [2015] and Walton et al. [2015, 2017] combined the physical realism of dynamical downscaling and the computational efficiency of statistical downscaling together to form a new dynamical-statistical “hybrid” downscaling approach for projecting regional climate changes over the Los Angeles area and the Sierra Nevada. This report builds upon the hybrid downscaling technique to project future temperature changes across the entirety of California at 9 km. All available CMIP5 GCMs under multiple greenhouse gas emissions are downscaled for both the middle and end of the 21st centuries.

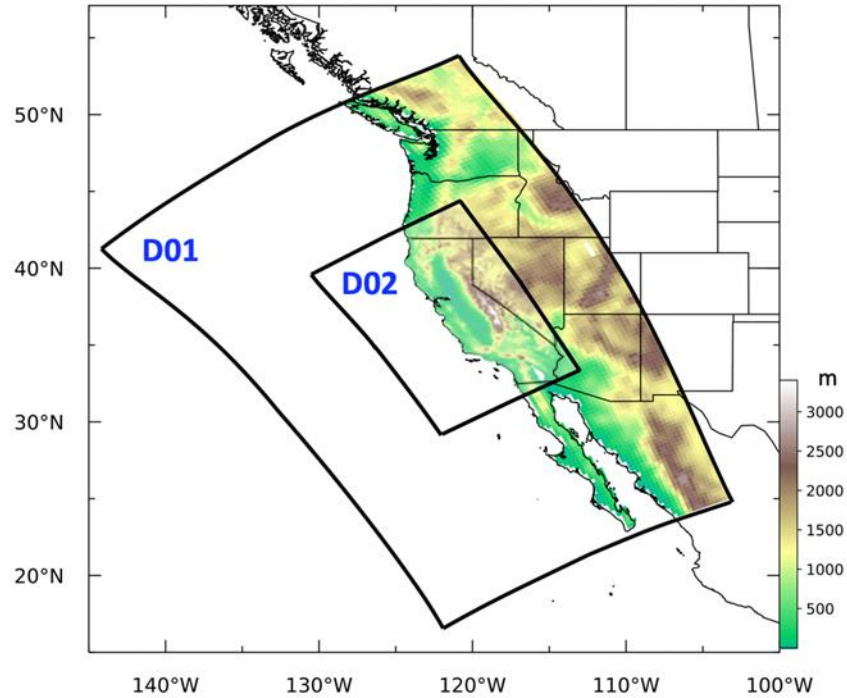
2. Methods

In this study, temperature projections from 31 CMIP5 GCMs are downscaled using a hybrid dynamical-statistical downscaling approach for analyzing high-resolution future temperature changes over California. The hybrid downscaling approach starts by using an RCM to first dynamically downscale historical and future high-resolution patterns. The historical simulations from this step are compared to observed gridded datasets to ensure their validity. Then, statistical relationships are developed between the raw GCM output driving the dynamically downscaled simulations and the downscaled changes themselves, in essence determining how to re-produce dynamically downscaled simulations through statistical means alone. These relationships are then applied to other GCMs to efficiently downscale their coarse-scale features to finer scales, forming an essential high-resolution ensemble of future temperature patterns.

2a. Dynamical downscaling

The National Center for Atmospheric Research Weather Research and Forecasting (WRF) model, version 3.5, [Skamarock et al. 2008] has been applied to dynamically downscale historical data and future projections over California. WRF has been extensively tested and proved to credibly simulate regional climates with physical consistency over the state [Lo et al. 2008; Bukovsky and Karoly 2009; Gilliam and Pleim 2010]. WRF’s configuration was tested with multiple modules and parameterizations to determine the best configuration for the complicated topographic area over California. In this study, WRF is coupled to the Noah Land Surface Model with Multi-Parameterization options [Noah-MP; Niu et al. 2011]. Two one-way nested domains with 27 km and 9 km resolution were simulated in this study (Figure B1-1). The 27 km domain simulates the large-scale general circulation around California and provides boundary conditions to the 9 km domain. There are 43 total vertical layers in the atmosphere and 30 layers below 3 km to improve the simulation of surface and boundary layer. Additional configuration details can be found in Walton et al. [2017].

Figure B1-1: Elevation (m) and model setup in this study with two one-way nested WRF domains (labeled D01 and D02) at resolutions of 27 and 9 km



Source: University of California, Los Angeles

A 1991-2000 historical simulation is first generated using 6-hourly North American Regional Reanalysis (Mesinger et al. 2006) data as boundary conditions. Five future climates spanning 2091-2100 are then simulated using the pseudo-global warming (PGW) method (Schär et al. 1996; Sato et al. 2007; Rasmussen et al. 2011). These future climates are based on five GCMs under RCP8.5: CNRM-CM5, GFDL CM3, INM-CM4.0, IPSL-CM5ALR, and MPI-ESM-LR; see Appendix b. In the PGW method, a future climate is produced by re-simulating the historical simulation with boundary conditions perturbed by end-of-century (2081-2100 minus 1981-2000) changes in temperature, specific humidity, zonal and meridional winds, and geopotential height according to the GCM in question. This method allows for a clear comparison between future and historical climates and avoids issues of internal variability from the GCM. However, it should be noted that variability between the historical and future projections are constant in a pseudo-global warming approach. For instance, the frequency of storms is constant in both time periods, but future magnitudes will differ. Overall, this method is best interpreted as examining how an observed historical climate may look in the future if everything else is held constant but large-scale climate changes in temperatures, humidity, pressure, and winds are imposed on the boundaries on the historical climate within the region in question.

2b. Statistical Downscaling

The statistical portion of the hybrid downscaling approach begins by developing a statistical emulator of the high-resolution temperature changes produced by the WRF simulations in section 2a (referred to as "StatWRF" in Walton et al. 2017). Two physical features have been considered in statistical models to reconstruct temperature distributions over California [Walton et al. 2015; 2017]. One of the most important factors is the relationship between snow albedo feedback (SAF) and temperature. Following Walton et al. [2015, 2017], here the

total snow cover fraction (SCF) data from WRF output to understand the effect of SAF on temperature has been used. Equation 1 shows the relationship between the variations of SCF and surface temperature:

$$T_{reg}' = T' - \alpha \cdot SCF' + residual \quad (B - 1)$$

Primes indicate anomalies either from the historical or future periods, T_{reg} is the regional mean temperature over the California, and α is the SAF strength representing the impact of SCF on temperature. The residual term refers to the intercept term in the linear regression, which can be ignored because T_{reg}' is small and $T' - T_{reg}'$ and SCF' fluctuate around zero. This equation shows that the temperature anomaly in any grid cell (T') can be decomposed into the change of background temperature anomaly (T_{back}') and the effect of the SCF anomaly. To estimate the impact factors of SCF on temperature, in each month, a linear regression analysis was applied to ($T' - T_{reg}'$) and (SCF') to generate the α value from all combined years in the historical and future time periods. When calculating the local SAF strength α , the additional warming contributed from the local SCF can be subtracted from the temperature change to produce a "background warming" ΔT_{back} in each grid cell of a given month:

$$\Delta T_{back} = \Delta T - \alpha \cdot \Delta SCF \quad (B - 2)$$

where Δ presents the climatological differences between WRF's future and historical runs. The value of ΔT_{back} is an estimation of temperature warming without the effect of local SAF. To estimate the background warming change, Walton et al. [2015, 2017] found that the regional-mean temperature warming and the dominant spatial variability pattern from the WRF background warming are key factors to reconstruct the background warming amount from the GCM.

$$\Delta T_{back}(x, y) = \Delta T_{ReMean} + \beta (\Delta T_{east} - \Delta T_{west}) PC1(x, y) \quad (B - 3)$$

Equation B-3 shows the formula of reconstructing background warming from the GCM. ΔT_{ReMean} contains the GCM regional climatological temperature difference; $PC1(x, y)$ is the spatial variability pattern identified via principal component analyses generated from the background warming patterns of the five WRF simulations, and represents the dominant background temperature change; $(\Delta T_{east} - \Delta T_{west})$ is the climatological temperature difference between land and ocean in GCM to setup a physical constraint of the temperature gradient in all GCMs; and β is temperature gradient stretch between land and ocean over the study area generated from the linear regression of the GCM-sampled warming difference $(\Delta T_{east} - \Delta T_{west})$ and the eigenvalue of $PC1$ to determine the value of β that appropriately scales the GCM warming differences to approximate $PC1$ loadings, while minimizing error. To constrain the background warming with zero east-west gradient, the intercept in the linear regression is set to zero. The east-west grid locations having the least error are located over the southern Sierra Nevada (120.13° W, 32.05° N) and the coastal ocean (115.74° W, 34.63° N). Since coarse-resolution GCMs poorly resolve SAF and its influences on regional mean temperatures (T_{ReMean}), the GCM ΔT_{ReMean} calculated from the mean temperature over California land areas is not consistent with the WRF ΔT_{ReMean} from December to April. To better estimate the ΔT_{ReMean} from the GCM in this season, a grid point in GCMs is used which can represent the ΔT_{ReMean} in WRF by selecting the point in GCM with the lowest root-mean-square error against the WRF ΔT_{ReMean} , and which is located at 34.85° N and 119.15° W.

The last step in the statistical model is to estimate the SCF change in the GCM. To understand the relationship between SCF and temperature, a logistic regression function between T and SCF from WRF output (1 historical and 5 future runs) is applied in Equation B-4:

$$SCF(T) = \frac{1}{1 + \exp[c(T - T^*)]} \quad (B - 4)$$

where c and T^* are constants computed via logistic regression. The change of SCF can be obtained through equation B-5:

$$\Delta SCF(T) = \frac{1}{1 + \exp[c(\Delta T + T_{hist} - T^*)]} - SCF_{hist} \quad (B - 5)$$

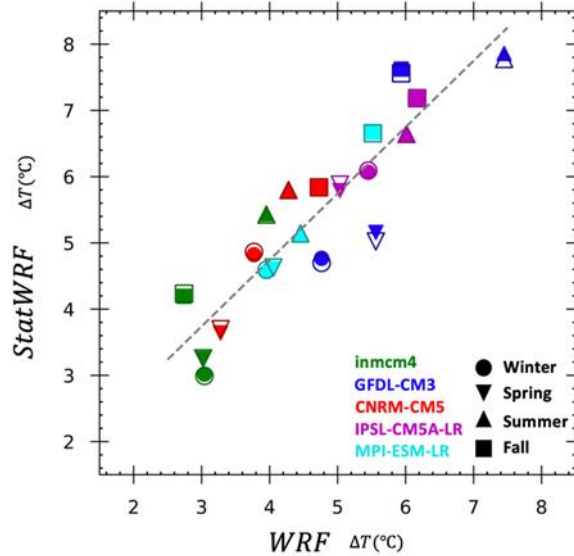
Equations B-3 and B-5 create the reconstruction of background warming and SCF changes from the WRF output that is applied to the CMIP5 CGMs output to estimate the multi-model temperature change in Equation B-2.

3. Results

3a. Evaluating Hybrid Model Performance

A cross-validation exercise is used to test how robust the hybrid model, StatWRF, is when re-creating downscaled features from the dynamical model, WRF, when only 4/5 downscaled models are used to predict changes from the 5th model. In essence, this is a leave-one-out-cross-comparison technique that reveals how sensitive statistical relationships are to its training dataset. The exercise is repeated for all combinations of the five models for seasonal changes, yielding 20 total data points for evaluation. The resulting scatter plot of this cross-validation exercise of regional-mean temperature changes is presented in Figure B1-2. The dynamical results from WRF are displayed on the x-axis, with the hybrid results on the y-axis, where the hybrid results are colored according to the model that is left-out in the validation exercise. The figure shows excellent agreement for all models and all seasons ($r^2 \sim 0.82$), indicating that the statistical relationships in StatWRF are not highly sensitive to the choice of 5 models versus 4 models in its training dataset. This provides more confidence that the hybrid technique can credibly be applied to any GCM to efficiently downscale future temperature changes.

Figure B1-2: Elevation (m) and model setup in this study with two one-way nested WRF domains (labeled D01 and D02) at resolutions of 27 and 9 km

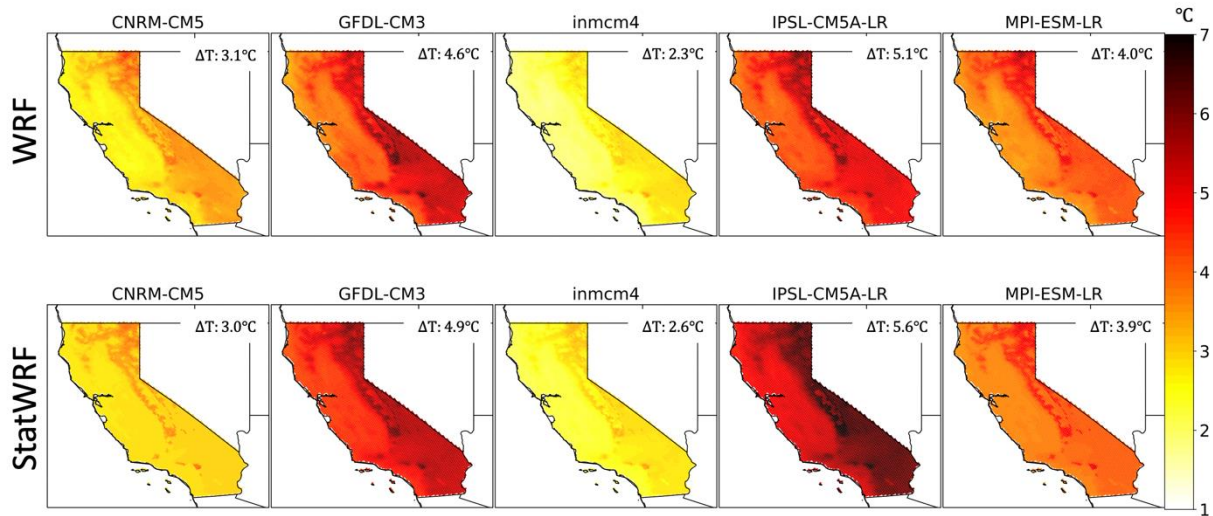


Warming values represent a downscaling of regional-mean temperature changes between the 1981–2000 and 2081–2100 periods in different seasons. Dashed line is the least squares line.

Source: University of California, Los Angeles

Moreover, Figure B1-3 further shows comparison between StatWRF (using all 5 dynamically downscaled results) and WRF output in March when is expected have the largest change of snow cover fraction [Bales et al. 2011; Walton et al. 2017; Sun et al. 2019]. Specifically, it shows the end-of-century projected temperature changes for each of the 5 downscaled GCMs according to StatWRF and WRF in March. The figure shows that StatWRF can successfully emulate WRF’s spatial detail of temperature changes (spatial correlation coefficient > 0.94 with 99 percent confidence), particularly the coastal gradient and sharply varying elevation-based gradients of temperature across the Sierra Nevada and other mountain regions. During the melting season, the middle-high elevations (1,500-3,000 meters) have the largest temperature changes across the state, which is related to the SAF as large snowpack reductions in these elevations dramatically increase future temperatures [Sun et al. 2015; Walton et al. 2017]. Moreover, the high variance of temperature changes across the 5 models demonstrates the necessity of examining multi-model ensembles to better capture the range of potential future scenarios over California.

Figure B1-3: (top) WRF March warming patterns (°C). (bottom) StatWRF March warming patterns



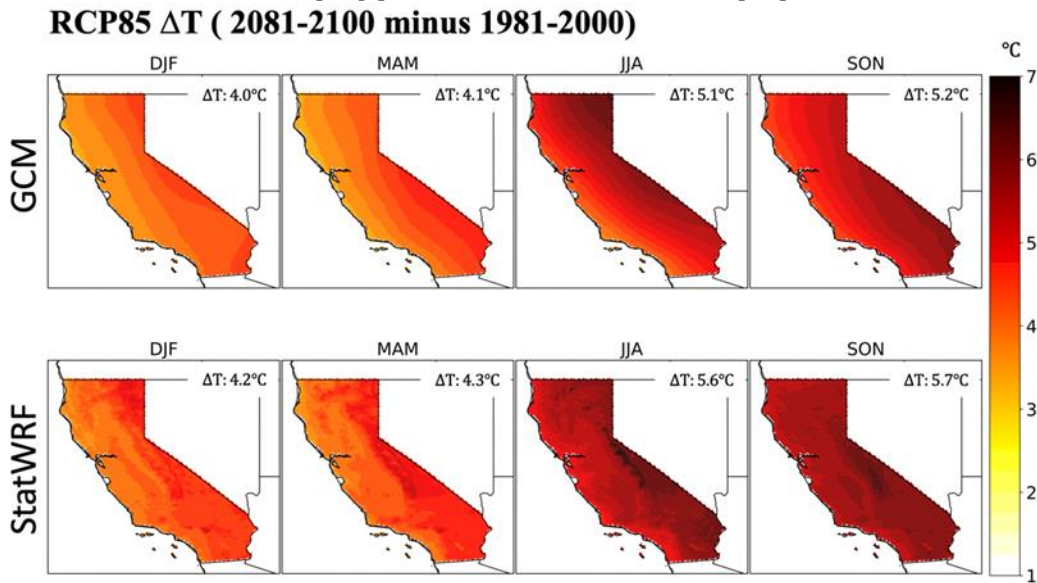
Warming patterns represent a downscaling of GCM temperature changes between the 1981–2000 and 2081–2100 periods.

Source: University of California, Los Angeles

3b. Value Added from Downscaling

With confidence in the ability for the hybrid model to credibly downscale warming signals over California using the 5 dynamically downscaled GCMs (Figures B1-2 and B1-3), then temperature changes downscaled for 31 CMIP5 GCMs using the hybrid approach. Figure B1-4 reveals the ensemble mean of seasonal temperature changes under RCP8.5 at the end of 21st century between simple linearly interpolated output of 31 CMIP5 GCMs and their hybrid downscaled patterns using StatWRF. Both GCM and StatWRF ensemble-mean temperature changes show coastal-to-inland temperature gradient patterns, but only StatWRF is able to resolve fine-scale geographic features across the state, critical for providing information for at local scales. In general, the downscaled datasets project 5.0 °C warming on an annual-average for the entire state by the end of the century, with more warmth in mountain regions (5.5°C, > 1500m) and less warmth in Central Valley and coast regions (4.7 °C), In addition, in the peaks of the Sierra Nevada (>3,000m) temperature changes show less warming than middle-high elevation areas (1,500-3,000m) in the winter and spring. On the contrary, in the summer and fall, warmer temperatures in the peaks of the Sierra Nevada are much warmer than lower-lying areas. Surface hydrological changes in snow water equivalent, snowmelt timing, and initiation of evaporation from soils under the warming temperature may result in different warming rates over different elevations [Walton et al. 2017; Sun et al. 2019]. These features of temperature changes do not exist in the coarse-resolution GCM projections, highlighting the importance and value added of downscaling GCMs to finer scales for more accurate projections of temperature change over California.

Figure B1-4: Temperature changes between 2081–2100 and 1981–2000 for (top) linearly interpolated GCM ΔT ($^{\circ}\text{C}$) averaged from 31 RCP8.5 GCMs, and (bottom) as in (top), but for StatWRF ΔT ($^{\circ}\text{C}$)

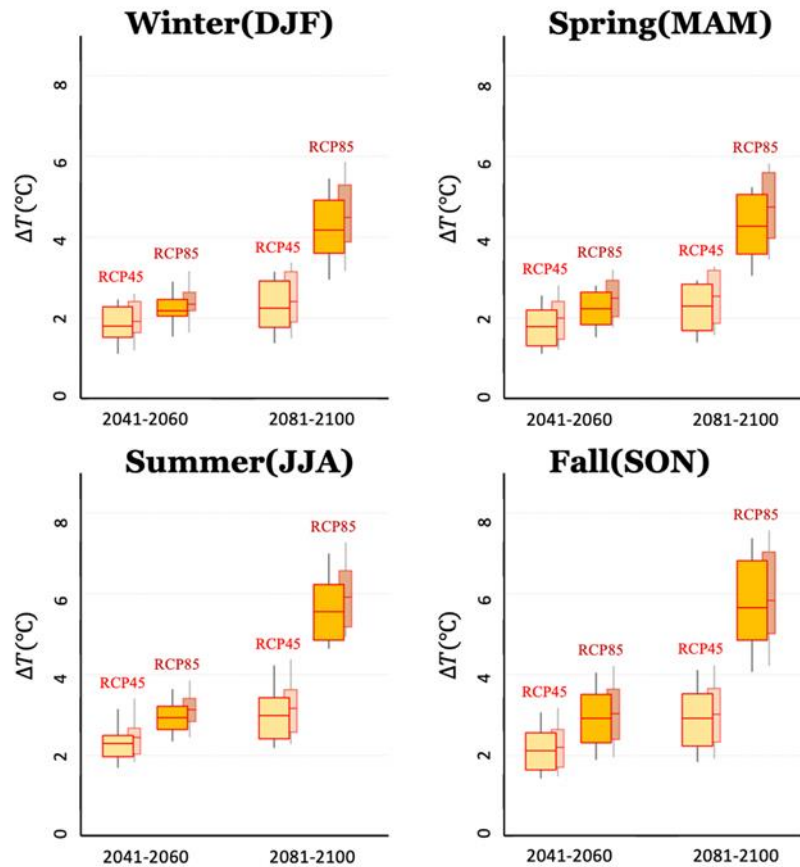


Source: University of California, Los Angeles

3c. Impact of Different Greenhouse Gas Emissions Scenarios

To assess the impact of different greenhouse gas pathways in the 21st century on California climate, Figure B1-5 compares seasonal-mean temperatures over the entire state and just the high-elevations between RCP4.5 and RCP8.5 during the middle and the end of the 21st centuries. During the middle of the 21st century, statewide ensemble-mean temperature changes between RCP4.5 and RCP8.5 are about 2.0 and 2.5 $^{\circ}\text{C}$ warmer compared to the historical climate (1981-2000), respectively. A similar result is found when only considering high-elevation regions. As such, there is not a significant difference in temperatures across the state by mid-century between the two greenhouse gas scenarios. However, at the end of the 21st century, the projections of ensemble-mean temperature changes under the RCP8.5 scenario show dramatic warming of about 4.2 $^{\circ}\text{C}$ warmer in the winter and spring and 5.6 $^{\circ}\text{C}$ warmer in the summer and fall, which is about 2.3 $^{\circ}\text{C}$ warmer than the RCP4.5 scenario. In addition, temperature changes over high-elevation areas (> 1,500m) are about 0.4 $^{\circ}\text{C}$ warmer than in low-elevation areas (\leq 1,500m) in all seasons.

Figure B1-5: StatWRF ΔT warming estimations in California between 2041-2060 and 1981-2000 periods and between 2081-2100 and 1981-2000 for RCP4.5 and RCP8.5



The line within the box indicates ΔT ensemble mean; the bottom and top of box indicate the ensemble 25 percent to 75 percent range, and the vertical lines extending from the box represent the 10 percent to 90 percent ensemble range. The light-color bar on the right shows ΔT for elevations that are higher than 1,500 meters.

Source: University of California, Los Angeles

4. Summary

In this report, a hybrid dynamical–statistical approach (StatWRF) was used to downscale the CMIP5 GCMs to 9 km resolution for fine-scale temperature projections over California during the 21st century. A cross-validation exercise is used to demonstrate the credibility of StatWRF successfully reproducing fine-scale features of temperature changes from the full dynamical solution from WRF. To reduce the uncertainty of physics contained in GCMs and across different greenhouse gas emissions scenarios, StatWRF is used to downscale 31 CMIP5 GCM models under two emissions scenarios: RCP4.5 and RCP8.5. The downscaled ensemble reveals that statewide temperatures under RCP4.5 (RCP8.5) are projected to increase by about 2.0 (2.5) $^{\circ}\text{C}$ in the middle of the 21st century and 2.6 (5.0) $^{\circ}\text{C}$ at the end of 21st century compared to the historical (1981-2000) climate. There are clear patterns of changes according to elevation and by season. Mid- and high-elevation areas (>1,500 m) are projected to experience more warmth than low-elevation areas (< 1,500 m) due to the presence of the snow albedo feedback. In terms of seasonality, temperatures in the dry season are projected to warm about 1.4 $^{\circ}\text{C}$ more

than changes in the wet season. These fine-scale warming patterns with season and elevation in the high-resolution downscaling projections are generally absent in the GCMs. Thus, using a hybrid downscaling approach to credibly and efficiently project changes in local temperature variations that incorporate variations of snow cover fraction, snow water equivalent, and soil moisture across California [Howat and Tulaczyk 2005; Pagán et al. 2016; Sun et al. 2019].

Overall, the findings in this report indicate that a hybrid-downscaling approach that combines the benefits of physical realism associated with dynamical downscaling and the computational efficiency of statistical downscaling can provide a credible way to downscale a large ensemble of GCM temperature projections. These high-resolution projections of future climate provide important and necessary information for understanding regional climate changes and adaptation planning in California. Looking forward, there are expected advancements in both GCMs and RCMs, both of which offer opportunities to generate more reliable projections and accurate downscaled projections over California. In preparation for the next IPCC report, a new phrase of GCMs and associated intercomparison project, CMIP6, is currently being conducted. As CMIP6 GCMs become available, they will offer new global-scale datasets that may improve upon CMIP5 projections and offer better large-scale inputs to a hybrid downscaling model. RCMs like WRF are also continuously being updated and improved through new parameterizations, which should further improve the accuracy of downscaled projections.

References

- Bales, R. C., J. J. Battles, Y. Chen, M. H. Conklin, E. Holst, K. L. O'Hara, P. Saksa, and W. Stewart, 2011: Forests and water in the Sierra Nevada: Sierra Nevada watershed ecosystem enhancement project. Sierra Nevada Research Institute Rep. 11.1, 39 pp. [Available online at <http://ucanr.edu/sites/cff/files/146199.pdf>.]
- Benestad, R. E., I. Hanssen-Bauer, and D. Chen, 2008: Empirical-Statistical Downscaling. World Scientific, 228 pp.
- Berg, N., A. Hall, F. Sun, S. Capps, D. Walton, B. Langenbrunner, and J. D. Neelin, 2015: Twenty-first-century precipitation changes over the Los Angeles region. *J. Climate*, 28, 401–421, doi:10.1175/JCLI-D-14-00316.1.
- Bukovsky, M. S., and D. J. Karoly, 2009: Precipitation simulations using WRF as a nested regional climate model. *J. Appl. Meteor. Climatol.*, 48, 2152–2159.
- Gilliam, R. C., and J. E. Pleim, 2010: Performance assessment of new land surface and planetary boundary layer physics in the WRF-ARW. *J. Appl. Meteor. Climatol.*, 49, 760–774, doi:10.1175/2009JAMC2126.1
- Howat, I. M., and S. Tulaczyk, 2005: Trends in spring snowpack over a half-century of climate warming in California, USA. *Ann. Glaciol.*, 40, 151–156, doi:https://doi.org/10.3189/172756405781813816.
- Intergovernmental Panel on Climate Change, 2014: Climate change 2014: Impacts, adaptation, and vulnerability. Contributions of working group II to the fifth assessment report. Cambridge, England/New York, NY: Cambridge University Press.

- Knutti, R., and J. Sedláček, 2012: Robustness and uncertainties in the new CMIP5 climate model projections. *Nat. Climate Change*, 3, 369–373, doi:10.1038/nclimate1716.
- Lo, J. C. F., Z. L. Yang, and R. A. Pielke Sr., 2008: Assessment of three dynamical climate downscaling methods using the Weather Research and Forecasting (WRF) model. *J. Geophys. Res.*, 113, D09112. doi:10.1029/2007JD009216.
- Mass, C. F., D. Ovens, K. Westrick, and B. A. Colle, 2002: Does increasing horizontal resolution produce more skillful forecasts? *Bull. Amer. Meteor. Soc.*, 83, 407–430, doi:10.1175/1520-0477(2002)083<0407:DIHRPM.2.3.CO;2.
- Niu, G.-Y., and Coauthors, 2011: The community Noah land surface model with multiparameterization options (Noah-MP): 1. Model description and evaluation with local-scale measurements. *J. Geophys. Res.*, 116, D12109, doi:10.1029/2010JD015139.
- Pagán, B. R., A. Moetasim, D. Rastogi, D. R. Kendall, S. Kao, B. S. Naz, R. Mei, and J. S. Pal., 2016: "Extreme Hydrological Changes in the Southwestern US Drive Reductions in Water Supply to Southern California by Midcentury." *Environmental Research Letters* 11 (9): 1–11. doi:10.1088/1748-9326/11/9/094026.
- Plummer, D. A., and Coauthors, 2006: Climate and climate change over North America as simulated by the Canadian RCM. *J. Climate*, 19, 3112–3132, doi:10.1175/JCLI3769.1.
- Rasmussen, R., and Coauthors, 2011: High-resolution coupled climate runoff simulations of seasonal snowfall over Colorado: A process study of current and warmer climate. *J. Climate*, 24, 3015–3048, doi:10.1175/2010JCLI3985.1.
- Sun, F., A. Hall, M. Schwartz, D. B. Walton, and N. Berg, 2016: Twenty-first-century snowfall and snowpack changes over the Southern California mountains. *Journal of Climate*, 29(1), 91–110. <https://doi.org/10.1175/JCLI-D-15-0199.1>
- Sun, F., N. Berg, A. Hall, M. Schwartz, and D. Walton, 2019: Understanding end-of-century snowpack changes over California's Sierra Nevada. *Geophysical Research Letters*, 46, 933–943. <https://doi.org/10.1029/2018GL080362>
- Sato, T., F. Kimura, and A. Kitoh, 2007: Projection of global warming onto regional precipitation over Mongolia using a regional climate model. *J. Hydrol.*, 333, 144–154, doi:10.1016/j.jhydrol.2006.07.023.
- Schär, C., C. Frie, D. Luthi, and H. C. Davies, 1996: Surrogate climate-change scenarios for regional climate models. *Geophys. Res. Lett.*, 23, 669–672, doi:10.1029/96GL00265.
- Skamarock, W. C., and Coauthors, 2008: A description of the Advanced Research WRF version 3. NCAR Tech. Note NCAR/TN-4751STR, 113 pp., doi:10.5065/D68S4MVH.
- Taylor, K. E., R. J. Stouffer, and G. A. Meehl, 2012: An overview of CMIP5 and the experiment design. *Bull. Am. Meteorol. Soc.* 93, 485–498

- Walton, D. B., F. Sun, A. Hall, and S. Capps, 2015: A hybrid dynamical–statistical downscaling technique. Part I: Development and validation of the technique. *J. Climate*, 28, 4597–4617, <https://doi.org/10.1175/JCLI-D-14-00196.1>.
- Walton, D. B., A. Hall, N. Berg, M. Schwartz, and F. Sun, 2017: Incorporating snow albedo feedback into downscaled temperature and snow cover projections for California’s Sierra Nevada. *J. Climate*, 30, 1417–1438, <https://doi.org/10.1175/JCLI-D-16-0168.1>.

APPENDIX B-2: Regarding 1981–2014 90-m Temperature Simulations and End-of-21st-Century 90-m Temperature Simulations

By Hsin-Yuan Huang and Alex Hall
University of California, Los Angeles
Department of Atmospheric and Oceanic Sciences
Institute of the Environment and Sustainability

Acronyms

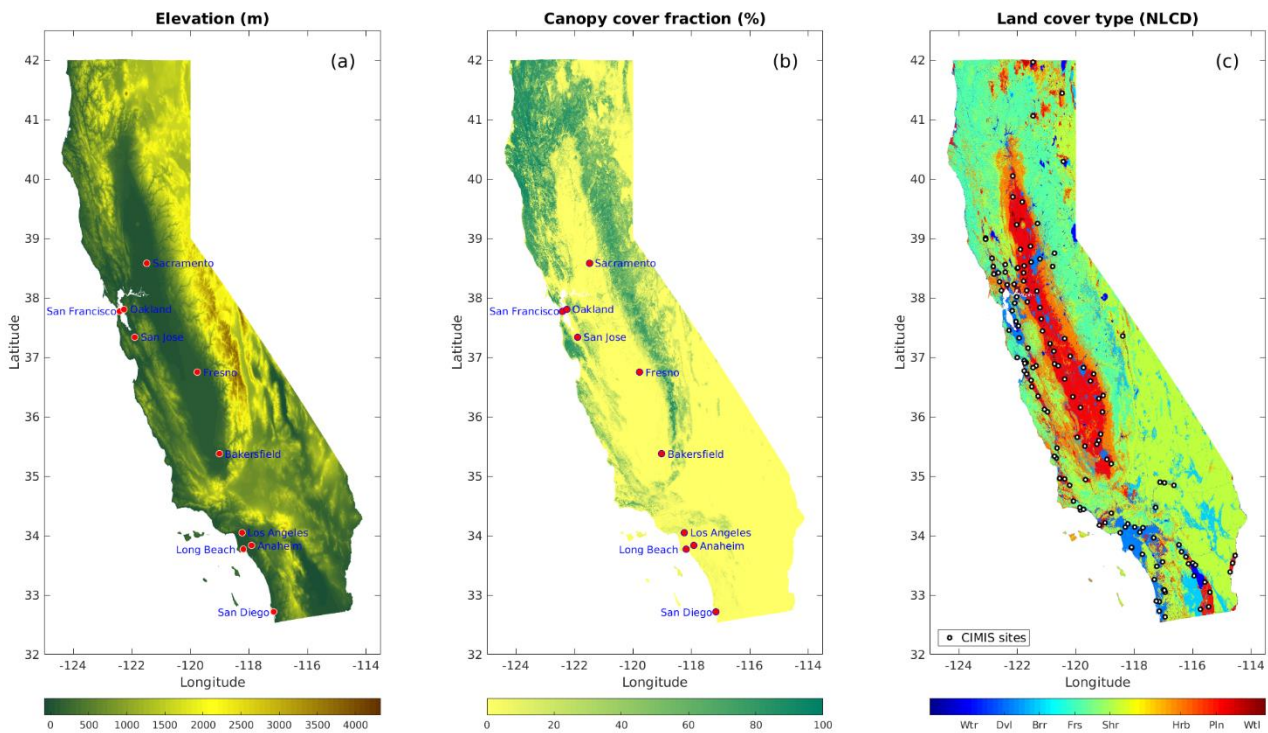
Term	Description
CIMIS	California Irrigation Management Information System
CMIP5	Coupled Model Intercomparison Project, Phase 5
CNRM-CM5	GCM from Centre National de Recherches Météorologiques (France)
GCM	Global climate model
GFDL-CM3	GCM from National Atmospheric and Oceanic Administration/Geophysical Fluid Dynamics Laboratory (USA)
INMCM4	GCM from Institute of Numerical Mathematics (Russia)
IPSL-CM5A-LR	GCM from L'Institut Pierre-Simone Laplace (France)
MPI-ESM-LR	GCM from Max Planck Institute for Meteorology (Germany)
NCEP	National Centers for Environmental Prediction
Ta	Air temperature
WRF	Weather Research and Forecast Model

I. Introduction

Climate change is expected to have significant impacts on air temperature in State of California, but these impacts are not yet quantified at very fine scales (e.g., hundreds of meters or finer). Global climate models (GCMs) are the most powerful tools climate scientists have to simulate the climate system and project future climates. This study uses data from a subset of GCM outputs in Phase 5 of the Coupled Model Intercomparison Project (CMIP5), which is the collection of GCM experiments underlying the 5th Assessment Report by the Intergovernmental Panel on Climate Change (IPCC) and represents the latest generation of GCMs. However, GCMs are very low in spatial resolution, outputting climate data points that represent very large areas (e.g., 100 km resolution or larger). For this reason, GCMs do not represent the complex topography of State of California, and therefore do not produce climate change projections that are spatially explicit enough to be employed in adaptation planning. Thus, the use of a regional climate model (e.g., Weather Research and Forecasting, WRF) to “downscale” GCM information to finer spatial scales (e.g. on the order of 10 km resolution) is required to obtain more details about near-surface atmospheric temperature.

The WRF model is a next-generation mesoscale numerical weather prediction system designed for both atmospheric research and operational forecasting applications. The model serves a wide range of meteorological applications across scales from tens of meters to thousands of kilometers. In the late 1990's, the development of WRF began at the National Center for Atmospheric Research, the National Oceanic and Atmospheric Administration, the National Centers for Environmental Prediction (NCEP), the Air Force Weather Agency, the Naval Research Laboratory, and the University of Oklahoma. WRF can produce simulations based on actual atmospheric conditions or idealized conditions. WRF offers operational forecasting on a flexible and computationally efficient platform, while reflecting recent advances in physics, numerical, and data assimilation contributed by developers from the expansive research community. WRF is currently in operational use at NCEP and other national meteorological centers as well as in real-time forecasting configurations at laboratories, universities, and private companies. Using reanalysis data as well as GCM data as a forcing to drive WRF simulations, this study simulates near-surface atmospheric conditions in a 9 km resolution grid covering the entire State of California (Figure B2-1a, topography shown at 90 m resolution).

Figure B2-1: Study domain's a) elevation, b) canopy cover fraction, and c) land cover type in 90-m resolution. Abbreviations in c) represent Water body (Wtr), Developed (Dvl), Barren (Brr), Forest (Frs), Shrubland (Shr), Herbaceous land (Hrb), Planted (Pln), and Wetland (Wtl)



Top 10 largest cities are shown in red dots. The black dots shown in c) are CIMIS sites where observations are collected

Source: University of California, Los Angeles

Though WRF is a powerful tool to simulate atmospheric variables of interest, it still has limitations when capturing geographical variations in soil and topography, which is on the order of a couple hundred meters or less. To perform WRF simulations with resolutions of

hundreds of meters is theoretically possible but not feasible due to the limitation of parameterizations included in the model. Therefore, the research group employed other approaches to downscale 9 km WRF outputs to even finer spatial scales necessary for detailed analyses. Details of this technique will be described in the Methodology section, followed by a brief discussion of the simulation results.

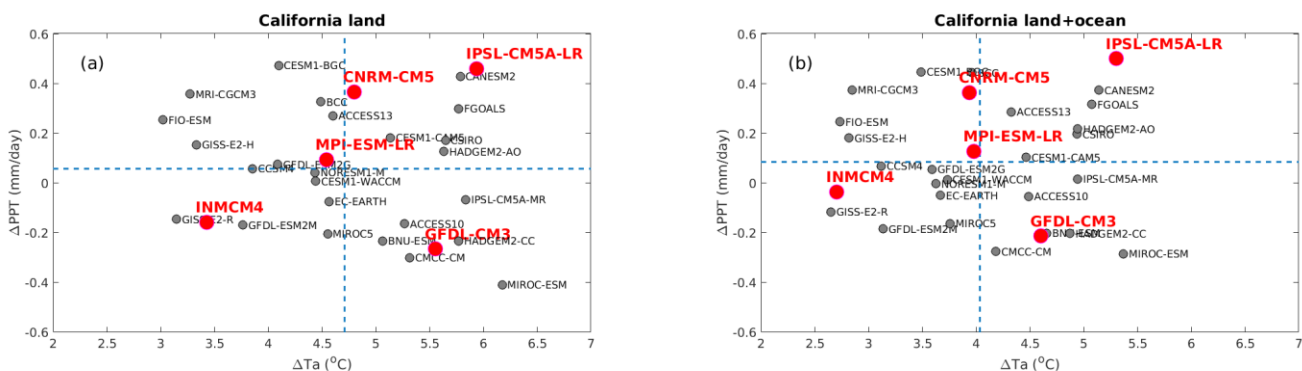
II. Methodology

1. Selection of Global Circulation Models

Since the changes in surface air temperature and precipitation between the future projections and the current climate are the key atmospheric characteristics to affect near-land variables, the research group selected a subset of GCMs to downscale air temperature based on these two variables. The 20-year mean changes in air temperature and daily precipitation between the end of the century (2081–2100) under the greenhouse gas emissions scenario of RCP8.5 and historical baseline (1981–2000) are shown in Figure B2-2. Each dot (gray markers) represents data from a CMIP5 GCM. GCM data over the entire California land domain are shown in the left panel and data for California land and coastal ocean domains are in the right panel.

Five selected GCMs are shown in red dots. MPI-ESM-LR is one GCM representing nearly no change in precipitation between the future projection and historical data. IPSL-CM5A-LR shows a much warmer and wetter future climate projection, while INMCM4 projects a lesser increase in air temperature and a reduction in precipitation. Additional two GCMs also selected that representing a warmer but dryer condition (GFDL-CM3) and a less warm but wetter condition (CNRM-CM5), to show the spread in GCM uncertainty.

Figure B2-2: Mean changes of surface air temperature (ΔT_a) and daily precipitation (ΔPPT) between future GCM simulations (2081–2100 with scenario RCP 8.5) and historical baseline (1981–2000)



a) Averaged over California land grids and b) averaged over California land grids and surrounding oceanic grids.

Source: University of California, Los Angeles

2. Fine-scale Downscaling Technique

The research group use the MicroMet scheme introduced in Liston and Elder (2006)¹ to downscale WRF 9 km resolution near-surface air temperature (at 2-m height) to 90-m resolution over the study domain covering the entire State of California as shown in Figure B2-1. This method is a quasi-physically based, high-resolution meteorological distribution model. It is designed specifically to produce high-resolution meteorological forcing distribution required to run a land surface model. Two basic assumptions of this method are: 1) all available data, at a given time, are spatially interpolated over the domain, and 2) physical sub-models are applied to each variable to improve parameter realism at a given point in space and time.

The spatial interpolation (horizontal and vertical) using a Barnes objective analysis scheme (e.g., Koch et al., 1983²), which applies a Gaussian distance-dependent weighting function and the weighting function, w , is described as:

$$w = \exp \left[-\frac{r^2}{f(dn)} \right],$$

where r is the distance between the observation and a grid point, and $f(dn)$ defines a filter parameter whose value gives how smooth the interpolation will be. Since the grid point values are weighted averages of the surrounding stations (i.e., lower-resolution grid points), the gridded values are always less than the maximum and greater than the minimum value surrounding the point. This method is able to achieve good success with high-resolution topography data (e.g., Digital Elevation Model³) and remotely sensed observations (e.g., Landsat data⁴).

Dodson and Marks (1997)⁵ summarize two of the most realistic and general methods used to distribute point air temperature data over mountainous terrain: assuming 1) neutral atmospheric stability, and 2) a constant linear lapse rate. They conclude that the constant linear lapse rate method most successfully reproduces the natural environment, but also note that lapse rates can vary widely over space and time. Since air temperature is highly affected by elevation, the elevation information is considered in downscaling temperature estimate (T).

First, the large-scale air temperatures (9 km resolution) are adjusted to a common level (i.e., sea level) using the formula of lapse rate. The reference-level large-scale temperatures are then interpolated to the model grid (i.e., 90 m resolution) using the Barnes objective analysis

¹ Liston G. E., and K. Elder (2006), A meteorological distribution system for high-resolution terrestrial modeling (MicroMet). *J. Hydromet.*, 7, 217-234.

² Koch, S. E., M. desJardins, and P. J. Kocin (1983), An interactive Barnes objective map analysis scheme for use with satellite and conventional data. *J. Climate Appl. Meteor.*, 22, 1487-1503.

³ <https://www.usgs.gov/faqs/what-are-digital-elevation-models-dems>.

⁴ https://www.nasa.gov/mission_pages/landsat/main/index.ht.

⁵ Dodson, R., and D. Marks (1997), Daily air temperature interpolation at high spatial resolution over a large mountainous region. *Climate Res.*, 8, 1-20.

scheme. The gridded topography data and lapse rate are then used to adjust the reference-level gridded temperatures to the elevations provided by the topography dataset, using

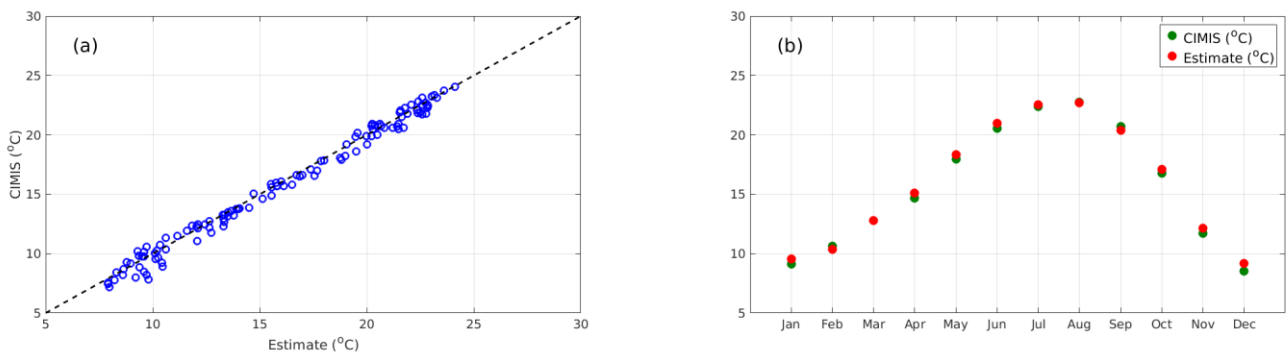
$$T = T_0 - \Gamma(z - z_0),$$

where T_0 is the interpolated temperature on Barnes scheme, Γ is a seasonal lapse rate, z is the elevation from topography dataset, z_0 is the reference-level elevation surface. For more details, the reader is referred to Liston and Elder (2006).

3. Model performance evaluation

The data of estimated air temperature (T_a) using above model is first compared to point-scale observations to see the model performance. The observations are collected from California Irrigation Management Information System⁶ (CIMIS) sites shown in Figure B2-1c. CIMIS is a program unit in the Water Use and Efficiency Branch, Division of Statewide Integrated Water Management, California Department of Water Resources, that manages a network of over 145 automated weather stations in California. It is clear that good agreement exists between model estimates and observations (Figure B2-3a). The correlation coefficient is 0.99 and the root-mean-square-error is about 0.7 °C. The model also well reproduces the seasonal cycle of air temperature and fits well with monthly mean observations (Figure B2-3b). This comparison provides us confidence to apply this technique to downscale WRF T_a outputs to a 90-m resolution.

Figure B2-3: Comparison of T_a between observations collected in CIMIS sites and model estimates: a) all data from October, 1991 to September 2001, b) monthly mean. Data are averaged across all 137 CIMIS sites



Source: University of California, Los Angeles

III. Overall Pictures of Downscaled Air Temperature

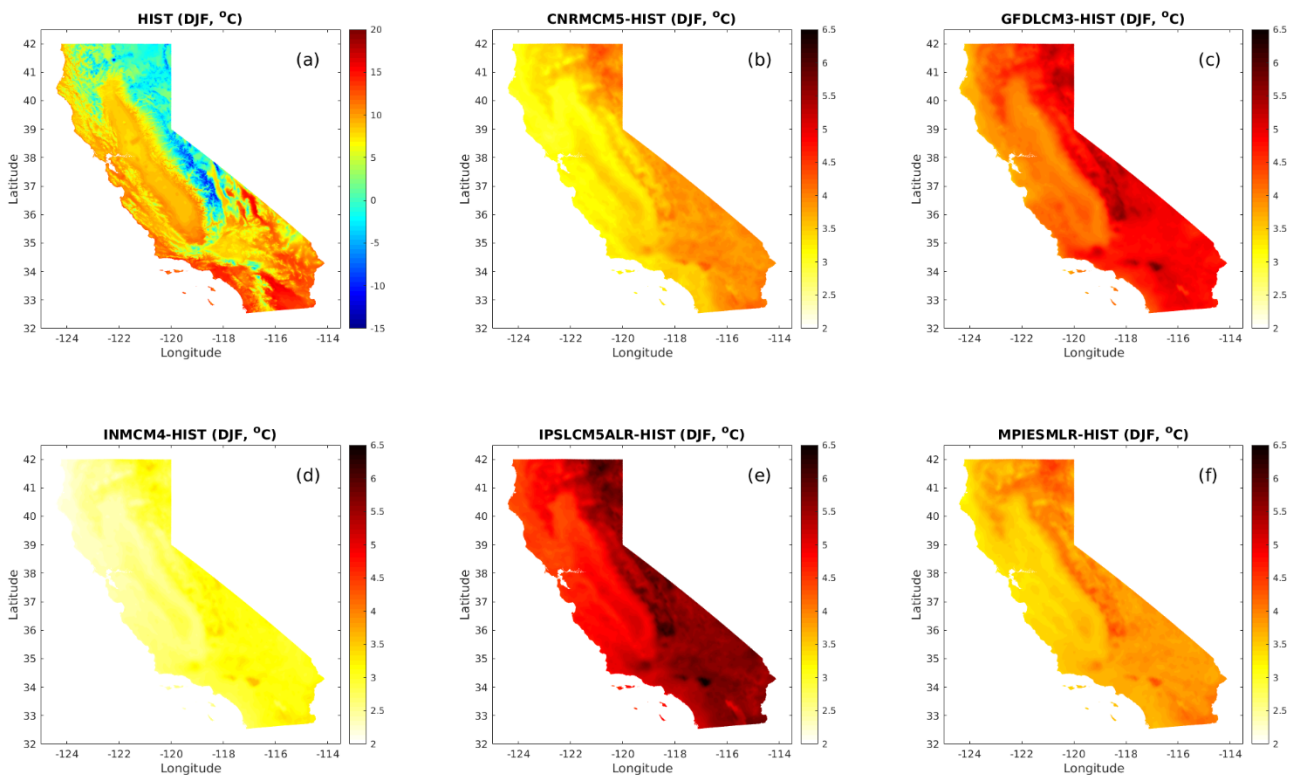
1. Temperature change in winter months

The research group first take a look at air temperature (T_a) in winter months (e.g., December, January, and February). The climatology of historical temperature data is shown in Figure B2-4a. It is clear that T_a is significantly affected by topographic elevation and land surface type.

⁶ <https://cimis.water.ca.gov/>

Higher Ta is seen in the coastal urban area and Mojave Desert, and lower Ta is seen in California’s Sierra Nevada, where most precipitation and snow accumulate. Projected temperature change from five selected GCMs (projection minus historical data) are shown in subplots 4b-4f. An overview shows that larger increases of Ta are seen in IPSL-CM5A-LR and GFDL-CM3 models, and smaller increases are seen in CNRM-CM5 and INMCM4. This result is consistent with Figure B2-2. For each projection, the smaller increase in Ta is seen in coastal urban areas and the Central Valley, whereas the larger increase is usually seen in mountainous regions, especially the Sierra Nevada. This is because of the difference in lapse rate between low-elevation and high-elevation areas simulated in future projections. Another reason could be due to differences in land surface type, where ground temperatures in urban areas are higher than those over vegetated regions.

Figure B2-4: Average air temperature in winter months (December, January, and February): a) historical and b–f) projected temperature change from selected GCMs



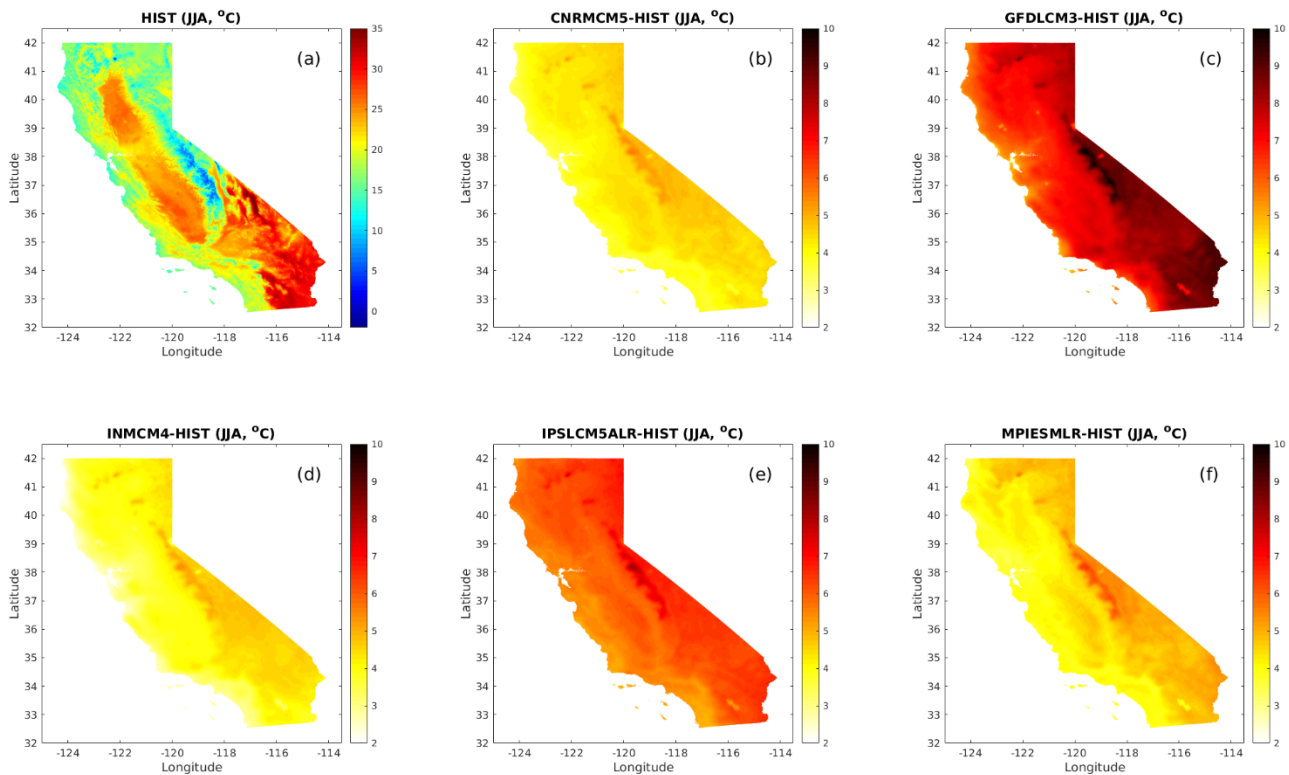
Source: University of California, Los Angeles

2. Temperature change in summer months

Results averaged over summer months (June, July, and August) are shown in Figure B2-5. The general pattern shown in Figure B2-5 is similar to what has been seen in Figure B2-4, but with greater magnitude. However, the GFDL-CM3 model here shows the largest increase in mean temperature over the entire study domain for summer months. There is a larger model spread during summer months than winter months. This indicates that at least within the small subset of downscaled GCMs analyzed in this study, models converge to a greater extent in their projections of future temperature over California during the cold season than they do in the warm season. However, the inclusion of more GCMs would likely increase the spread during

both seasons, so caution should be applied when interpreting these results, which are based only on a few GCMs. For more details about increase in Ta versus topography, the reader is referred to Sun et al. (2016)⁷.

Figure B2-5: Average air temperature in winter months (June, July, and August): a) historical and b–f) projected temperature change from selected GCMs



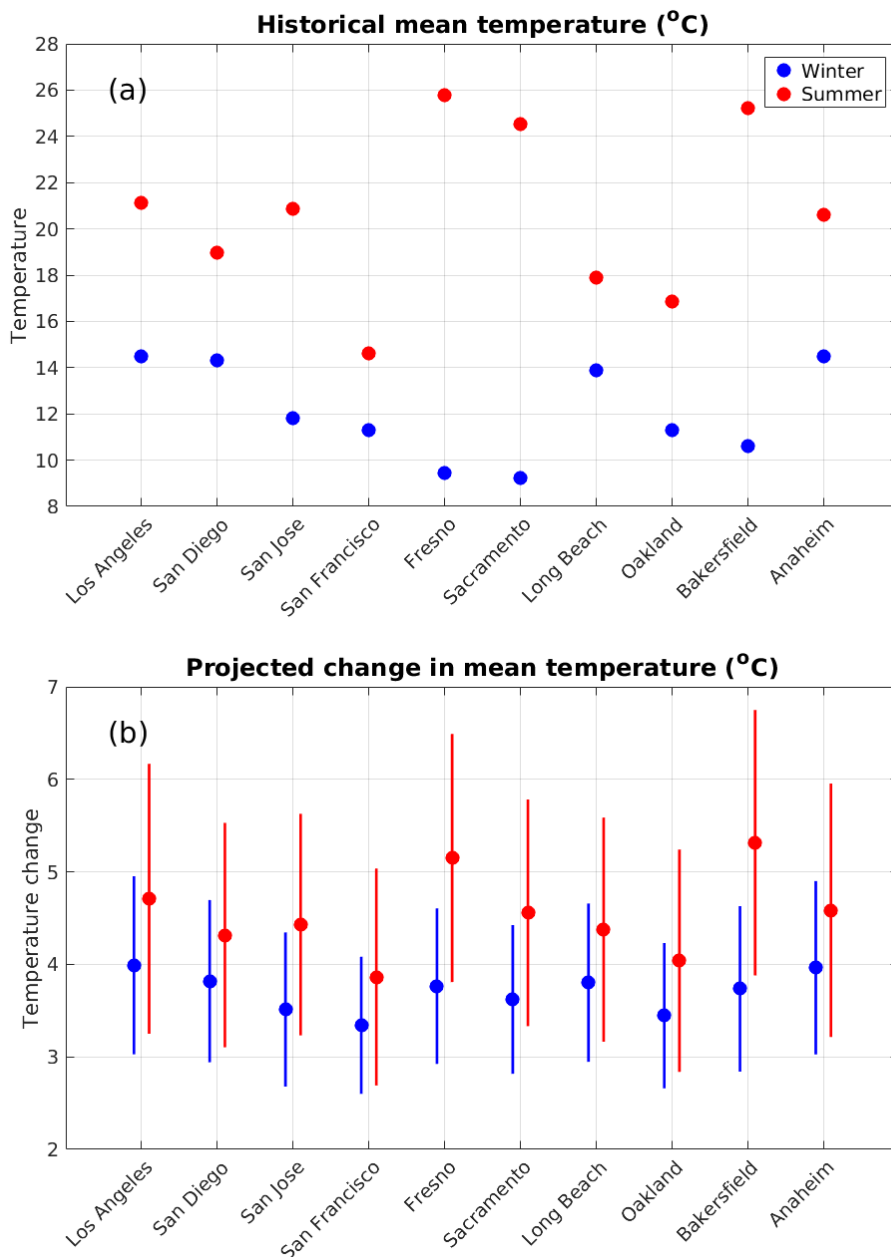
Source: University of California, Los Angeles

3. Temperature changes in big cities

Figure B2-6a shows the historical mean temperatures for winter (blue dots) and summer months (red dots). In winter months, temperatures in Southern California cities are generally higher than those in Northern California cities, as expected. However, in summer months, Sacramento and Fresno are hotter than other cities in Northern California. The reason could be the lack of sea breeze cooling down the air temperature in these cities located in the Central Valley. Figure B2-6b shows there is a larger spread of GCM projections (standard deviation shown as vertical bars) in summer than in winter, which is consistent with previous figures. The average increase in temperature is about 3.5 and 4.5 °C in winter and summer months, respectively. Larger differences in temperature increase between winter and summer are seen in Fresno and Bakersfield, both located in the Central Valley, a result similar to those shown in previous maps.

⁷ Sun, F., A. Hall, M. Schwartz, D.B. Walton, and N. Berg, (2016), Twenty-first century snowfall and snowpack changes over the Southern California mountains. *Journal of Climate*, 29(1), 91-110.

Figure B2-6: a) Mean air temperature for winter months (December-February, blue dots) and summer months (June-August, red dots) during the historical time period for major cities in State of California. b) Projected temperature changes from GCMs. The vertical bar represents standard deviation cross GCMs



Source: University of California, Los Angeles

VII. Data Description

1. Data files

Monthly air temperature data in 90-m resolution are saved in gridded format based on latitude and longitude information in /Surface folder.

2. Data format

Data are saved in a HDF5 file format, with unit of °C. The file name is in a format of

T2D_{model}_{rcp option}_{year}_{month}.h5

The parameters, text in {}, are:

model: HIST (historical data)

CNRMCM5, GFDLCM3, INMCM4, IPSLCM5ALR, and MPIESMLR (future projection)

rcp option: N/A for historical data

85 for GCM future projection

year: Data year (1981-2014 in historical and 2091-2100 for future projections)

month: Data month

For example, T2D_HIST_1981_01.h5 is the monthly temperature data for January, 1981. Dimensions of each file are 13450 (points in latitude) x 7886 (points in longitude). Data with NaN value indicates grid outside the simulation domain.

APPENDIX C:

Regional Climate Symposia Summary

The Local Government Commission (LGC) and Climate Resolve, in partnership with the California Energy Commission (CEC) and various local partners, organized a series of regional climate symposia to disseminate findings from California’s Fourth Climate Change Assessment, including deeper dives into the energy sector. The Symposia served as valuable venues to share best-available science, research findings, and adaptation strategies and tools, as well as to bring practitioners together from across each region.

Event	Date	Location	Lead	Partners
Inland Deserts Climate Symposium	10/12/18	Palm Desert, CA	Climate Resolve	LGC, CEC, OPR, CNRA
Los Angeles Climate Symposium	11/2/18	Long Beach, CA	Climate Resolve	LGC, CEC, OPR, CNRA, Los Angeles Regional Collaborative for Climate Action and Sustainability, Aquarium of the Pacific
San Joaquin Valley Climate Symposium	12/4/18	Fresno, CA	LGC	CEC, CNRA, Fresno Council of Governments, UC Merced, Central Valley Community Foundation
Central Coast Climate Symposium	12/10/18	San Luis Obispo, CA and Santa Cruz, CA	LGC	CEC, CNRA, California Water Boards Central Coast, Central Coast Climate Collaborative, UC Santa Cruz

Source: University of California, Irvine and University of California, Los Angeles

Participation

LGC and Climate Resolve worked proactively to conduct targeted outreach and work with local partners to attract a diverse range of participants across sectors. Through mass emailing campaigns, targeted invitations, recruitment of promotional partners, and engagement with local media outlets, organizers worked to attract both practitioners and members of the public. Each symposium was well-attended and received overwhelmingly positive feedback from both participants and speakers.

Region	Total Participants	Public Agencies*	Non-profit Organizations*	Private Sector Companies*
Inland Deserts	143	19	10	5
Los Angeles	150	28	22	6
San Joaquin Valley	77	16	23	13
Central Coast	154	33	21	18
Total	524	96	76	42

*Counts reflect unique agencies, organizations, and/or companies rather than the total number of public, non-profit, or private sector participants. Public members, academic institutions, and universities are not reflected in these columns.

Source: University of California, Irvine and University of California, Los Angeles

Speakers and Panelists

LGC and Climate Resolve managed all aspects of planning and hosting the symposia, including working closely with partners to develop the agenda, and inviting and coordinating with speakers and panelists. Each symposium featured a mix of presentations and panel discussions featuring leading climate experts.

Event	Public Agencies	Non-profits, Universities, and Private Sector
Inland Deserts	CA Assemblymember Eduardo Garcia Louise Bedsworth, SGC Guido Franco, CEC Daniel Tirado-Lopez, Torres Martinez Desert Cahuilla Indians	UC Riverside: Francesca Hopkins, William Porter, Cindy Yanez, Darrel Jenerette, Lynn Sweet, Hoori Ajami, Elia Scudiero Amir Aghakouchak, UC Irvine Silvia Paz, Alianza Coachella Valley Humberto Lugo, Comite Civico del Valle Peter Satin, Mojave Desert Land trust Colin Barrows, Friends of the Desert Mountains Amber Amaya, Coachella Unincorporated Rebecca Zaragoza, Leadership Counsel Pueblo Unido CDC: Yaneth Andrade, Serio Carranza

Event	Public Agencies	Non-profits, Universities, and Private Sector
Los Angeles	CA State Senator Ricardo Lara City of Long Beach: Councilmember Jeannine Pearce, Christopher Koontz Joey Wraithwall, CNRA Nuin-Tara Key, OPR Sarah Risher, CalOES Elizabeth Rhoades, LA County DPH Kelly Trainor Gamino, South Coast AQMD Juliette Finzi-Hart, USGS Heather Tomley, Port of Long Beach	Laurel Hunt, Los Angeles Regional Collaborative for Climate Action UCLA: Alex Hall, Neil Berg, Katharine Reich, Eric Fournier, Stephanie Pincetl Nancy Thomas, UC Berkeley George Ban-Weiss, USC Edith de Guzman, TreePeople Dan Cayan, Scripps Institute for Oceanography
San Joaquin Valley	Martha Guzman Aceves, CPUC CEC: Alana Mathews, Laurie ten Hope, Susan Wilhelm Mayor Jose Gurrola, City of Arvin Tom Jordan, SJV APCD Sarah Risher, CalOES Matt Rogers, U.S. Senator Kamala D. Harris	UC Merced: Joshua Viers, Josué Medellín- Azuara Julia Hatton, Rising Sun Energy Center Russ Teall, Biodico Zero Net Energy Farms
Central Coast	City of San Luis Obispo: Mayor Heidi Harmon, Chris Read Supervisor Ryan Coonerty, Santa Cruz County Dominic Roques, Central Coast Water Resources Control Board CEC: Laurie ten Hope, Guido Franco OPR: Jennifer Phillips, Nuin-Tara Key Li Erikson, USGS Anna Olsen, Cachuma Resource Conservation District	UC Santa Cruz: Ruth Langridge, Gary Griggs Melissa Rohde, The Nature Conservancy Monique Myers, California Sea Grant Geoffrey Danker, SoCalGas

Source: University of California, Irvine and University of California, Los Angeles

Inland Deserts Symposium

The Inland Deserts Symposium featured a diverse array of climate presentations and speakers made the event very special and it was noted that this was something attendees really appreciated. Panel topics included: energy; biodiversity & ecosystems; public health; community development, land use, and transportation; and water & agriculture. Coachella Valley Assemblymember Eduardo Garcia spoke at the end about legislative priorities on climate change and making them relevant to the Inland Deserts area, like with the Salton Sea work. Photos of the event.

Some testimonials from the event:

- “The next generation of children will be faced with many issues associated with climate change. We’re being faced with unprecedented changes...the new normal of what to expect and how to prepare for it. You have to be proactive and reactive,” - attendee Alan Hurt, College of the Desert Professor, as quoted in NBC article
- “Higher temperatures, more intense droughts and more damaging wildfires and floods are just some of the climate change effects already being seen in the California desert — and residents of low-income, minority communities in the Coachella Valley are most likely to suffer the consequences of those environmental stresses.” - reporter, Sammy Roth as quoted in Desert Sun article
- “Climate Resolve did an excellent job of hosting the roll out event in the Desert region of California, which is not well connected to activities out of Sacramento or to the climate movement in the greater Los Angeles area. They were able to build a diverse group of stakeholders, activists, and interested parties, and their sensitivity to the local perspective really made the event a success. In addition, Natalie was a pleasure to work with.” - UCR Lead Author of Inland Deserts Report, Francesca Hopkins, personal testimony.

Los Angeles Region Symposium

The Symposium was attended by 150 representatives from state and local government, academic institutions, and community-based organizations. The panel topics focused on themes in the LA Region report: more frequent natural disasters like wildfires, sea-level rise, drought, flooding, and extreme heat, as well as increased pressure on the region’s electrical grid. The symposium and report also highlighted the acute public health vulnerabilities of low-income communities in the face of climate change.

Moreover, the symposium demonstrated tools and resources (like Cal-Adapt, Adaptation Planning Guide, and ResilientCA.org) for practitioners, and provided a space where climate experts and stakeholders networked with each other. The event’s keynote speaker was local California State Senator Ricardo Lara who talked about climate change priorities for low-income communities of color. Photos of the event.

Some testimonials from the event:

- “Just wanted to send my gratitude for you all hosting this free climate change event. Beautiful venue, awesome content, great new tools for me to play around with, and new contacts to continue discussions. Success, indeed.” Attendee, Robyn Eason- West Hollywood Chief Sustainability Officer, personal testimony
- “I was able to network with and hear from the presenters that are critical to the work I do in the LA Region.” Attendee, Lolly Lim, UCLA staff, personal testimony
- “Great event, awesome venue. Really liked Sea Level Rise panel. Jerry Schubel was a perfect moderator that hit the key questions.” Attendee, Alexander Yee, CA Coastal Commission staff, personal testimony.

San Joaquin Valley Climate Symposium

Researchers, agency leaders, and community practitioners came together at the San Joaquin Valley Climate Symposium to highlight climate change risks and impacts, as well as to

demonstrate progress towards a resilient future. The Symposium launched an overview of California's Fourth Climate Change Assessment and presentations on the key climate impacts facing the San Joaquin Valley. CPUC Commissioner Martha Guzman Aceves provided a lunch keynote, exploring affordable energy options and energy access improvements for San Joaquin Valley residents. In the afternoon, two panel discussions bridged across sectors to dive deeper into adaptation opportunities. The first focused on challenges and innovations in creating an energy system of the future, and the second highlighted examples of on-the-ground adaptation efforts, best practices, and replicable strategies. The Symposium concluded with closing remarks from Matt Rogers from U.S. Senator Kamala D. Harris' office. Overall, the Symposium was a great success with many participants expressing their desire for additional climate-focused events. This may demonstrate an unmet need in the San Joaquin Valley – a region experiencing the impacts of climate change firsthand with a growing workforce and communities committed to climate action and resilience.

Media coverage:

- Interview: KFCF 88.1 Climate Politics, November 30, 2018
- KPFA 94.1
- Fresno Community Alliance
- California Energy Commission

Feedback received through the evaluation:

- "I would like to commend Local Government Commission, UC Merced, California Energy Commission, California Public Utilities Commission, Rising Sun Energy Center and all other guest speakers for taking the time to be present in the San Joaquin Valley to discuss in depth on this topic of climate adaptation. CCAC looks forward to further staying in contact with you all and continue to move towards 100 percent clean energy for not just their communities in the San Joaquin Valley, but for all communities in the State of California. Thank you." – Angela Islas, Central California Asthma Collaborative
- "Please continue bringing us together--great conversation, learning, and sharing!" – Participant
- "Terrific job! Thanks for an excellent event." – Participant
- "Thank you for the Symposium. I found it very interesting and important." – Participant

Central Coast Climate Symposium

In order to maximize participation, and in recognition of travel-related challenges in the region, LGC conducted the Central Coast Climate Symposium in a co-located format by connecting the San Luis Obispo location to the Santa Cruz location via webcast. The Symposium included an overview of California's Fourth Climate Change Assessment and key findings from the Central Coast Regional Report. A series of presentations and panel discussions aimed to dig deeper into the key climate risks and adaptation opportunities in the region including: coast and ocean; water, agriculture, and ecosystems; and the energy system. Participants also learned about state tools and resources including Cal-Adapt and the Adaptation Clearinghouse, engaged in table discussions to identify opportunities and resources to accelerate adaptation and enhance coordination efforts in the region. San Luis Obispo's Mayor Heidi Harmon provided welcoming remarks, and Santa Cruz County's Supervisor Ryan Coonerty provided closing remarks. Overall, the Symposium was well-attended, covered a

diverse range of topics critical to the Central Coast region, and provided valuable networking opportunities for participants.

Media coverage:

- California Energy Commission
- UC Santa Cruz

Feedback received through the evaluation:

- “Was very grateful I was able to attend. It was excellent getting to see others working with these issues, hearing the data, and being able to network.” – Participant
- “Thank you for hosting this event! Overall it was helpful and I appreciated seeing what other community members and jurisdictions were there. It was also nice to have people at the State level to make the connection.” – Participant
- “Thank you so much for bringing it directly to the Central Coast!” – Participant
- “Thank you for a really well orchestrated symposium!” – Participant

Contact

Inland Empire and Los Angeles Symposia: Natalie Hernandez | Climate Resolve,
nhernandez@climateresolve.org

San Joaquin Valley and Central Coast Symposia: Julia Kim | Local Government Commission.
jkim@lgc.org

APPENDIX D:

Dynamic Modeling of Grid-Scale Hydrogen Energy Storage Using the Natural Gas System

California has set ambitious goals to reduce the state's reliance on fossil fuels and move towards zero-carbon energy sources. However, the variability of renewable energy sources has brought increased attention to the requirements for energy storage systems, especially for large scale integration into the electricity sector. To mitigate the intermittency of renewable energy, different energy storage technologies, such as hydroelectric storage, compressed air energy storage, batteries, hydrogen energy storage (HES), capacitors, and various other energy storage technologies are being deployed. Some energy storage systems (e.g. batteries) are well suited for short-term storage, while other systems (e.g. hydroelectric storage, hydrogen energy storage) can utilize independent power and energy scaling to accomplish seasonal energy storage (Beaudin et al., 2010; Maton et al., 2013). Hydrogen energy storage is especially growing in demand due to the significantly higher storage capacity, however, the integration of hydrogen storage to the grid is not straight-forward. Further research is required to model this integration process.

In areas such as California where high levels of renewable power generation are already grid-connected, Hydrogen Energy Storage has been shown to be promising for increasing solar and wind market penetration. Repurposing the existing natural gas infrastructure to transport and store hydrogen may significantly accelerate the adoption of hydrogen and reduce the initial infrastructure investment.

Additionally, the motivation to use the existing natural gas infrastructure instead of building new hydrogen infrastructure and equipment is to reduce the initial cost and gradually phase in hydrogen and mix it with natural gas. This is similar to mixing ethanol to gasoline. Over time, it may be possible to retrofit the natural gas infrastructure to transport hydrogen and retire natural gas to support the goal of carbon neutrality, though this option should be compared with other decarbonization alternatives.

Hydrogen energy storage systems generate hydrogen gas from water using electrolysis as the main conversion technology which can be dynamically powered to complement renewable intermittency. Hydrogen energy storage can become cost effective by using inexpensive or otherwise curtailed renewable energy, storing the hydrogen, and subsequently using the hydrogen for various purposes (e.g., to produce electricity via a fuel cell for power generation or transportation applications). One of the biggest challenges in moving toward 100 percent renewable energy portfolio is the integration of the renewable sources to the grid.

The overarching goal of this appendix is to model the integration of hydrogen energy storage with large-scale renewable power using the capabilities of the existing California natural gas infrastructure. The research team analyzed the dynamics associated with grid demand, renewable power, pressure, and hydrogen energy storage capacity in detail, and simulated higher level analysis for the southern California region. In doing so, the scenario that was chosen to be modeled included assumptions of:

- Only 100 percent renewable energy penetration to meet all electric demand in Southern California through scaling solar PV installations throughout southern California (i.e., no change in wind power generation),
- All overgeneration and curtailment is used to produce hydrogen in the Southern California,
- All of the hydrogen is transmitted via the existing natural gas transmission system to existing natural gas storage facilities.

The results suggest that existing natural gas storage facilities may be converted to hydrogen storage facilities using proton exchange membrane (PEM) electrolysis. In addition, PEM fuel cell systems can be used to dispatch the hydrogen back to the grid as power. This analysis portrays that the dynamics of Southern California's natural gas storage system can support renewable gas integration. The provided framework can help to use the existing natural gas infrastructure for storage and transportation of hydrogen as one the major sources of green fuel for the future. Decision makers in the energy sector can use the information from this research to plan for and minimize the potential damage resulting from such hazards.

Additionally, the dynamic modeling of grid-scale hydrogen energy storage discussed in this appendix could be used when considering expanding hydrogen energy storage while building a hydrogen gas network with multiple gas inlet points and compressor stations for the whole southern California territory. The framework described could be used to investigate the dynamics of the SoCal natural gas infrastructure evolution to support 100 percent sustainable and renewable gas use that can benefit people of southern California.

I. Approach

The research team modeled the integration of hydrogen energy storage into the energy grid. This was done to investigate the maximum contribution that southern California natural gas transmission pipelines and underground storage facilities could make to transport and store pure hydrogen for carbon neutral energy portfolio to meet southern California's electric demand.

a. Method

The implications of a hydrogen energy storage system utilizing California's existing natural gas infrastructure were analyzed and developed in MATLAB and MATLAB/Simulink. The goal is to investigate the capabilities and vulnerabilities of Southern California (SoCal) natural gas storage facilities and main transmission pipelines owned by SoCalGas Company to absorb otherwise curtailed renewable power when renewable penetration is 100%. The analysis herein assumes that adequate hydrogen production equipment is available when the renewable power exceeds the demand to produce hydrogen in order to either store in the storage facilities or inject hydrogen into the pipeline. The study also assumes that adequate power generation equipment is available to generate electric power by dispatching hydrogen from the storage facilities when the demand is higher than renewable power.

b. Model Components

The Implications of Renewable and Demand Power

The hourly renewable power generation data was obtained from the California Independent System Operator (CAISO; <http://oasis.caiso.com/mrioasis/logon.do>). CAISO reports renewable power generation real-data on an hourly basis for three zones; NP15, ZP26, and SP15. Wind and solar data for zone SP15, which is the SoCal region, was obtained. For 100 percent renewable penetration of the SoCal region for the entire 2017 year, the solar PV and wind were considered as potential new renewable power sources. The renewable power profile from PV was thus scaled up to produce a total energy amount that meets the total SoCal demand on an annual basis considering also the round-trip efficiency of the energy storage system. Some curtailment was allowed for all scenarios (i.e., power generation amount is allowed to exceed that required to meet demand). The hourly demand data for the Southern California Edison (SCE) also was taken from CAISO. Total SCE hourly demand was then scaled up to match the southern California electricity demand.

SoCal Natural Gas Underground Storage and Transmission Pipelines

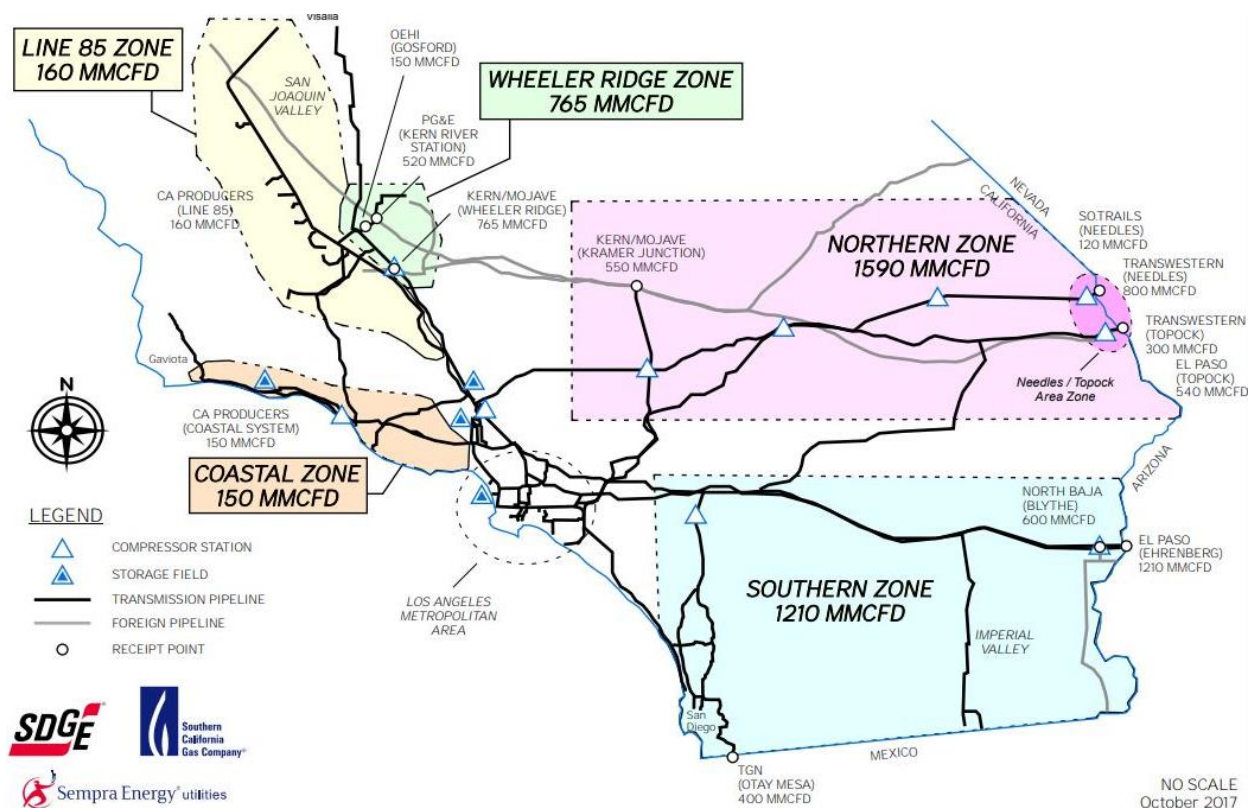
Table 1 lists SoCal natural gas underground storage facilities with respect to their capacities (based on <https://www.eia.gov/state/maps.php>). SoCalGas system map is presented in Figure D-1 (<https://scgenvoy.sempra.com/>). All four natural gas underground storage are shown in the map. Four main transmission receipt points were selected to inject hydrogen: El Paso, Blythe, Topock, and Needles. Pipes diameter, length, and ID number were taken from California Natural Gas pipeline and station (<https://www.arcgis.com/home/webmap/viewer.html>). The maximum operation pressure for SoCalGas transmission pipelines with diameter 30" and 36" is 860 psi and the minimum compressor station suction pressure is 475 psi. SoCalGas natural gas transmission pipelines are American Petroleum Institute (API) steel 5L grades B, X52, X56, X60, and X65.

Table D-1: Southern California Gas Company Natural Gas Underground Storage

Storage Facility	Working Capacity (m³)
Aliso Canyon	2,435,262,000
Honor Rancho	685,271,400
La Goleta	608,815,500
Playa del Rey	67,960,800
Total	3,797,309,700

Source: University of California, Irvine and University of California, Los Angeles

Figure D-1: SoCalGas System Map



Source: University of California, Irvine and University of California, Los Angeles

Fuel Cell and Electrolyzer

There are various types of electrolyzers with features that depend upon their electrolyte type: Proton exchange membrane (PEM) electrolysis using solid polymer electrolyte membranes, Solid oxide electrolysis (SOE) using a solid metal oxide electrolyte, Alkaline electrolysis (AE) using aqueous alkaline electrolyte solution (Schiebahn et al., 2015). SOE systems have advantages compared to PEM and Alkaline electrolyzers. First, the operation temperature of SOEs is high (900-950· C) which leads to a lower required electrical energy and faster electrochemical kinetics (lower activation losses) that lead to lower voltages (and lower energy) to produce hydrogen. Second, SOE systems can continuously operate below the thermoneutral voltage (i.e., at greater than 100 percent electrical efficiency) if a source of high-grade heat is available. This is an advantage, since electricity is more costly than thermal energy (Mohammadi and Mehrpooya, 2018). On the other hand, PEM electrolyzers can operate under pressurized conditions (even creating higher hydrogen pressure through electrochemical pumping) and both PEM and alkaline electrolyzers can operate in a highly dynamic fashion. In this study PEM fuel cell/electrolyzer (PEMFC) was used in the modeling.

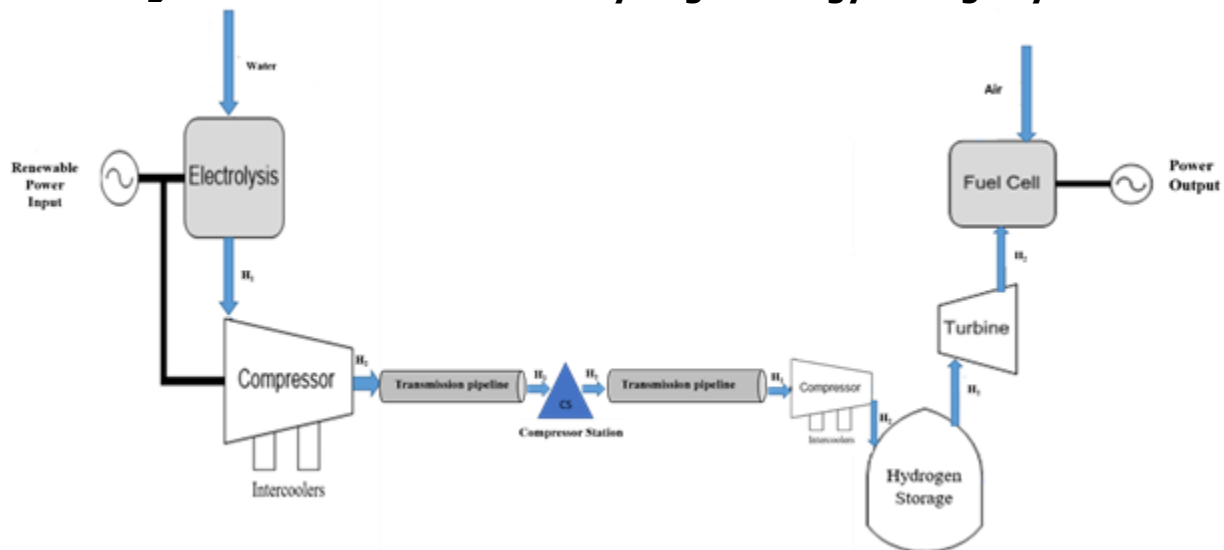
Hydrogen Energy Storage System

Figure D-2 shows a schematic of the hydrogen energy storage system. When the renewable power is higher than the demand the excess power will be directed to the PEM Electrolysis Cell (PEMEC) to produce hydrogen. Hydrogen then is pressurized in a two-stage compressor before injection into the transmission pipelines. Hydrogen then is transferred to the underground storage facilities through a network of pipelines. When the demand power is greater than the

renewable power, hydrogen is withdrawn from the storage facilities and is allowed to expand through a turbine before being directed to PEMFC to generate electricity. The hydrogen energy storage facility model used in this work was initially developed and is described in Maton et al. (2013). This storage facility model assumes that the pressurized gas facility is governed by cylindrical, one dimensional radial heat transfer, and negligible convective heat transfer within the storage facility. In the original model it was assumed that the hydrogen is produced next to the storage and there was no pipeline in the modeling. Model components are simulated with the following assumptions in Maton et al. (2013):

- The compressor isentropic efficiency is 0.75.
- The turbine isentropic efficiency is 0.82
- PEM fuel cell system efficiency of 58 percent (LHV).
- PEM electrolyzer system efficiency of 57 percent (HHV).
- Electrolyzer H₂ outlet pressure of 13.1 bar.

Figure D-2: Schematic of the Hydrogen Energy Storage System



Source: University of California, Irvine and University of California, Los Angeles

II. Results

This section presents a gedanken experiment (thought experiment) which is aimed at determining the magnitude of the contribution that the natural gas system could make toward balancing a highly renewable electric grid in the future. The assumptions that are made regarding the amount of solar and wind power considered, regional transmission of renewable power, potential for other technologies (e.g., battery energy storage, demand response) to help manage grid dynamics, etc. are not consequential to determining capabilities and challenges of using the gas system for this purpose. In addition, the potential use of the gas system for renewable hydrogen has many research and development challenges that must first be overcome before one should consider implementing grid scale hydrogen energy storage in California.

Nonetheless, in areas like California where high levels of renewable power generation are already grid-connected, Hydrogen Energy Storage (HES) has been shown to be promising for

increasing solar and wind market penetration (González et al., 2004). California is also interested in using hydrogen to fuel its transportation sector (California Fuel Cell Partnership, 2016; E4Tech, 2015), which produces the largest percentage of greenhouse gases.

To adopt hydrogen as one of the major sources of green fuel of the future, several obstacles need to be addressed. Statewide infrastructure for Hydrogen requires high initial investment compared to the existing infrastructure for fossil fuels. The existing of this cost-effective alternative makes commercial justification for investment in hydrogen in the private sector difficult, which slows down the transition to hydrogen (Myers Jaffe et al., 2017).

One approach suggested to lower the initial investment needed for Hydrogen fuel system is to utilize the existing natural gas infrastructure for storage and transportation of Hydrogen (Myers Jaffe et al., 2017). Repurposing the existing natural gas infrastructure to transport and store Hydrogen significantly accelerate the adoption of Hydrogen and reduces the initial investment.

A robust transportation infrastructure is needed to transport and store the hydrogen that is produced at the site of wind or solar farms using the excess power which is far from urban centers in CA. There are several Hydrogen transportation methods in the industry today, including dedicated pipelines, and specially made trucks. There is no one-solution-fits-all for delivery of hydrogen. Several studies have discussed the similarities between natural gas and hydrogen and the potential to utilize the existing natural gas infrastructure to transport hydrogen (Melaina et al., 2013; Myers Jaffe et al., 2017). Some of these projects are several decades old and go back to the year 1980.

In the present work, solar and wind resource dynamics, considering spatially resolved resource availability at each hour during the year, were analyzed to simulate large-scale implementation of combined solar and wind power resources sufficient to meet the entire annual southern California electric energy demand. For each hour in which excess power is available from the renewable sources such power is directed to PEM (Proton Exchange Membrane) system to produce hydrogen. Produced hydrogen from the PEMEC (Proton Exchange Membrane Electrolysis) is then transported through four main transmission pipelines to be stored in a model of the existing natural gas underground storage resources. When the grid demand is greater than the available renewable power, hydrogen is removed from the storage resources and provided to PEMFC (Proton Exchange Membrane Fuel Cell) to return power to the grid. The pressure dynamics during simulation time period were analyzed for all of hydrogen being stored. The goal of the work is to determine how much pure hydrogen can be carried out by Southern California Gas Company (SoCalGas) main transmission pipelines and underground storages under pressure limitation for 100 percent renewable energy penetration scenario.

The scenario analyzed here in this thought experiment is in fact, the worst-case scenario (e.g., one that doesn't consider other approaches or technologies that could also help manage a highly renewable electric grid, such as battery energy storage, regionalization, and demand response) to investigate the maximum contribution that southern California natural gas transmission pipelines and underground storage facilities could make to transport and store pure hydrogen for a 100 percent renewable energy portfolio to meet southern California electric demand. In the studied scenario, it was assumed that the amount of wind generation will be the same as 2017 and that solar generation is then scaled up to meet the entire

southern California electric demand. This scenario should not be considered a realistic scenario, but rather, one intentionally conceived to introduce the maximum need for dynamically supporting the electric grid with the goal of this thought experiment being to determine the capacity (pressure and flow dynamics) of the southern California natural gas infrastructure to transport and store hydrogen for this purpose.

It should be noted that blending hydrogen into the natural gas infrastructure is still in the early stages of research and one of the challenges of employing existing natural gas infrastructure to transport hydrogen is embrittlement and fatigue crack growth rate enhancement features of hydrogen on natural gas pipelines. Hydrogen molecules are significantly smaller than methane gas, which gives hydrogen a much faster leakage rate, and increases the corrosive effect of Hydrogen on metals (Djukic et al., 2015; Wasim et al., 2019). In California today, hydrogen is transported through specialty pipelines that are specifically designed from carbon steels that are well-suited to long term exposure to pure hydrogen.

Considering these challenges for introducing hydrogen into natural gas pipelines, careful analysis has been done to study the effect of injecting a blend of natural gas and hydrogen into the existing pipelines. Several studies have investigated the corrosion and cracks that have appeared in natural gas pipelines that transported a mixture of hydrogen and natural gas (Ogden et al., 2018). It is shown that mixing low percentage of Hydrogen (<15 percent by volume) does not materially increase the corrosiveness of the gas and therefore does not reduce the durability of the pipelines (Melaina et al., 2013). This same study did find increased risk, even from low blends of hydrogen, on distribution systems that would have to be addressed to enable blending. Melaina et al. (2013) also noted that there are site-specific conditions that need to be considered on a case-by-case basis for incompatibility with low amounts of hydrogen blending. On the other hand, the idea of storing hydrogen in the existing natural gas underground storage has been around since 1970. In fact, hydrogen has been stored in underground storage reservoirs in some countries and is currently stored in salt caverns in the U.S. To store such large scale of hydrogen, natural gas underground geological reservoirs in the form of salt caverns, depleted oil and gas fields, and aquifers are the only options available to-date.

In this study, the research team assumes that natural gas infrastructure (pipeline and underground facilities) may be used as hydrogen facilities that operate in the same pressure range with adequate modifications. What modifications may be required are not known at this time and should be a matter of future research and development. It is worth mentioning that the purpose of the study is not to determine the optimum mix of solar and wind generation in the southern California region for 100 percent renewable energy penetration but to investigate the capabilities and vulnerabilities (pressure and flow dynamics) of southern California natural gas infrastructure to transport and storage of hydrogen. Simply put, this study will answer the question: are there enough existing underground natural gas storage and transmission pipelines to transport and store hydrogen for the extreme case of meeting all of the hourly resolved annual electric demand by use of hydrogen energy storage in existing natural gas infrastructure alone?

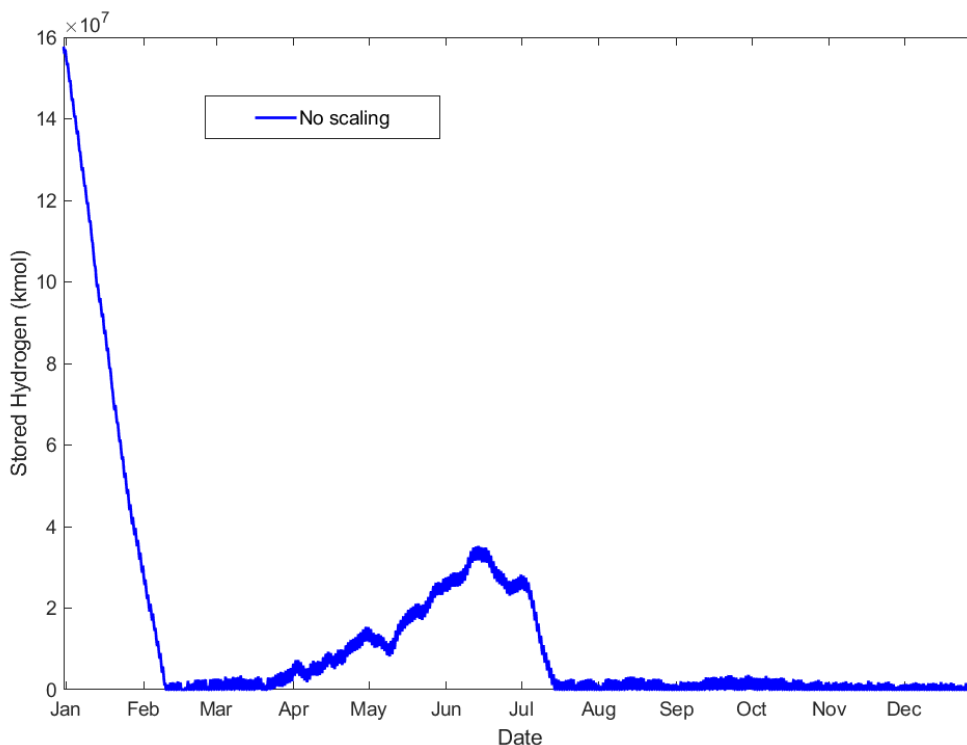
To determine the capacity of SoCalGas pipelines to accommodate hydrogen, the hydrogen energy storage system was modeled to facilitate integration of the 100 percent penetration of

renewable power sources into the electric power grid using existing natural gas infrastructure with the maximum storage capacity of 3,797,309,700 m³.

For 100 percent renewable energy penetration, the calculated scaling factor for renewable power to match the demand exactly was found to be 6.77 with the assumption of only scaling solar PV installations throughout the SoCal (i.e., no change in wind power generation). This results in a maximum renewable energy generation of 138,720 GWh. An additional scaling factor to account for hydrogen energy storage system maximum and minimum pressure and flow constraints must be used on top of the 6.77 factor. The determination of this additional scaling factor requires the following: (a) store as much otherwise curtailed renewable power as hydrogen as possible, (b) allow for the hydrogen energy storage to always be in use (not completely depleted or completely charged), and (c) result in a fill level at the end of the year that is the same as the fill level at the beginning of the year.

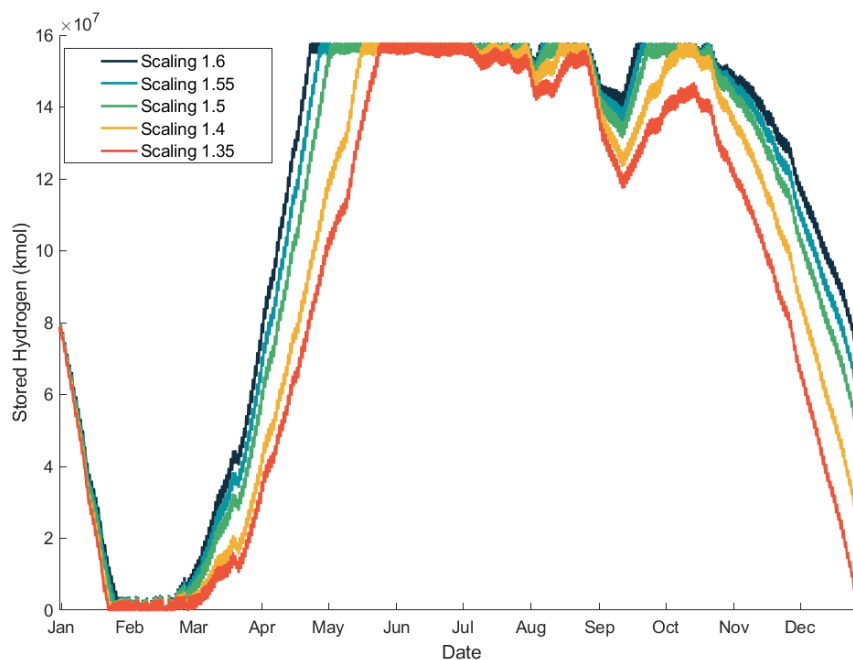
As shown in Figure D-3, for 6.77 scaling factor the hydrogen energy storage system depletes completely early in February and the fill level is very low at the end of the year. To address this, it was assumed that the hydrogen energy storage facility starts at half capacity and the scaling factor is varied from 1.35 to 1.6. The results of these simulations are shown in Figure D-4. Note that the factor of 1.6 is the optimum scaling factor due to the mentioned criteria which is the fill level at the end of the year is very close to the starting point. While the 1.6 scaling factor does not fully discharge in the early months, which is good, it does result in the additional installation of solar PV that must be curtailed (whenever the hydrogen energy storage system is full) leading to higher overall cost. The factor of 1.6 was selected as the additional scaling factor on top of the 6.77 based on above conditions which results to the overall scaling factor of 10.83 and total renewable energy capacity of 216,452 GWh required to balance generation with demand throughout the year using a hydrogen energy storage system.

Figure D-3: Annual Hydrogen Energy Storage Capacity Starting at Full Capacity



Source: University of California, Irvine and University of California, Los Angeles

Figure D-4: Annual Hydrogen Energy Storage Capacity for Various Scaling Factors Starting at Half Capacity



Source: University of California, Irvine and University of California, Los Angeles

To analyze the flow characteristics at the inlet of the pipeline a series of equations (continuity, momentum, energy) need to be solved. One dimensional, transient, and compressible flow is modeled with the following assumptions:

- Isothermal flow: The change of temperature is negligible throughout the pipeline
- Constant compressibility factor
- The convective inertia term in the momentum equation is negligible
- Horizontal pipe ($\theta = 0$)

By assuming isothermal flow, the energy equation drops, and momentum and continuity equations are solved in terms of mass flow rate $m' = ruA$ and where r, u and A are the density of the gas, velocity and the cross-sectional area of the pipe, respectively. The compressibility factor (Z) is a function of temperature and pressure but for the transient isothermal analysis it is adequate to take Z at the average system pressure and temperature (Kiuchi, 1994). According to Kiuchi, (1994) the effect of the convective inertia term in the momentum equation (second term in equation (3.2)) is much smaller than the others, and as a result it could be negligible. The continuity equation, momentum equation, compressibility factor (ideal gas law), and friction factor are expressed in the following forms (3.1 to 3.4), respectively (Abbaspour and Chapman, 2008; Kiuchi, 1994):

$$\frac{\partial r}{\partial t} + \frac{\partial (ru)}{\partial x} = 0 \quad (3.1)$$

$$\frac{\partial (ru)}{\partial t} + \frac{\partial (ru^2)}{\partial x} + \frac{\partial p}{\partial x} = -\frac{fru|u|}{8} p D - rgsin\theta \quad (3.2)$$

$$\frac{p}{r} = \frac{ZRT}{M} \quad (3.3)$$

$$f^{0.5} = -2\log \left(\frac{e}{3.7D} + \frac{2.51}{Re f^{0.5}} \right) \quad (3.4)$$

where $r, u, p, f, Z, T, R, M, Re, D, e$ are the density of the gas, velocity, pressure, friction factor, compressibility, temperature, molar mass, Reynolds number, diameter of the pipe, and the roughness of the pipe, respectively. The friction factor is from the Coplebrook friction factor equation, which is an experimentally derived equation commonly used in the natural gas industry (Abbaspour and Chapman, 2008). In equation (3.2), as it was mentioned before, θ is zero for the horizontal pipeline.

The simplified version of the continuity and momentum equations that result is written in terms of \dot{m} as presented below (Abbaspour and Chapman, 2008; Kiuchi, 1994):

$$\frac{\partial p}{\partial t} + \frac{ZRT}{MA} \frac{\partial \dot{m}}{\partial x} = 0 \quad (3.5)$$

$$\frac{\partial \dot{m}}{\partial t} + A \frac{\partial p}{\partial x} = -\frac{fZRT\dot{m}|\dot{m}|}{2DAp} \quad (3.6)$$

A fully implicit finite difference method is used to solve the above equations which is time independent and conditionally stable, and also making it easier to take larger time steps compared to the time dependent explicit method (Kiuchi, 1994). The partial time derivative, the spatial derivatives, and the individual terms are given in equations (3.7 to 3.9), respectively, by (Abbaspour and Chapman, 2008; Kiuchi, 1994):

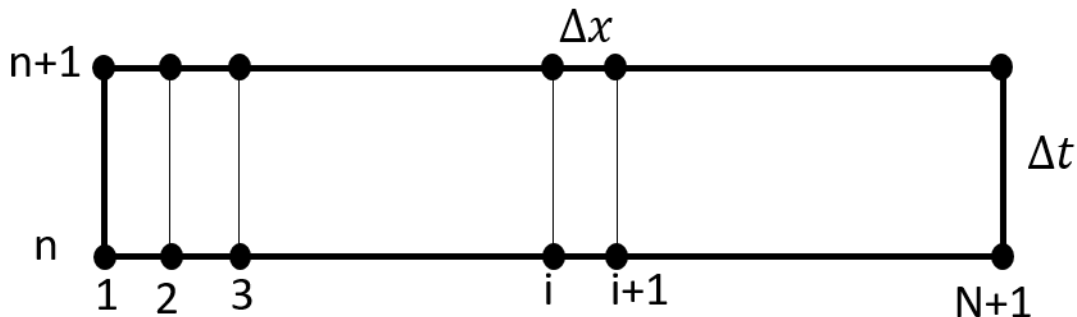
$$\frac{\partial Y}{\partial t} = \frac{(Y_{i+1}^{n+1} + Y_i^{n+1} - Y_{i+1}^n - Y_i^n)}{2 \Delta t} + O(\Delta t) \quad (3.7)$$

$$\frac{\partial Y}{\partial x} = \frac{(Y_{i+1}^{n+1} - Y_i^{n+1})}{\Delta x} + O(\Delta x^2) \quad (3.8)$$

$$Y = \frac{(Y_{i+1}^{n+1} + Y_i^{n+1})}{2} + O(\Delta x^2) \quad (3.9)$$

Y in the above equations represents mass flow rate \dot{m} and pressure (p). The pipeline is divided into N sections as it is shown in Figure 5. Therefore, it has N+1 nodes in the x direction and Δx is the distance between each of the nodes. The time step Δt is defined between the old-time level (n) and the new-time level (n+1). The number of unknowns comprising of \dot{m} and p at the new time level (n+1) is 2(N+1) can be reduced to 2N equations by setting boundary conditions. The Taylor expansion method is applied to solve the nonlinear term in the momentum equation.

Figure D-5: Annual Hydrogen Energy Storage Capacity for Various Scaling Factors Starting at Half Capacity



Source: University of California, Irvine and University of California, Los Angeles

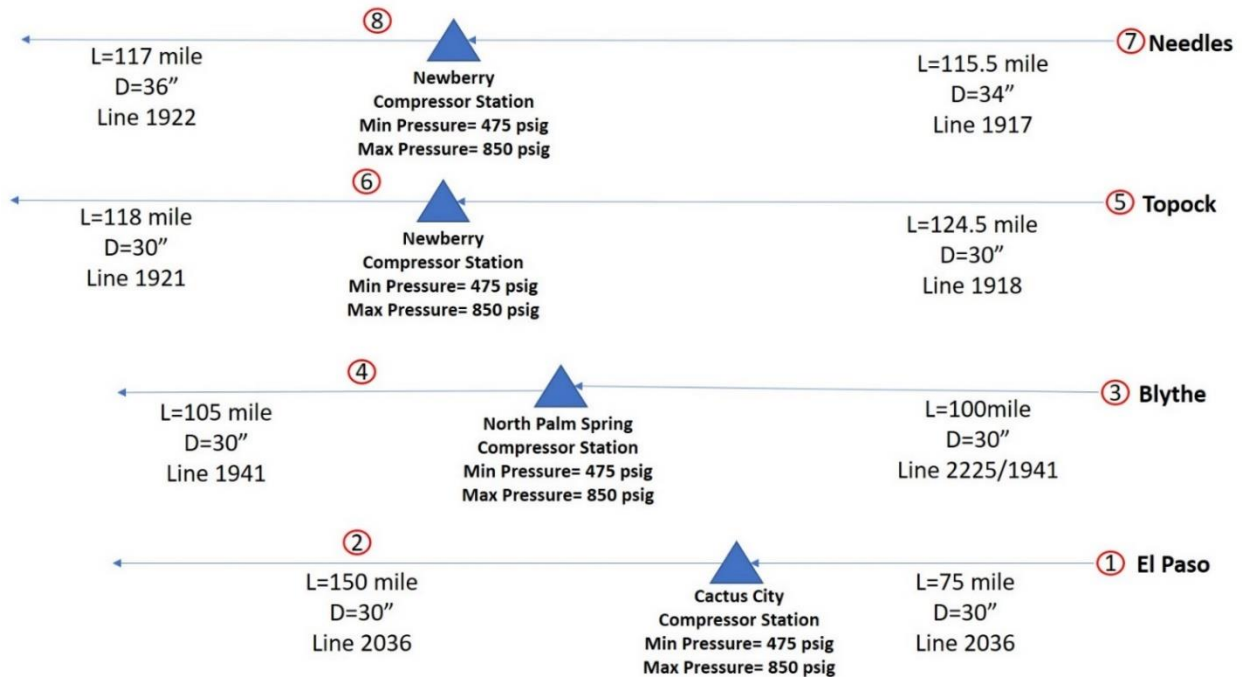
The initial condition is set to the steady state which basically means $\frac{\partial p}{\partial t} = 0$ and $\frac{\partial \dot{m}}{\partial t} = 0$. As a result, the second term in (3.5), $\frac{\partial \dot{m}}{\partial x}$ will be zero. Thus, at the initial steady state condition the

mass flow rate through the pipe will be constant. The simplified momentum equation expressed in (3.10) at the initial condition. Where p_{in} and p_{out} are pressure at the inlet and outlet of the pipeline respectively. Equation (3.10) shows the pressure drop from the inlet to the outlet is not linear under these initial conditions.

$$p_{in}^2 - p_{out}^2 = \Delta x \frac{fZRT\dot{m}|\dot{m}|}{pA^2} \quad (3.10)$$

For the current analyses, the pressure at the exit of the pipeline is maintained constant at 475 psi: $p(L, t) = 475 \text{ psi}$. The mass flow rate at the inlet of the pipe is equal to the hydrogen produced from the PEMEC: $\dot{m}(0, t) = f(t)$. Where $f(t)$ is the mass flow profile. Figure 6 shows the information of pipelines used in the modeling.

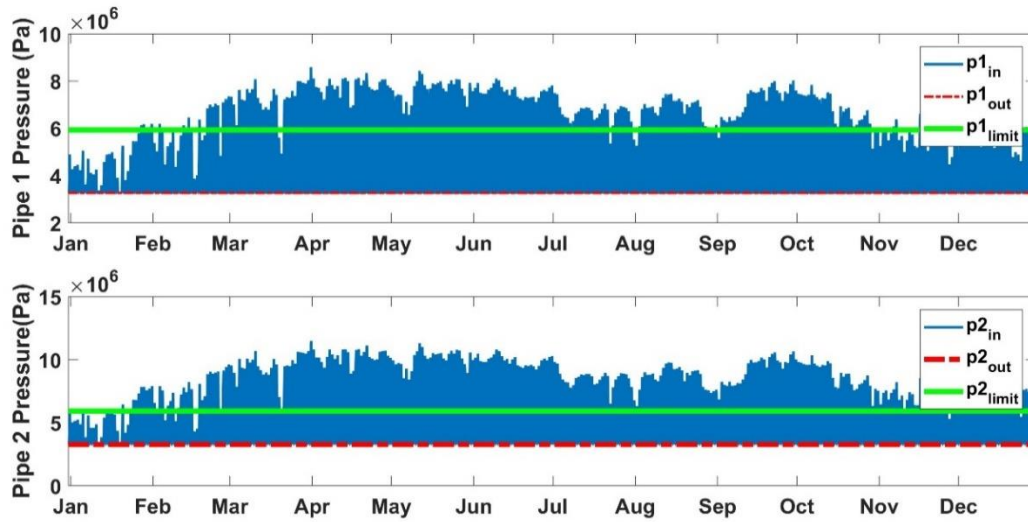
Figure D-6: SoCal Transmission Pipelines Used in Modeling



Source: University of California, Irvine and University of California, Los Angeles

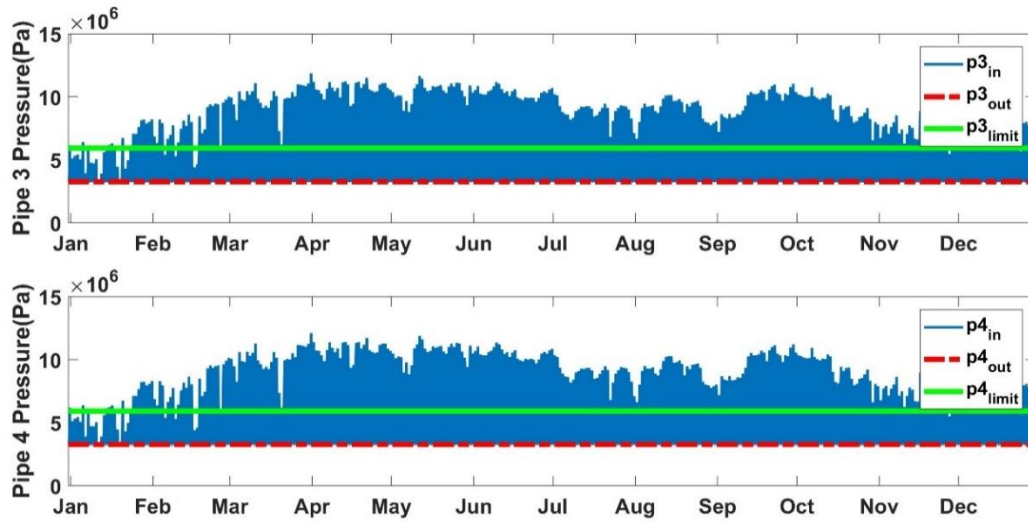
As shown in Figures D-7 to D-10, the annual pressure fluctuation exceeds the maximum operation pressure which is 850 psi. In order to deliver all the hydrogen produced at the renewable sites to the underground storages more pipes will be needed. It was found that by using four main transmission pipelines owned by SoCalGas Company, only 40 percent of the hydrogen produced can be delivered to the underground fields without pressure going above the limit as it is shown in Figures D-11 to D-14. It should be noted that these results are only for the 100 percent renewable energy penetration to meet all electric demand in Southern California. Land-use requirement for solar PV installation to reach 100 percent renewable energy penetration in SoCal is summarized in Table D-2. SoCal solar generation in 2017 was 19,138 GWh so to reach 100 percent renewable energy portfolio, 188,148 GWh additional solar energy needs to be generated. This amount of solar generation requires at least 526,815 acres of land for 2-axis Concentrator photovoltaics (CPV).

Figure D-7: Annual Pressure Fluctuation for 100% Hydrogen Delivered Through Pipe 1-2



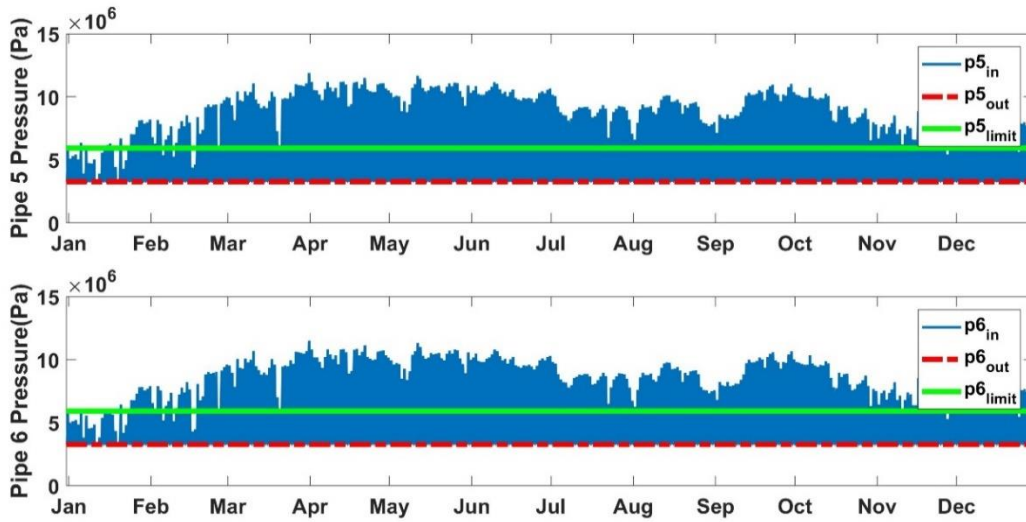
Source: University of California, Irvine and University of California, Los Angeles

Figure D-8: Annual Pressure Fluctuation for 100% Hydrogen Delivered Through Pipe 3-4



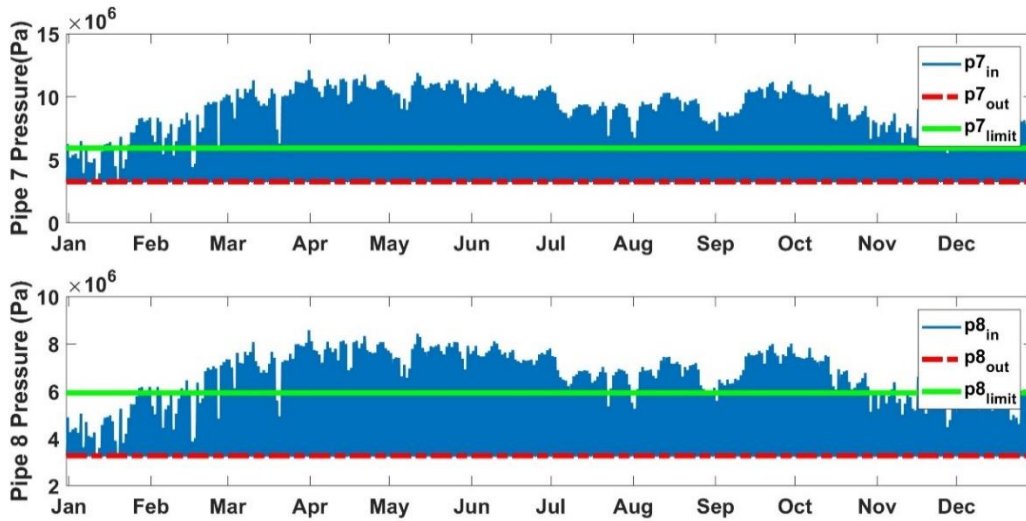
Source: University of California, Irvine and University of California, Los Angeles

Figure D- 9: Annual Pressure Fluctuation for 100% Hydrogen Delivered Through Pipe 5-6



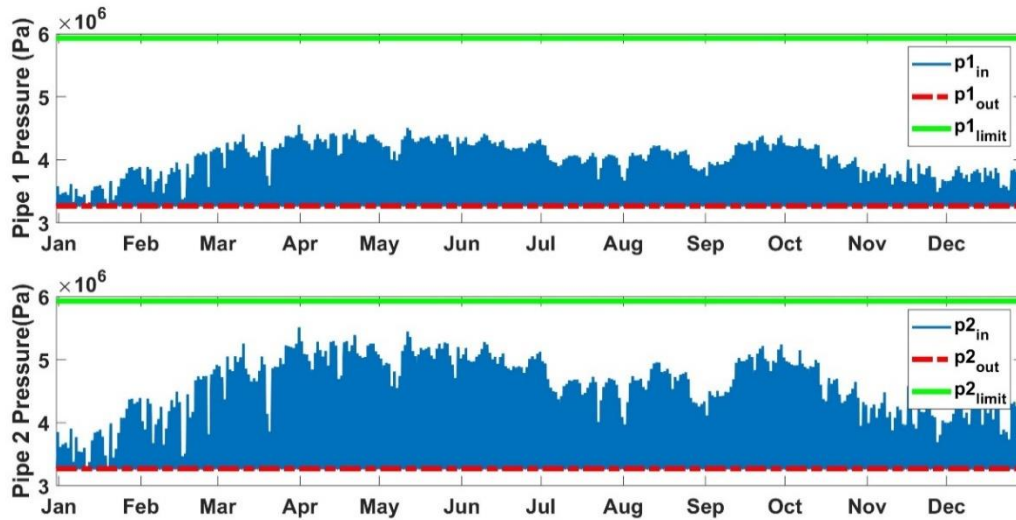
Source: University of California, Irvine and University of California, Los Angeles

Figure D-10: Annual Pressure Fluctuation for 100% Hydrogen Delivered Through Pipe 7-8



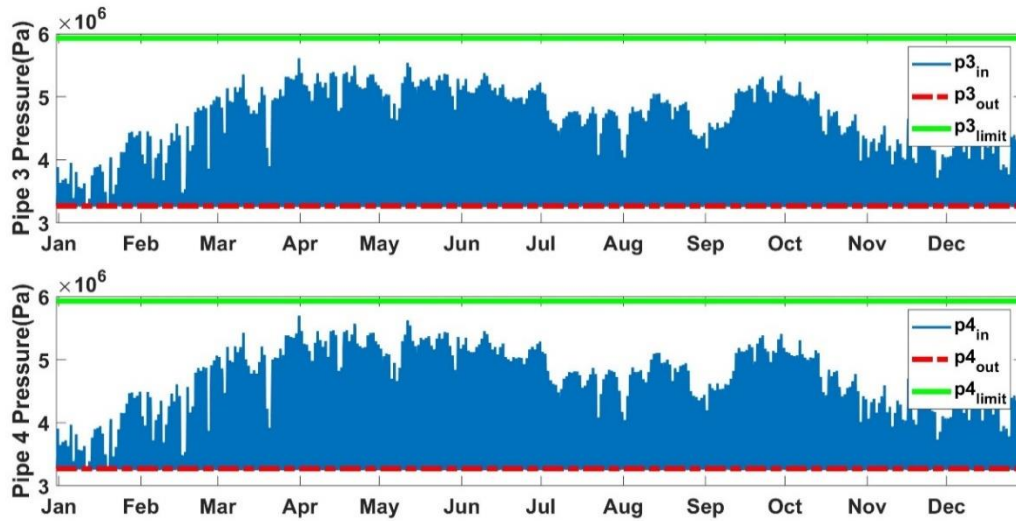
Source: University of California, Irvine and University of California, Los Angeles

Figure D-11: Annual Pressure Fluctuation for 40% Hydrogen Delivered Through Pipe 1-2



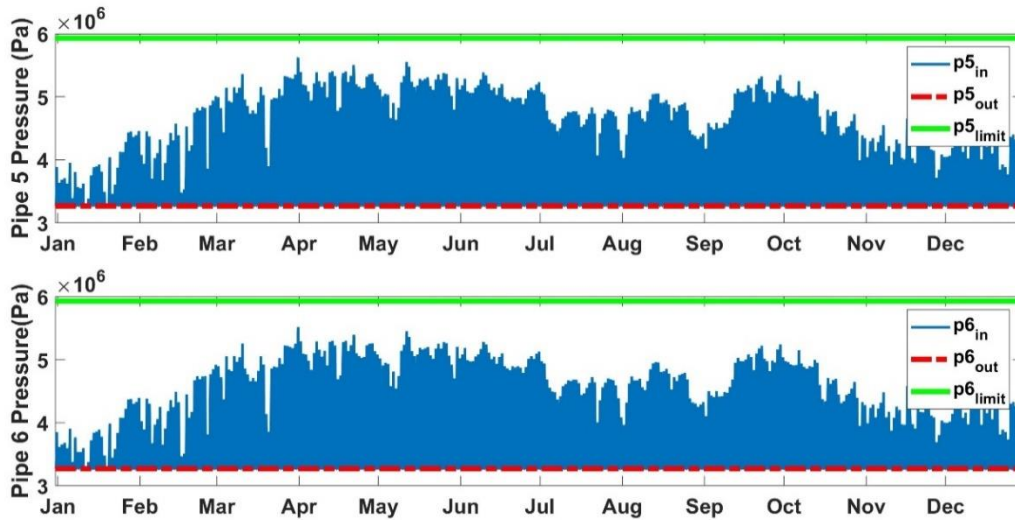
Source: University of California, Irvine and University of California, Los Angeles

Figure D-12: Annual Pressure Fluctuation for 40% Hydrogen Delivered Through Pipe 3-4



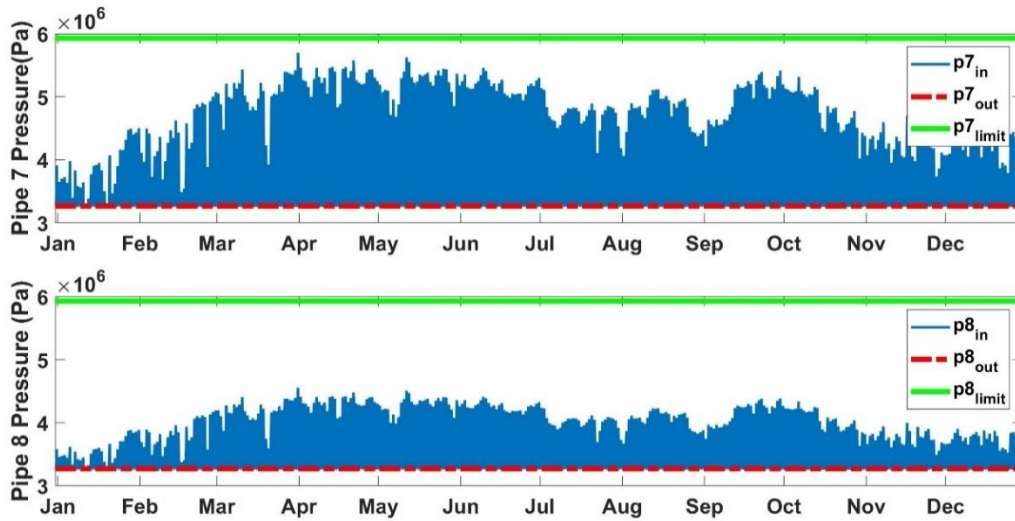
Source: University of California, Irvine and University of California, Los Angeles

Figure D-13: Annual Pressure Fluctuation for 40% Hydrogen Delivered Through Pipe 5-6



Source: University of California, Irvine and University of California, Los Angeles

Figure D-14: Annual Pressure Fluctuation for 40% Hydrogen Delivered Through Pipe 7-8



Source: University of California, Irvine and University of California, Los Angeles

Table D-2: Land Use Requirement for Different Solar PV Power Plants in SoCal

Solar Technology	Generation-weighted average land use (acres/GWh/yr)	Acres	Mile ²	Length_Mile (L*L)
Fixed	3.7	696149.38	1087.73	32.98
1-axis	3.3	620889.99	970.14	31.14
2-axis CPV	2.8	526815.74	823.14	28.69

Source: University of California, Irvine and University of California, Los Angeles

The study set out to examine the capacity of existing natural gas infrastructure to facilitate integration of the 100 percent penetration of renewable power sources into the electric power grid in southern California. The study examined whether existing natural gas infrastructure would provide sufficient capacity to transport and store hydrogen for the extreme case of meeting all the electric demand by use of hydrogen energy storage in existing natural gas infrastructure alone. The hydrogen energy storage system was modeled to facilitate that integration using the existing natural gas infrastructure's working capacity (of max. 3.8 billion m³). In the simulation, constraints of hydrogen delivery when the natural gas storage facilities are not next to the renewable energy resources (typically in the desert) are overcome.

A key finding was that the dynamics for transferring hydrogen to the underground storage resources through a long gas transmission pipelines and the dynamics associated with mass flow rate and pressure are reasonable for developing and operating a hydrogen energy storage system that can meet the electricity demand. However, only 40 percent of the hydrogen modeled to be produced at the renewable sites can be transferred along the examined (existing) four main transmission pipelines owned by SoCalGas Company to the underground storage fields without exceeding standard pressures.

References

- Abbaspour, M., Chapman, K.S., 2008. Nonisothermal Transient Flow in Natural Gas Pipeline. *J. Appl. Mech.* 75, 031018. <https://doi.org/10.1115/1.2840046>
- Beaudin, M., Zareipour, H., Schellenberglabe, A., Rosehart, W., 2010. Energy storage for mitigating the variability of renewable electricity sources: An updated review. *Energy for Sustainable Development* 14, 302–314. <https://doi.org/10.1016/j.esd.2010.09.007>
- California Fuel Cell Partnership, 2016. Medium- & Heavy-duty Fuel Cell Electric Truck Action Plan for California.
- Djukic et al., 2015; Djukic, M.B., Sijacki Zeravcic, V., Bakic, G.M., Sedmak, A., Rajcic, B., 2015. Hydrogen damage of steels: A case study and hydrogen embrittlement model. *Engineering Failure Analysis* 58, 485–498. <https://doi.org/10.1016/j.engfailanal.2015.05.017>
- E4Tech, 2015. The Fuel Cell Industry Review.
- González, A., McKeogh, E., Gallachóir, B.Ó., 2004. The role of hydrogen in high wind energy penetration electricity systems: The Irish case. *Renewable Energy* 29, 471–489. <https://doi.org/10.1016/j.renene.2003.07.006>
- Kiuchi, T., 1994. An implicit method for transient gas flows in pipe networks. *International Journal of Heat and Fluid Flow* 15, 378–383. [https://doi.org/10.1016/0142-727X\(94\)90051-5](https://doi.org/10.1016/0142-727X(94)90051-5)
- Maton, J.-P., Zhao, L., Brouwer, J., 2013. Dynamic modeling of compressed gas energy storage to complement renewable wind power intermittency. *International Journal of Hydrogen Energy* 38, 7867–7880. <https://doi.org/10.1016/j.ijhydene.2013.04.030>

- Melaina, M.W., Antonia, O., Penev, M., 2013. Blending hydrogen into natural gas pipeline networks. a review of key issues. National Renewable Energy Laboratory.
- Mohammadi, A., Mehrpooya, M., 2018. A comprehensive review on coupling different types of electrolyzer to renewable energy sources. *Energy* 158, 632–655. <https://doi.org/10.1016/j.energy.2018.06.073>
- Myers Jaffe, A., Dominguez-Faus, R., Ogden, J., Parker, N.C., Scheitrum, D., McDonald, Z., Fan, Y., Durbin, T., Karavalakis, G., Wilcock, J., Miller, M., 2017. The Potential to Build Current Natural Gas Infrastructure to Accommodate the Future Conversion to Near-Zero Transportation Technology (Institute of Transportation Studies, Working Paper Series No. qt2tp3n5pm). Institute of Transportation Studies, UC Davis.
- Ogden, J., Jaffe, A.M., Scheitrum, D., McDonald, Z., Miller, M., 2018. Natural gas as a bridge to hydrogen transportation fuel: Insights from the literature. *Energy Policy* 115, 317–329. <https://doi.org/10.1016/j.enpol.2017.12.049>
- Schiebahn, S., Grube, T., Robinius, M., Tietze, V., Kumar, B., Stolten, D., 2015. Power to gas: Technological overview, systems analysis and economic assessment for a case study in Germany. *International Journal of Hydrogen Energy* 40, 4285–4294. <https://doi.org/10.1016/j.ijhydene.2015.01.123>
- Wasim, M., Li, C.-Q., Mahmoodian, M., Robert, D., 2019. Mechanical and Microstructural Evaluation of Corrosion and Hydrogen-Induced Degradation of Steel. *J. Mater. Civ. Eng.* 31, 04018349. [https://doi.org/10.1061/\(ASCE\)MT.1943-5533.0002560](https://doi.org/10.1061/(ASCE)MT.1943-5533.0002560)